TRIBOLOGICAL AND MECHANICAL CHARACTERIZATION OF POLYELECTROLYTE MULTILAYER NANOASSEMBLIES

by

PREM VENKATACHALAM PAVOOR

Bachelor of Chemical Engineering
Department of Chemical Technology, University of Mumbai, Mumbai, India, 2000

Master of Science, Chemical Engineering Practice
Massachusetts Institute of Technology, Cambridge, Massachusetts, 2002

Submitted to the Department of Chemical Engineering
in partial fulfillment of the requirements for the degree of

DOCTOR OF PHILOSOPHY IN CHEMICAL ENGINEERING PRACTICE

at the

MASSACHUSETTS INSTITUTE OF TECHNOLOGY
[June 2005]
SEPTEMBER 2003

© 2003 Massachusetts Institute of Technology. All rights reserved.

Signature of Author_____
Department of Chemical Engineering
September 5, 2003

Certified by:_____
Robert E. Cohen
St. Laurent Professor of Chemical Engineering
Thesis Advisor

Certified by:_____
Anuj Bellare
Assistant Professor of Orthopaedic Surgery
Harvard Medical School
Thesis Co-advisor

Accepted by:_____
Daniel Blankschtein
Professor of Chemical Engineering
Chairman, Committee for Graduate Students

MASSACHUSETTS INSTITUTE OF TECHNOLOGY
SEP 0 2 2004
LIBRARIES

ARCHIVES

Tribological and Mechanical Characterization of Polyelectrolyte Multilayer Nanoassemblies

by

Prem Venkatachalam Pavoor

Submitted to the Department of Chemical Engineering on September 5, 2003,
in partial fulfillment of the requirements for the degree of
Doctor of Philosophy in Chemical Engineering Practice

Abstract

Over the last decade, the sequential layer-by-layer assembly of oppositely charged polyelectrolytes has received much interest for the deposition of film architectures, ranging from tens to hundreds of nanometers in thickness, that can be precisely tuned as a function of the processing conditions. The resulting polyelectrolyte multilayer (PEM) constructs are being investigated as biomaterials, photonic structures, electrochemical devices, and separation membranes. There is a distinct lack of literature, however, on the friction-and-wear behavior of these nanocoatings, and their exploitation in systems with tribological problems of practical relevance. In addition, their mechanical properties, crucial for the success of almost all applications being studied, have not been systematically characterized.

This thesis focuses on the elucidation of the tribological and mechanical properties of PEMs composed predominantly of weak polyelectrolytes--poly(allylamine hydrochloride) (PAH) and poly(acrylic acid) (PAA). In general, the friction coefficients of PAH/PAA PEM-coated substrates were at least marginally higher than those exhibited by their uncoated counterparts, in the absence of substrate wear. The films, however, demonstrated a significant capacity for wear prevention of underlying substrates in the dry state, and also in the presence of bovine calf serum, used to simulate joint synovial fluid. In the latter case, a significant decrease in wear rates, in tests using a clinically relevant number of cycles and articulation pattern, pointed to the efficacy of PEM-coated systems for wear reduction in total joint replacement prostheses; wear particle-induced implant loosening remains a major cause of revision surgeries. To tune the frictional response of PEMs without compromising their wear-retarding behavior, various strategies were explored; these included surface capping with a block co-polymer, *in-situ* synthesis of silver nanoparticles in the films, and assembly of composites containing PAH and multi-wall carbon nanotubes. The engineered coatings find possible applications in microelectromechanical systems (MEMS) where friction, wear, and stiction can be detrimental to device performance.

Nanoindentation was employed to probe the mechanical behavior of these ultra-thin films. It was demonstrated that the modulus and hardness of PAH/PAA PEMs could be tuned as a function of the pH of the polyelectrolyte solutions used for their assembly. The mechanical response of these structures was superior to either parent polyelectrolyte and also commercially used polymeric systems. The mechanical properties were studied at ambient conditions and in the presence of a liquid medium.

Thesis Supervisors: Robert E. Cohen, St. Laurent Professor of Chemical Engineering
Anuj Bellare, Assistant Professor of Orthopaedic Surgery, Harvard Medical School

Acknowledgements

This thesis has been made possible by collaborations spanning across departments at MIT, and research institutions in the Greater Boston area. I have been extremely fortunate to work with a number of talented and dedicated individuals during this research phase of the PhDCEP project. Each one of them has, in his/her unique way, contributed to my personal and professional growth.

First, however, I would like to thank my advisor, Prof. Robert Cohen. As far as selecting the right advisor to make one's Ph.D. experience intellectually fulfilling, I couldn't have made a better choice. In addition to generously funding my research through his St. Laurent Professorship, Prof. Cohen's enthusiasm and encouragement always lifted my spirits in times (and there were quite a few of these!) when my research faced hurdles. His support and optimism, in conjunction with his clear thoughts on a field that was beyond his primary circle of expertise, are the primary reason for my being in a position to write this thesis. He has been nothing short of a model advisor. I also thank him for patiently reading and revising drafts of my thesis and articles. My project has also benefited a great deal from having a co-advisor in Prof. Anuj Bellare. Anuj's big picture perspective and practical outlook on research helped me bridge the gap between fundamental work and its real-world applications. I thank him for setting up the collaboration with Hysitron, Inc. for nanoindentation studies, and his guidance in designing the macroscale wear tests, and in the supercritical CO_2/organic additive work, reported in Appendix D.

I am grateful to my thesis committee--Prof. Michael Rubner, Prof. Mary Boyce, and Prof. Ken Beers for bringing their expertise, in different areas, to dwell on this interdisciplinary field of tribology of thin polymer films. This work has benefited greatly from numerous discussions with Prof. Rubner, including his suggestion of block copolymer surface-capping of PEMs. I also thank him for giving me access to the dipping machines in his lab during the initial phases of the project. I thank Prof. Boyce for helping me get started on the nanoindentation work, through collaborations with Prof. Ned Thomas, and access to the AFM in his lab. I also thank her for suggesting the use of the scratch tester developed by Hang Qi, a student in her group.

The biaxial apparatus in the laboratory of Prof. Lallit Anand has been a crucial element of my thesis work. I am extremely thankful to Prof. Anand for arranging for me to get trained on that apparatus and the microindenter (before I moved on to the Triboindenter®), and allowing me to use the facilities in his lab. I also thank him for tips on nanoindentation experiments. Initial testing on the biaxial apparatus was done in conjunction with its "creator", Dr. Brian Gearing. I learnt a lot from Brian, over the one year that I worked with him before his thesis defense; his views on work, music, and life made the long hours spent in his lab less monotonous. He also introduced me to the joy of seeing the sun rise, from the confines of a lab!

The work in Appendix D is almost entirely the effort of my UROP, John Dise. I had an extremely positive experience working with John for the one year that he spent in our lab. I had heard that the choice of a UROP student was critical to a graduate student's piece of mind. I have no doubts in saying that I made an excellent choice (John, on his part, may beg to differ!). I wish him the best of luck in all his future endeavors.

The last three years would not have been as enjoyable and fulfilling without the members of the Cohen group. I have had the privilege of interacting with a group of friendly and knowledgeable graduate students and post-docs--Dr. Jeff Abes, Roger Aronow, Ryan Bennett, Dr. Russell Gorga, Heejae Kim, Ed Kopesky, Dr. Yonghwan Kwon, Daeyeon Lee, Adam Nolte, Michelle Poliskie, Sharon Soong, Dr. Yonathan Thio, Dr. Tom Wang, and Benjamin Wang. In particular, I thank Tom for helping me get started on the multilayer work, and patiently answering all my questions during the initial phases of my project. I am grateful to Heejae for giving me access to the optical microscope in Prof. Hammond's lab and for useful discussions, to Jeff for help with TEM imaging, to Russell for TEM collaboration on the MWNT-composite part of the project, and to Adam for proof-reading my thesis. Finally, I'd like to thank Yonathan; from discussions about work, food, and the future, to assistance whenever need be, Yonathan made the road to the thesis less bumpy and more intellectually interesting.

This thesis has benefited deeply from collaborations with several groups. At Massachusetts General Hospital, I thank Dr. Orhun Muratoglu for agreeing to run wear tests on our materials, in spite of his cramped schedule, and for supplying the needed substrates. I appreciate help from Mary O'Keefe and Nathaniel Hawkins in running the tests. Nat was kind enough to come in over the weekends to start my experiments. At Brigham and Women's Hospital, I thank Mary Beth Turell for being a great resource and source of help, from assisting with wear testing to preparing serum. I thank Ying Lee for general assistance and for helping John get trained on the fatigue tester. I thank Nicoli Ames and Yujie Wei for making me feel at home in the Anand lab. I thank Hang Qi for running scratch tests on his micro-tester; along with Brian and Nicoli, Hang was my link to the world of elasticity, plasticity, and Mechanical Engineering! I am thankful to members of the Rubner group for help and useful discussions during the course of the project. In particular, I would like to acknowledge Dr. Jonas Mendelsohn and Michael Berg for useful tips on the multilayer process. I also thank Jeeyoung Choi for advice and tips on the block copolymer surface-capping experiments. I thank Manish Bajaj for help with preparing self-assembled monolayers, and with ellipsometric and contact angle measurements, Dr. Itzik Sabba for advice on preparing stable dispersions of MWNTs and for access to the sonicator in Prof. Ned Thomas's lab, and Panitarn Wanakamol for patient assistance with initial work on the AFM-nanoindenter. I thank LaShanda James-Korley and Greg Pollock for training John on the DSC instrument, and Ethan Parsons for help with the tensile tests at constant true strain rates. I would also like to express my gratitude to Michael Timko for helping me set up the Parr reactor for $ScCO_2$ testing, for lending me a back pressure regulator, and for his expertise with high-pressure systems. I am grateful to Tim McClure and Libby Shaw, MIT Center for Materials Science and Engineering, for training on the AFM, profilometer, DSC, and FT-IR. My work has been greatly expedited by prompt service from the MIT Machine Shop and Peter Morley. I am grateful to Peter for help in designing the mating surfaces for the biaxial apparatus, and the tool holder for polishing. The collaboration with Hysitron, Inc. was instrumental in the development of Chapter 5 of this thesis (all measurements with the cube-corner indenter tip, and dynamic mechanical analysis in Appendix B). I thank Dr. Dehua Yang for prompt processing of the samples, Andrew Strom for patiently answering my questions, and Alissa Wild for testing the specimens. I also thank Alan Schwartzman for running my samples on the Triboindenter® at the MIT Nanomechanical Technology

Laboratory. In addition, discussions with Prof. Martin Schmidt and Prof. Mark Spearing were extremely useful in understanding the tribological issues in MEMS devices.

The final appendix in this thesis, describing a possible commercial venture arising from the project, owes a great deal to the efforts of David Lipman and Michael Berg, with whom I worked jointly towards a 50K entry at MIT.

I'd like to thank Danielle Delgado, Suzanne Easterly, Annie Fowler, Jennifer Shedd, Arline Benford, and Elaine Aufiero for looking after the administrative part of the program and for ensuring that I did not have to worry about those details. I also thank Una Sheehan for help in scheduling meetings with Prof. Boyce.

It's easy to get bogged down by work at MIT, particularly in the time-constrained PhDCEP program. I am grateful to all my friends here for helping me get away from the lab on Fridays and on evenings over the weekend. Away from work, I've been lucky to have some of my closest friends as roommates; Jeremy Johnson, Joe Moritz, and Jamie Stankiewicz have made my years at MIT a lot more fun. I thank them for periodically serving as a sounding board for my woes. Our mutual admiration for beer and Chinese food further facilitated the bonding process! I also thank Nicoli Ames, Brian Baynes, Manish Bajaj, Michael Berg, Reuben Domike, Stephen Fox, Kyle Jensen, Saif Khan, Meegan LeMott, Kathryn Miller, Jatin Misra, Jeff Peterson, Evan Piland, Michael Raab, Bala Rao, Greg Randall, Hameer Ruparel, and Harpreet Singh for their friendship and for keeping me sane. I must also acknowledge Dr. John Friedly, Dr. William Dalzell, and Prof. Alan Hatton for the Practice School experience.

Finally, I would like to thank my parents, Venkatachalam and Manjari Pavoor. My thesis would not have reached completion without their undying support and love. I thank them for listening to all my petty problems. They have truly lived the PhDCEP experience through me, and words cannot express my gratitude to them. I am grateful to my brother Tej for his constant encouragement, keeping me in touch with happenings in Bombay, and for being a great sibling. I dedicate this thesis to my parents, brother, and my grandmother, Leela Mastakar Rele, the most important people in my life.

TABLE OF CONTENTS

List of Tables

List of Figures

List of Abbreviations and Symbols

A	Projected contact area at peak load
DSC	Differential scanning calorimetry
E_i	Indenter elastic modulus
E_r	Effective modulus
E_s	Sample elastic modulus
E'	Storage modulus
E"	Loss modulus
EB	Ethyl n-butyrate
FT-IR	Fourier transform infrared
H	Hardness
h_c	Contact depth
h_{max}	Penetration depth at peak load
MWNT	Multi-wall carbon nanotube
P_{max}	Peak indentation load
PAA	Poly(acrylic acid)
PAH	Poly(allylamine hydrochloride)
PEM	Polyelectrolyte multilayer
PS-PAA	Polystyrene-block-poly(acrylic acid)
PSS	Poly(sodium 4-styrenesulfonate)
S	Unloading stiffness
$ScCO_2$	Supercritical carbon dioxide
SEM	Scanning electron microscope
TGA	Thermo-gravimetric analysis
TEM	Transmission electron microscope
μ	Coefficient of friction
ν_i	Poisson's ratio for indenter tip material
ν_s	Poisson's ratio for sample

Chapter 1 Introduction

1.1 What is Tribology?

The performance and longevity of moving systems in intermittent or continuous contact are often governed by the behavior at the articulating surfaces. Tribology, derived from the Greek word *tribos*, or rubbing, is the science of the interface between bodies in relative motion [1]; the associated areas of friction, wear, and lubrication are all encompassed by this field. An understanding of the friction-and-wear behavior is of prime importance in a number of devices and operations, ranging from those employed in large-scale industrial applications, including gears, sliders, bearings, cams, turbines, and metal cutting, to micro-mechanical devices, and biological systems like total joint replacement prostheses. Tribology-related phenomena are thus omnipresent, and encountered at virtually all scales of operation.

Polymeric materials have received much attention in the tribological arena [1]. Compared with metallic components, polymers provide economically attractive bearing surfaces that are extremely wear resistant, and associated with low friction coefficients. In addition, an increased freedom of component design, reduced weight, corrosion protection, low noise emission, and vibration dampening make polymers the preferred materials for a variety of load-bearing applications, including tires, journal bearings, gears, shaft seals, ball-bearing cages, horse shoes [2], and hip and knee implants [3]. Polytetrafluoroethylene (PTFE), high-density (HD) and ultra-high molecular weight (UHMW) polyethylene (PE), polyoxymethylene, fluoroethylene propylene, polyimide,

polyurethane, and epoxies, are examples of tribologically relevant thermoplastic and thermosetting polymeric materials.

The primary focus of this thesis is wear reduction using polymer-based coating materials. The formation of wear particles has a deleterious effect on a number of operations; equipment malfunction and stoppage in industrial devices, and implant loosening [4] for orthopedic prostheses are some examples. It is generally believed that a decrease in friction coefficients manifests as reduced system wear. While often the case, low friction forces are not a prerequisite for a decrease in wear rates. Several systems [1], including the one discussed in this thesis, are known to eliminate wear without a decrease in the friction force. Conversely, for various linear semi-crystalline polymeric systems like PTFE, the friction forces in sliding contacts are confined to low values (coefficients around 0.1 [1]) by the formation of transfer films on the opposing counterface, a consequence of material wear. Lower friction forces, however, are beneficial in conjunction with reduced wear to facilitate smooth operation and economy of energy consumption; in extreme cases, high friction coefficients may render the device inoperable.

1.2 Tuning Tribological Properties via Coating Materials

The choice of bearing surface materials in a practically relevant tribological system is dictated by several factors including cost considerations, ease of fabrication, bulk mechanical rigidity, weight, ease of integration into the overall system, interaction with the environment, and ease of maintenance and repair. The friction-and-wear

behavior might often be a consequence of the materials selection process rather than a factor guiding their choice. Since tribological response is primarily associated with the articulating region, manipulating the nature of the surfaces in contact offers the potential to control the friction-and-wear behavior without affecting the choice of the bulk material. A variety of coatings like metallic carbides and nitrides, and diamond-like carbon, harder than the substrate materials, have been used with this objective in mind [5]; the coatings resist asperity penetration and plowing, and hence lower the friction coefficients and wear rates [1]. While polymeric bearing components might be limited in their utility owing to their poor dimensional stability compared with their metallic counterparts, thin polymer coatings can be used to tune the tribological properties of the system [5]. Most of these materials, mechanically softer than the substrate, prevent wear either by absorbing the applied stresses, preventing the deformation and wear of the underlying bulk bearing material, or by the formation of strongly adherent transfer films that lubricate the interface. The adhesion of the films plays an important role in the tribological response [5].

Thin polymeric coatings have been investigated as lubricants to reduce galling, and to increase the formability and corrosion resistance in sheet metal forming operations [6]. A perfluoropolyether film, less than 20 Å thick, is used as the lubricant layer in modern magnetic hard disk drives, to prevent wear during slider-disk interactions [7]. Soft organic coatings have been also used for microelectromechanical systems (MEMS) involving intermittent or continuous contact between structures. For such micron-scale systems, including motors, display-device mirror assemblies, accelerometers, and actuators, friction and wear can be detrimental to device life [8]. In addition, the

unintentional adhesion between microstructure surfaces (or *stiction*), when restoring forces are unable to overcome adhesive interactions due to capillary, electrostatic, or Van der Waal's forces, poses a serious problem both during the manufacturing process (release stiction) and during device operation (in-use stiction) [9]. A number of small hydrocarbon molecule- and polymer-based coatings have been investigated to alleviate the problems of stiction, friction, and wear associated with these mostly silicon-based MEMS devices; the use of self-assembled monolayers [8,10-12], Langmuir-Blodgett monolayers [13], and polymer nanocomposite films [14,15] has been reported.

Surface modification, for wear reduction in orthopedic implants, has been the focus of recent research (for a review, see ref. 16). Wear particle-induced loosening of hip replacement prostheses remains a major cause of revision surgeries for the commonly used metal/ultra-high molecular weight polyethylene (UHMWPE) [17] and metal/metal [18] ball/socket configurations; a forged cobalt-chromium-molybdenum alloy is generally used as the metallic counterface. In addition to loosening, metal/metal articulations are plagued by concerns of electrochemical corrosion [18], and carcinogenesis due to the dissemination of wear particles to the lymphatic and haematopoeitic systems [4,18]. While a variety of hard coatings, including diamond-like carbon [19-23] and titanium nitride [23], have been investigated for the metallic bearing surfaces, there is a distinct lack of literature on coating materials for UHMWPE to achieve wear reduction.

1.3 Mechanical Properties and Tribological Behavior

The tribological behavior of an articulating pair combination is intimately connected to the mechanical properties of the contacting surfaces [1]. The mechanical response of the surface can often be drastically different from that of the bulk; the presence of impurities, or chemically different surface layers are potential causes for deviations. The hardness of the coating material, defined as its resistance to plastic deformation (and mathematically, as the maximum applied load divided by the corresponding projected area of the indent), plays an important role in determining the merit of the surface modification technique. Higher hardness values lead to reduced levels of asperity penetration and plowing [1], and hence decreased friction coefficients and system wear.

For thin films, particularly those less than a micron in thickness, the elucidation of mechanical properties is often complicated by effects from the underlying substrate. Nanoindentation facilitates the measurement of the mechanical response of such small quantities of materials, without the influence of the substrate's stress field [24]. By indenting the material to a certain force (or depth) and then withdrawing the tip, at a desired rate, a load-displacement (P-h curve) is obtained. This curve is a characteristic of the material being tested. Various properties, including the elastic modulus and hardness, can be elicited by analysis of this curve [25].

1.4 Surface Modification through Polyelectrolyte Multilayers

Over the last decade, the layer-by-layer assembly of polyelectrolytes has been shown to be a versatile technique for the deposition of ultra-thin films, tens-hundreds of nanometers thick [26]; polyelectrolytes are polymers with ionizable groups on each monomer repeat unit. First introduced by Decher [27], the technique uses the sequential adsorption of oppositely charged polyelectrolytes for the construction of architectures that can be precisely tuned as a function of processing conditions or polyelectrolyte pair [28-30]. Electrostatic interactions between the functional groups of the two polyelectrolytes are the driving force for this self-assembly method, which proceeds by the reversal of surface charge at each adsorption step [28]. The resulting polyelectrolyte multilayer (PEM) films have been explored for several applications including tailoring cell-surface interactions [31,32], biocompatible coatings for bone implants [33], vehicles for drug delivery [34-36], protein-resistant coatings for contact lenses [26], photonic structures [37-39], electrochemical devices [40-42], anti-reflective materials [43], and separation membranes[44,45].

Initial reported research on PEM assembly utilized strong polyelectrolytes for film construction [46]; these systems are characterized by a high degree of ionization of the functional groups over a range of solution pH values. The thickness was controlled by varying the number of adsorbed layers or the concentration of inorganic salts in the assembly solutions [28]; the thickness exhibited an almost linear dependence on these variables. The salt ions shield charges on the polyelectrolyte chain, thus allowing for a more loopy coil configuration and increased thicknesses. The potential for film build-up using weak polyelectrolytes was investigated in detail by Rubner and co-workers [29,30]. The degree of ionization of such a polyelectrolyte is intimately connected to its pKa, and

hence the pH of the solution. At values of pH below and close to the pKa, the functional groups in the polyelectrolyte chain are only partially ionized, allowing for a random coil configuration in solution. Above the pKa, a high degree of ionization straightens out the chains due to electrostatic repulsion between neighboring groups. By manipulating the pH values of the assembly solutions of polyacrylic acid (PAA) (pKa ~ 5) and poly(allylamine hydrochloride) (PAH) (pKa ~ 9), it was demonstrated that precise control over the layer organization and thickness, interfacial roughness, and nature of functional groups at the surface could be obtained [30]; the latter parameter influenced the contact angles of the assembled structures. Structures of the repeat units of PAH and PAA are depicted in Figure 1-1. It was demonstrated that the PAH/PAA pH combination could tune film thicknesses from about 0.5 nm to 14 nm per adsorbed PAH/PAA bilayer, and contact angles from about 5° for a PAA dominated surface to as high as 60° for one that was composed predominantly of PAH [30]. It must be mentioned that although assembled by a layer-by-layer technique, neutron and x-ray reflectometry [46], and a less direct method employing the introduction of metallic nanoclusters in the films [47], have been used to demonstrate that the internal structure of the PEMs consists of a relatively interpenetrated network; the interpenetrations between layers are at least on the same order as the individual layer thicknesses. Though the internal structures have been termed "fuzzy"[46], the processing conditions control the physical and chemical properties of the film surface [30].

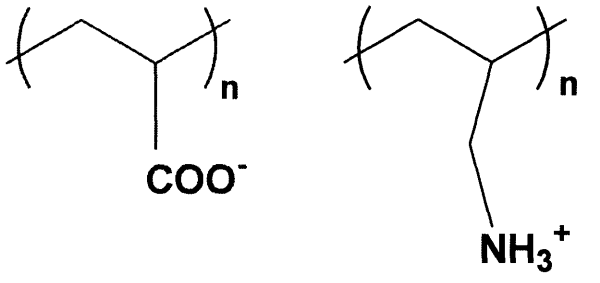

Poly(acrylic acid) (PAA)

Poly(allylamine hydrochloride) (PAH)

Figure 1-1 Structures of repeat units of PAA and PAH

In addition to tunable architectures, PEMs provide the advantage of being easy to fabricate. Assembly is aqueous based, and proceeds at ambient conditions. The entire layer-by-layer assembly process can be automated [29]. A distinct advantage of these films over other surface modification techniques, like self-assembled monolayers [9], is that PEMs can be assembled on a wide variety of substrates with little or no pretreatment. Strongly adhering PAH/PAA films, resistant to scotch-tape peel tests, have been formed on glass, polystyrene, polyethylene, silicon, and stainless steel in this study. Being conformal, substrates of complex shapes can be coated successfully, with uniformity over large areas.

Once assembled, PAH/PAA PEMs provide rich templates for further processing. Choi and Rubner [48] have demonstrated the adsorption of a block co-polymer onto the assembled PEM surface to impart a high degree of hydrophobicity to the structure; contact angles as high as 85° were reported for these modified films, with an initial contact angle of 40°. The bulk structure of the PAH/PAA film also serves as a template for the *in-situ* introduction of metallic and semiconducting nanoparticles [47]. While the ionized functional (carboxyl) groups of PAA are electrostatically bound to those of PAH,

the unionized carboxylic acid groups can be utilized for metal ion loading through an ion-exchange process with a metallic salt solution; these concentrations of unionized –COOH groups are only present at certain pH combinations. The metal ions are subsequently converted to nanoparticles through reduction or substitution chemistry. Silver and lead sulfide are examples of some nanoclusters introduced in these films [47]. Finally, in addition to using a polyelectrolyte pair for PEM assembly, charged nano-objects have also been used for film construction (for a review, see ref. 49); dispersions of semiconducting nanoparticles like cadmium sulfide, lead sulfide, and titanium oxide, montmorillonite clay platelets, graphite oxide, and carbon nanotubes [50] have all been used in alternate adsorption steps with a polyelectrolyte for the construction of films.

In conclusion, PEMs provide ultra thin films with tunable architectures that have been exploited for a variety of applications. There are, however, only scattered reports on the tribological [51] and mechanical characterization [52,53] of these structures, and almost no reports on their exploitation as coatings for practically relevant systems. The mechanical robustness and structural integrity of the films, often taken for granted, is critical to the success of almost all applications being investigated.

1.5 Thesis Outline

This thesis focuses on the elucidation of tribological and mechanical properties of PAH/PAA-based polyelectrolyte multilayers; their potential application for wear reduction in orthopedic implants and MEMS devices is also addressed. Chapter 2 studies the friction-and-wear behavior of the PAH/PAA multilayer system, primarily using a

meso/micro-scale testing device. Chapter 3 addresses the potential of this system for wear reduction in total joint replacements, by tribological testing at physiological conditions of loading, motion, and surrounding environment. The purpose of Chapter 4 is to discuss and evaluate strategies for engineering the friction coefficients and wear behavior of PAH/PAA PEMs; strategies include the surface capping of the film with a block co-polymer, *in-situ* synthesis of silver nanoclusters within the PEM, and layer-by-layer assembly of composites containing PAH and multi-wall carbon nanotubes. The friction-and-wear response of these modified structures is correlated with their mechanical properties, elicited via nanoindentation. Chapter 5 involves the detailed elucidation of mechanical properties of PAH/PAA PEMs through nanoindentation, and studies the effect of film processing conditions on material modulus and hardness. Finally, conclusions and proposed future research directions for this project are contained in Chapter 6. Chapters 2-5, in part or whole, are being submitted for publication; there is some redundancy in content to allow for self-contained reading.

1.6 References

(1) Suh, N. P. *Tribophysics*; Prentice-Hall, Inc.: Englewood Cliffs, New Jersey, 1986.

(2) Mischler, S.; Hofmann, M. In *14th International conference on wear of materials*: Washington DC, USA, 2003.

(3) Wang, A.; Essner, A.; Polineni, V. K.; Sun, D. C.; Stark, C.; Dumbleton, J. H. In *New Directions in Tribology*; Hutchings, I. M., Ed.; Mechanical Engineering Publications Limited: Bury St Edmunds, UK, 1997; pp 443-458.

(4) Ingham, E.; Fisher, J. *Proc. Instn. Mech. Engrs. Part H-Journal of Engineering in Medicine* **2000**, *214 (H1)*, 21-37.

(5) Holmberg, K.; Matthews, A. *Coatings Tribology*; Elsevier Science B.V.: The Netherlands, 1994.

(6) Carlsson, P.; Bexell, U.; Olsson, M. *Wear* **2001**, *251*, 1075-1084.

(7) Khurshudov, A.; Waltman, R. J. *Wear* **2001**, *251*, 1124-1132.

(8) Sundararajan, S.; Bhushan, B. In *NATO advances study institute on fundamentals of tribology and bridging the gap between the macro- and micro/nano scales*; Bhushan, B., Ed.; Kluwer Academic Publishers: Keszthely, Hungary, 2000; Vol. 10, pp 821-850.

(9) Maboudian, R.; Ashurst, W. R.; Carraro, C. *Tribology Letters* **2002**, *12*, 95-100.

(10) DePalma, V.; Tillman, N. *Langmuir* **1989**, *5*, 868-872.

(11) Srinivasan, U.; Howe, R. T.; Maboudian, R. In *Tribology Issues and Opportunities in MEMS*; Bhushan, B., Ed.; Kluwer Academic Publishers: AA Dordrecht, The Netherlands, 1998; pp 597-605.

(12) Ashurst, W. R.; Yau, C.; Carraro, C.; Lee, C.; Kluth, G. J.; Howe, R. T.; Maboudian, R. *Sensors and Actuators A* **2001**, *91*, 239-248.

(13) Tsukruk, V. V.; Bliznyuk, V. N.; Hazel, J.; Visser, D.; Everson, M. P. *Langmuir* **1996**, *12*, 4840-4849.

(14) Tsukruk, V. V. *Tribology Letters* **2001**, *10*, 127-132.

(15) Tsukruk, V. V.; Nguyen, T.; Lemieux, M.; Hazel, J.; Weber, W. H.; Shevchenko, V. V.; Klimenko, N.; Sheludko, E. In *Tribology Issues and Opportunities in MEMS*; Bhushan, B., Ed.; Kluwer Academic Publishers: AA Dordrecht, The Netherlands, 1998; pp 607-614.

(16) Dearnley, P. A. *Proc. Instn. Mech. Engrs. Part H-Journal of Engineering in Medicine* **1999**, *213 (H)*, 107-135.

(17) Kurtz, S. M.; Muratoglu, O. K.; Evans, M.; Edidin, A. A. *Biomaterials* **1999**, *20*, 1659-1688.

(18) Savarino, L.; Granchi, D.; Ciapetti, G.; Cenni, E.; Pantoli, A. N.; Rotini, R.; Veronesi, C. A.; Baldini, N.; Giunti, A. *J. Biomed. Mater. Res. (Appl. Biomater.)* **2002**, *63*, 467-474.

(19) Hauert, R. *Diamond and Related Materials* **2003**, *12*, 583-589.

(20) Platon, F.; Fournier, P.; Rouxel, S. *Wear* **2001**, *250*, 227-236.

(21) Saikko, V.; Ahlroos, T.; Calonius, O.; Keranen, J. *Biomaterials* **2001**, *22*, 1507-1514.

(22) Kiuru, M.; Alakoski, E.; Tiainen, V.; Lappalainen, R.; Anttila, A. *J. Biomed. Mater. Res. Part B: Appl. Biomater.* **2003**, *66B*, 425-428.

(23) Onate, J. I.; Comin, M.; Braceras, I.; Garcia, A.; Viviente, J. L.; Brizuela, M.; Garagorri, N.; Peris, J. L.; Alava, J. I. *Surface and Coatings Technology* **2001**, *142-144*, 1056-1062.

(24) Fischer-Cripps, A. C. *Nanoindentation*; Springer-Verlag New York, Inc.: New York, 2002.

(25) Oliver, W. C.; Pharr, G. M. *J. Mater. Res.* **1992**, *7*, 1564-1583.

(26) Decher, G.; Schlenoff, J. B., Eds. *Multilayer thin films: Sequential assembly of nanocomposite materials*; Wiley-VCH Verlag GmbH & Co. KGaA: Weinheim, 2003.

(27) Decher, G.; Hong, J. D.; Schmitt, J. *Thin Solid Films* **1992**, *210*, 831-835.

(28) Dubas, S. T.; Schlenoff, J. B. *Macromolecules* **1999**, *32*, 8153-8160.

(29) Yoo, D.; Shiratori, S. S.; Rubner, M. F. *Macromolecules* **1998**, *31*, 4309-4318.

(30) Shiratori, S. S.; Rubner, M. F. *Macromolecules* **2000**, *33*, 4213-4219.

(31) Mendelsohn, J. D.; Yang, S. Y.; Hochbaum, A. I.; Colson, C. D.; Rubner, M. F. *Abstr. Pap. Am. Chem. Soc.* **2002**, *223: 397-COLL.*

(32) Mendelsohn, J. D.; Yang, S. Y.; Hiller, J.; Hochbaum, A. I.; Rubner, M. F. *Biomacromolecules* **2003**, *4*, 96-106.

(33) Tryoen-Toth, P.; Vautier, D.; Haikel, Y.; Voegel, J.; Schaaf, P.; Chluba, J.; Ogier, J. *J. Biomed. Mater. Res.* **2002**, *60*, 657-667.

(34) Caruso, F.; Sukhorukov, G. In *Multilayer thin films*; Decher, G.; Schlenoff, J. B., Eds.; Wiley-VCH Verlag GmbH & Co. KGaA: Weinheim, 2003.

(35) Caruso, F.; Trau, D.; Mohwald, H.; Renneberg, R. *Langmuir* **2000**, *16*, 1485-1488.

(36) Mohwald, H.; Donath, E.; Sukhorukov, G. In *Multilayer thin films*; Decher, G.; Schlenoff, J. B., Eds.; Wiley-VCH Verlag GmbH & Co. KGaA: Weinheim, 2003.

(37) Wang, T. C.; Cohen, R. E.; Rubner, M. F. *Abstr. Pap. Am. Chem. Soc.* **2002**, *223: 275-POLY.*

(38) Wang, T. C.; Cohen, R. E.; Rubner, M. F. *Adv. Mater.* **2002**, *14*, 1534-1537.

(39) Wang, T. C. *Polyelectrolyte multilayers as nanostructured templates for inorganic synthesis*, PhD Chemical Engineering, MIT, 2002.

(40) DeLongchamp, D. M.; Hammond, P. T. *Abstr. Pap. Am. Chem. Soc.* **2002**, *223:286-POLY.*

(41) DeLongchamp, D. M.; Hammond, P. T. *Abstr. Pap. Am. Chem. Soc.* **2002**, *223: 114-COLL.*

(42) DeLongchamp, D. M.; Kastantin, M.; Hammond, P. T. *Chem. Mater.* **2003**, *15*, 1575-1586.

(43) Hiller, J. A.; Mendelsohn, J. D.; Rubner, M. F. *Nature Materials* **2002**, *1*, 59-63.

(44) Tieke, B.; Pyrasch, M.; Toutianoush, A. In *Multilayer thin films*; Decher, G.; Schlenoff, J. B., Eds.; Wiley-VCH Verlag GmbH & Co. KGaA: Weinheim, 2003.

(45) Graul, T.; Schlenoff, J. B. *Anal. Chem.* **1999**, *71*, 4007-4013.

(46) Decher, G. *Science* **1997**, *277*, 1232-1237.

(47) Joly, S.; Kane, R.; Radzilowski, L.; Wang, T.; Wu, A.; Cohen, R. E.; Thomas, E. L.; Rubner, M. F. *Langmuir* **2000**, *16*, 1354-1359.

(48) Choi, J.; Rubner, M. F. *J. Macromol. Sci.-Pure Appl. Chem.* **2001**, *A38*, 1191-1206.

(49) Kotov, N. A. In *Multilayer thin films*; Decher, G.; Schlenoff, J. B., Eds.; Wiley-VCH Verlag GmbH & Co. KGaA: Weinheim, 2003.

(50) Mamedov, A. A.; Kotov, N. A.; Prato, M.; Guldi, D. M.; Wicksted, J. P.; Hirsch, A. *Nature Materials* **2002**, *1*, 190-194.

(51) Shuiying, G.; Laigui, Y. *Chinese Journal of Chemical Physics* **2002**, *15*, 132-136.

(52) Hsieh, M. C.; Farris, R. J.; McCarthy, T. J. *Abstr. Pap. Am. Chem. Soc.* **1999**, *218: 59-PMSE.*

(53) Gao, C.; Donath, E.; Moya, S.; Dudnik, V.; Mohwald, H. *Eur. Phys. J. E* **2001**, *5*, 21-27.

Chapter 2 Tribological Characteristics of Polyelectrolyte Multilayers[1]

2.1 Introduction

This chapter addresses the tribological behavior of polyelectrolyte multilayer (PEM) nanocoatings. The assembly of these films, first reported by Decher [1], involves the layer-by-layer adsorption of oppositely charged polyelectrolytes, leading to structures whose architectures are controlled by the choice of processing conditions and the polyelectrolyte pair. In this study, weak polyelectrolytes, for which the degree of ionization of the functional groups is a function of solution pH, were used to build the PEMs. Structures of the repeat units of the two polyelectrolytes used, poly(acrylic acid) (PAA) and poly(allylamine hydrochloride) (PAH), are depicted again (also in Figure 1-1), for the reader's convenience, in Figure 2-1. Rubner and co-workers [2,3] have demonstrated that by changing the pH of these polyelectrolyte solutions, relative to their pKa values, the extent of ionization of the functional groups, and hence the ionic-crosslink density of the PAH-PAA pair, can be controlled. This facilitates tuning of PEM architectures with respect to film thickness, interfacial roughness, and nature of functional groups at the surface (i.e., contact angle). Although assembled using a layer-by-layer technique, neutron and x-ray reflectometry [1], and a less direct method employing the introduction of metallic nanoclusters [4] have been used to show that the internal structure of these films consists of a relatively interpenetrated network. A schematic of the PEM structure is illustrated in Figure 2-2.

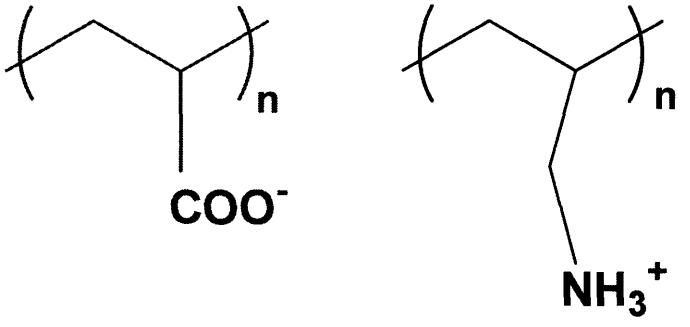

Poly(acrylic acid) (PAA)

Poly(allylamine hydrochloride) (PAH)

Figure 2-1 Structures of the repeat units of polyelectrolytes used for film assembly

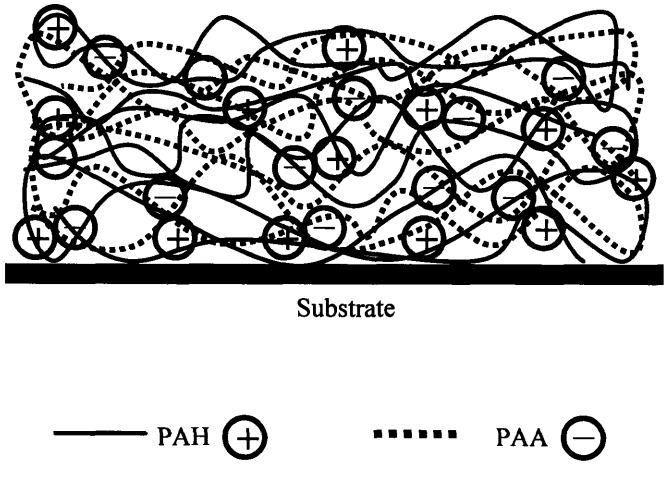

Figure 2-2 Schematic of the interpenetrated bulk structure of PEMs

In addition to tunable architectures, PAH-PAA PEMs provide the advantage of being easy to fabricate. Assembly is aqueous based, and proceeds at ambient conditions. The entire layer-by-layer assembly process can be automated [2]. A distinct advantage of these films over other surface modification techniques, like self-assembled monolayers [5], is that PEMs can be assembled on a wide variety of substrates with little or no

[1] Portions of this chapter appear in Wear **2004**, *256*, 1196-1207.

pretreatment. Strongly adhering films, resistant to scotch-tape peel tests [6], have been formed on glass, polystyrene [7], polyethylene, silicon, and stainless steel. Being conformal, substrates of complex shapes can be coated successfully, with uniformity over large areas.

Since their introduction, PEMs, assembled using various polyelectrolyte combinations, have attracted great interest (for reviews, see references 8-10) in photonic applications [11-13], anti-reflective coatings [7,14], separation membranes [15], and biocompatible films for bone [16] and artificial organ [17] implants. Their tribological properties, however, have received little or no attention [18]. This chapter focuses on the study of the friction-and-wear behavior of PEMs in the dry state (ambient conditions), and provides preliminary results of their performance in the presence of water and a biological medium. Prosthetic implants and microelectromechanical systems (MEMS) are some potential tribological application areas for these films. The detailed assessment of their performance in these areas is the subject of subsequent chapters.

2.2 Experimental Details

2.2.1 Materials

PAH (M_W = 70000) was purchased from Sigma-Aldrich (Milwaukee, WI). PAA (M_W = 90000) was obtained from Polysciences (Warrington, PA). Both these polymers were used without further purification. Deionized water (>18 MΩ cm, Millipore Milli-Q) was used for preparation of all aqueous solutions, and during rinsing procedures.

Bovine calf serum (79 g/l total protein), employed as a lubricant solution in certain tests, was purchased from JRH Biosciences (Lenexa, KS). The serum was diluted to 23 g/l using deionized water, following recommended procedures [19]. The solution also contained 20 mM of the sodium salt of ethylenediaminetetraacetic acid (EDTA), and 0.2 % by weight of sodium azide. Both these chemicals were obtained from Sigma-Aldrich (Milwaukee, WI).

Stainless steel sheets (type 316, #8 mirror finish), with an average roughness of approximately 6 nm, were purchased from McMaster-Carr (Dayton, NJ). Polished silicon wafers of <111> orientation were obtained from WaferNet (San Hose, CA). Glass microscope slides from VWR Scientific, Inc. (West Chester, PA) were used. The average roughness for both the glass and silicon substrates was less than 1 nm. These materials were all used, as received, as substrates for PEM assembly.

2.2.2 PEM Assembly and Thickness Measurements

Stainless steel, glass, and silicon slides were degreased in a detergent solution, via ultrasonication, for 15 minutes followed by ultrasonication in water for 10 minutes. After further rinsing them in water and drying by flushing with air, the slides were subjected to air-plasma treatment (5 min at 100 W-Harrick Scientific PDC-32G plasma cleaner/sterilizer). PAH and PAA aqueous solutions (0.01 M based on molecular weights of the repeat unit) were adjusted to the desired pH using 1 M HCl or 1 M NaOH. The PEMs were formed by immersing the slides into the PAH solution for 15 minutes, followed by three rinsing steps in water for 2, 1, and 1 minute respectively. The substrates were then immersed in the PAA solution for 15 minutes followed by identical

rinsing steps; this process built a PAH/PAA "bilayer". The cycle was repeated to build PEMs of the desired thickness. The immersion and rinsing steps were performed using an automated Zeiss HMS programmable slide stainer [2]. The PEM-coated substrates were finally dried by flushing with air at room temperature, and stored at ambient conditions for several hours before tribological testing. The films were assembled at a pH of 7.5 or 3.5 for the PAH assembly solution, and a pH of 3.5 for PAA, referred to as (PAH 7.5/PAA 3.5) or (PAH 3.5/PAA 3.5). The thickness of the PEMs, on glass substrates, was measured using a Tencor P-10 surface profiler.

2.2.3 Tribological Tests

2.2.3.1 Meso/micro-scale Biaxial Apparatus

Friction and wear behavior of PEMs was studied using a prototype meso/micro-scale flexure-based biaxial testing apparatus; details about the machine are given in reference 20. The normal force in this apparatus is controlled with a resolution of 80 μN over a range of 3.5 N. The shear force is measured with a resolution of 225 μN. Tangential displacements can be imposed in steps of 4 nm ranging from 0.5 μm/s to 600 μm/s. The entire system is mounted on a vibration-isolated table to minimize extraneous disturbances.

Flat-on-flat configurations were used for all tests. The apparatus is designed to hold the upper, smaller surface (a 1 mm or 2 mm diameter pin in this study) stationary, while the lower, larger block is subject to reciprocating motion. Coated and uncoated glass, silicon, and stainless steel slides were mounted on the lower surface using double-coated paper scotch tape. The upper pin counterface was made of D2 hardened tool steel

or type 316 stainless steel. It was either uncoated, or coated directly with the PEM films; in cases when an uncoated pin was articulated against the lower slider, it was polished to an average roughness of 1 μm using aluminum oxide film-coated disks. The polished pin was subsequently cleaned with acetone, and dried in a blast of air. A schematic of the mating surfaces used in this study is depicted in Figure 2-3.

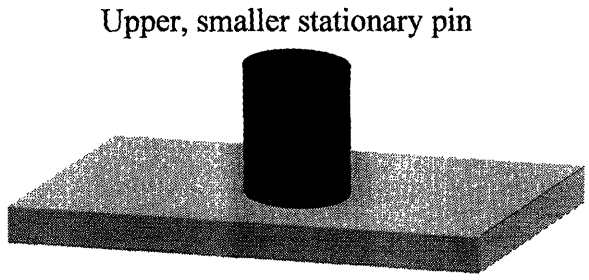

Figure 2-3 Pictorial representation of the mating surfaces used in the flexure-based biaxial apparatus

In all tests, the mating surfaces were subject to reciprocating motion over a 3 mm path length. The number of cycles was restricted to a maximum of 30, corresponding to an accumulated sliding distance of 180 mm. The sliding speed was 200 μm/s in all experiments. No effort was made to control the humidity in the test area; the ambient humidity levels were in the 15-55 % range over the duration of the experimental runs.

2.2.3.2 Pin-on-Disk Wear Testing Machine

Wear experiments were also carried out on a macroscale AMTI (Watertown, MA) Orthopod pin-on-disk wear-testing machine. Type 304 stainless steel pins, 9 mm in

diameter and 25 mm long, were machined to a hemispherical base with a point contact; they were subsequently polished, first using polishing paper, and then against a buffing compound, to obtain a mirror finish. The pin was made to articulate against coated and uncoated glass slides for approximately 2000 cycles of reciprocating motion at a normal load of 3.5 N. A path length of 2 cm, and a frequency of 1 Hz were used for all tests. Between tests, the pins were re-polished, and cleaned with water and ethanol, before drying in a stream of air.

2.2.3.3 Wear Track Analysis

Wear tracks, obtained during tribological tests using the apparatuses described in Section 2.2.3, were examined using an optical microscope. In addition, wear was characterized in terms of the topography of the wear track using a profilometer. The wear track was examined at three different points and a representative profile was chosen; in all cases, the surface profiles at different points along the wear track closely resembled each other.

2.3 Results and Discussion

2.3.1 Dry State Characterization

2.3.1.1 Effect of Normal Load on Coefficient of Friction

To study the friction behavior of PEM structures at varying normal loads, uncoated and 500 nm thick (40-45 bilayers), (PAH 7.5/PAA 3.5) PEM-coated stainless steel pins were articulated against glass slides. For these tests, the PEM constructs were assembled with PAH as the last adsorbed polyelectrolyte, i.e., an additional "half bilayer"

was employed. The average steady-state friction coefficients μ (ratio of tangential force to the normal force), over the course of three experiments at each load level, are plotted as a function of the applied nominal normal stress in Figure 2-4.

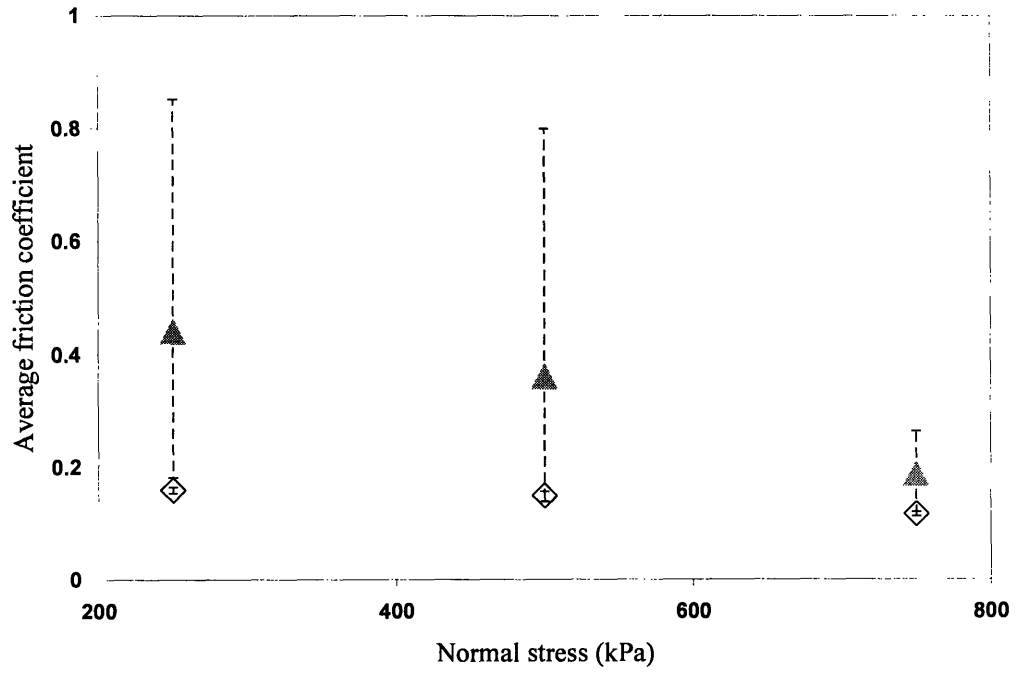

Figure 2-4 Average coefficients of friction for an uncoated stainless steel pin (diamonds), and a (PAH 7.5/PAA 3.5) 500 nm thick PEM-coated steel pin (triangles), sliding against glass at a normal stress of 250, 500, and 750 kPa; error bars reflect the maximum and minimum values obtained over three tests at each load level. Normal stresses are based on the pin diameter.

The coefficient of friction for the uncoated steel-glass combination remained almost unchanged (0.09-0.15, see Figure 2-4) over the range of stresses studied. On the other hand, when the pin was coated with PEMs, there was a wide range of friction forces observed at normal stresses of 250 and 500 kPa; the friction force was confined to a fairly narrow window at 750 kPa. There were no signs of wear particles, or rupture of the film

on the pin surface at all these stress levels. At a stress of 750 kPa, the film is likely to be compressed to a reasonably uniform thickness when the pin is in contact with the glass slide. Hence there was a smaller variation in the friction forces between tests. Minimal orientation in the sliding direction on account of the entangled structure of the PEMs, film adhesion to the glass surface, some asperity penetration, and film deformation lead to a friction force that is higher than that exhibited by the bare steel pin. At stresses of 250 and 500 kPa, a lower degree of conformal contact between the pin and the glass may lead to non-homogeneities in the film thickness along the pin-glass interface, resulting in a larger range of friction coefficients depending on the conformation of the film in the dominant contact region.

When PEMs are coated onto the pin, the entire film experiences the same forces and deformations as the larger slider moves past it. Since no film or substrate wear was observed at these stresses, these friction coefficients reflect the characteristics of the native material pair; these are the "true" coefficients exhibited by the films (on steel) against glass. Based on the adhesive component of friction force, Suh [21] predicts decreasing coefficients with an increase in normal load, for polymeric materials. This decrease in friction coefficient is related to the dependence of a polymer's shear strength on the applied hydrostatic pressure. An inkling of such a trend is observed in Figure 2-4.

We also carried out tests to examine the possible effect of the polyelectrolyte functional groups on the friction force. When assembled at the (PAH 7.5/PAA 3.5) pH condition, the surface layer of the PEM structure is enriched with functional groups from the last adsorbed polyelectrolyte; the bulk structure is still interpenetrated. This surface enrichment is reflected by the observed contact angles [3]. At the stress levels and mating-

surface geometries used in this study, the friction coefficient was not affected by the choice of PAH or PAA as the uppermost layer.

2.3.1.2 Wear Behavior of PEM-coated Substrates

The wear behavior of PEM-coated substrates was studied using (PAH 7.5/PAA 3.5) 500 nm PEM constructs; PAH was the last adsorbed polyelectrolyte. Figure 2-5 depicts the friction coefficient profile for the case of an uncoated tool steel pin against an uncoated sliding stainless steel substrate, over the 30-cycle duration of the test. Each curve in the graph represents the friction as the slider traverses the 3 mm path length; the change in sign indicates motion in the reverse direction. The evolution of the profile is similar to that described by Suh [21]. Initially, the friction force is largely a consequence of plowing of the surface by asperities. The steep increase in friction force is attributed to the generation of wear particles. The increase in friction coefficient is thus a consequence of evolution of the interface, and the observed values of μ in this region are not representative of the frictional interaction between the native materials (in the absence of wear).

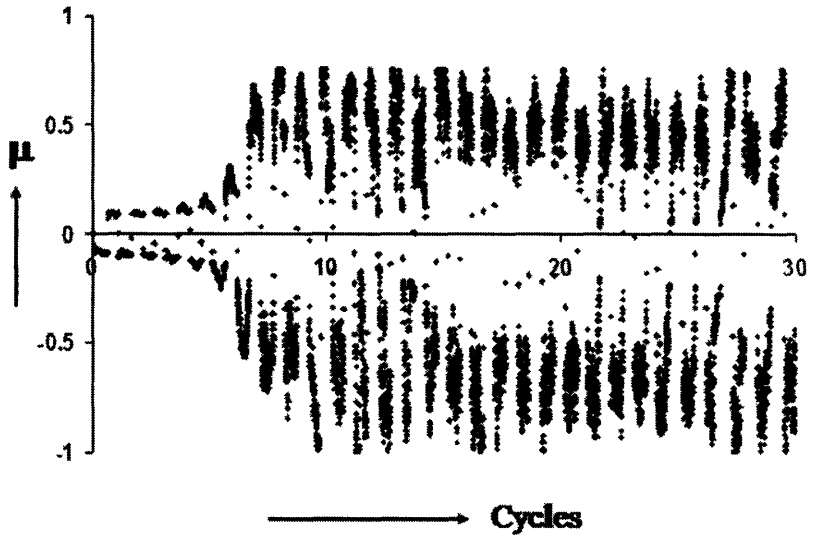

Figure 2-5 Friction profile for an uncoated tool steel pin slid against an uncoated stainless steel substrate. Normal stress 1 MPa based on diameter of pin

Figure 2-6 depicts the friction profile when the larger sliding steel substrate was coated with a 500 nm thick PEM assembly; the pin was uncoated. The frictional response in this configuration, unlike the case of the PEM-coated pin in Section 2.3.1.1, is expected to be influenced by the film characteristics, by the interface between the film and the substrate, and perhaps by the substrate itself. It is evident that the evolutionary nature of the friction profile was suppressed by the PEMs. The coefficient of friction remained almost constant in the range 0.5-0.6 during the duration of this test.

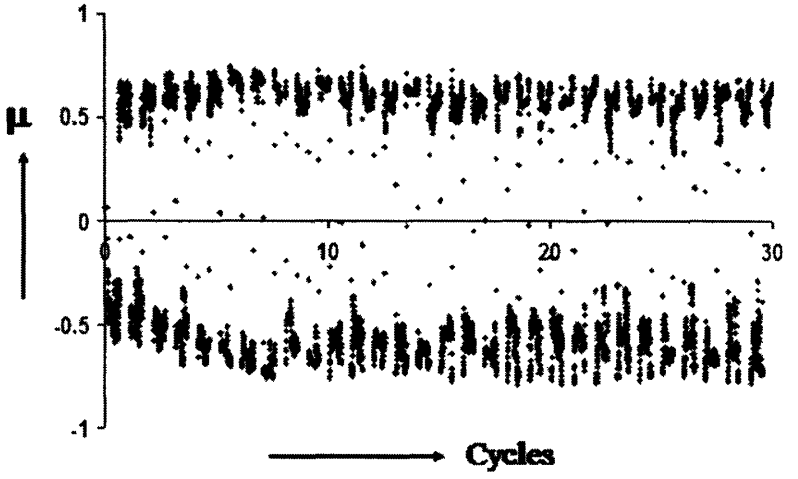

Figure 2-6 Friction profile for an uncoated tool steel pin sliding against a stainless steel slide coated with (PAH 7.5 / PAA 3.5) 500 nm PEM assembly. Normal stress 1 MPa based on diameter of the pin

To establish that an absence of evolution in the friction profile correlates with a virtual absence of substrate wear, the wear tracks, corresponding to the tests depicted in Figures 2-5 and 2-6, were analyzed using optical microscopy and cross-sectional surface profiling. The results are presented in Figure 2-7. For the case of the bare steel substrate, a distinct wear track was observed; at higher magnifications, the wear particles, the principal cause of evolution of the friction profile, could also be seen. Examination of the cross-section of the wear track revealed pile-up of material alongside gouges up to 1.5 μm in depth. By contrast, there was essentially no wear of the metal surface when coated with the PEM. It was evident from the wear track profile that the 500 nm film had delaminated over the width of the track, but the underlying metal surface was protected; in rare cases, the film was observed to have retained its integrity over the wear track. PEM film fragments could be seen in the optical micrographs on the wear track, mostly at the ends, or occasionally on the surface of the pin; the deformation, adhesion, and

dragging of these fragments at the interface results in the high observed friction forces. The mechanism of wear prevention evidently lies primarily in the presence of PEM fragments between the pin and the slider because the film is usually removed from parts of the track within the first few cycles of the test. There was no evidence of the metal debris or deep gouges that were apparent in the wear track for the uncoated metal-on-metal system.

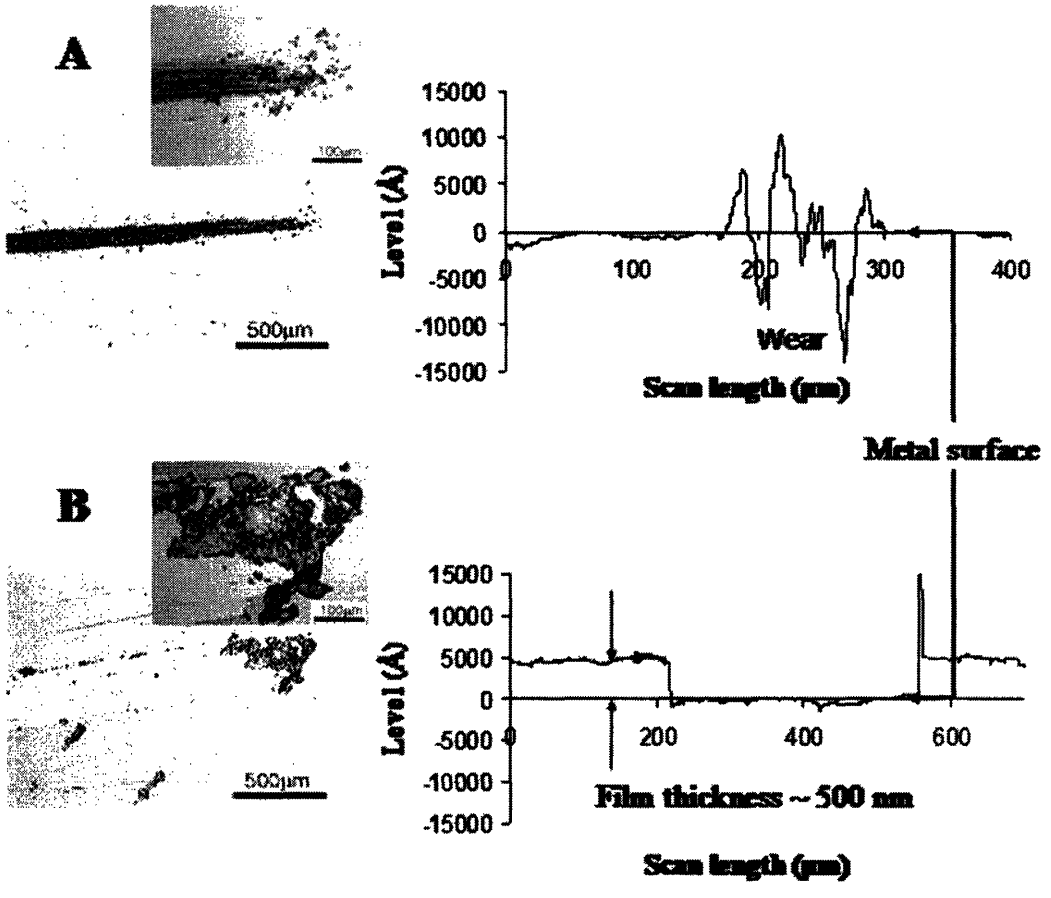

Figure 2-7 Optical micrographs (insets depict higher magnification images of the ends of the wear track) and cross-sectional surface profiles for A. Uncoated stainless steel slider, and B. Steel slider coated with (PAH 7.5 / PAA 3.5) 500 nm PEM construct. Counterface was uncoated tool steel pin, and normal stress was 1 MPa, in both cases.

The wear of a bare steel substrate over the 30-cycle duration of the test was also avoided when the pin was film-coated with a 500 nm PEM (similar to the configuration in Section 2.3.1.1). The evolution in the friction profile, depicted in Figure 2-8, is attributed to limited fragmentation of the film during the test, and not due to wear particles.

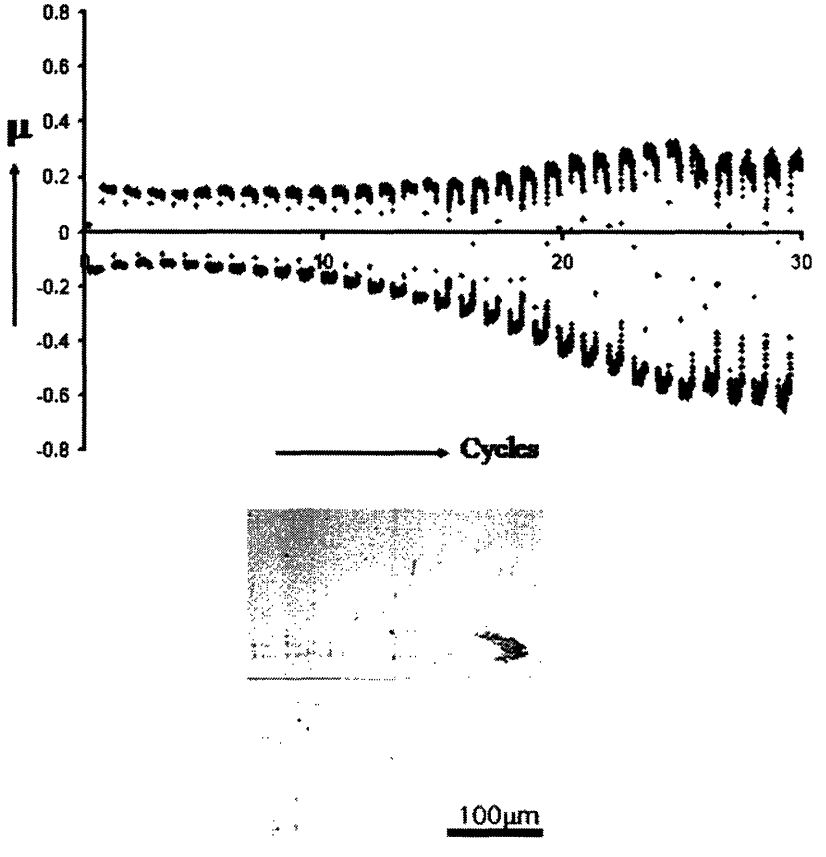

Figure 2-8 Friction profile and optical micrograph of the wear track for a (PAH 7.5/PAA 3.5) 500 nm PEM-coated stainless steel pin slid against bare stainless steel at a normal stress of 1 MPa

Several interesting observations can be made from the summary of the wear experiments in Table 2-1. All the 500 nm PEM constructs (Table 2-1, line 3-5) prevented

substrate wear. In the early stages of an experiment, the uncoated metal-on-metal pair has a low friction coefficient of 0.1; however, the generation of wear debris rapidly elevates this value (Figure 2-5). A relatively thick PEM coating (500 nm) elevates the value of μ substantially to approximately 0.6 (Table 2-1, line 3) but this value includes a mechanism of dragging and deforming PEM film-debris at the pin-slider interface. Thinner PEM films (compare Table 2-1, line 6, 7 and 8) show promise for simultaneously minimizing the friction coefficient and the wear of the substrate. A reduction in thickness compromises the wear-reducing efficacy of the PEM fragments (Table 2-1, line 7). This observation is also demonstrated by a 1 bilayer PEM assembly, approximately 9-15 nm thick on steel (for reference, a 20 nm film consists of 3 bilayers, while 7 bilayers are needed for a 70-80 nm thick film assembled at the (PAH 7.5/PAA 3.5) combination). Wear reduction was only occasionally observed for this very thin PEM; a low friction coefficient of 0.2 resulted in the absence of substrate wear. When the PEM is placed only on the pin (Table 2-1, line 4) the production of PEM film debris is almost negligible and the low value of the steel-steel friction coefficient is approached in the initial portion of the experiment. For the same thickness, PEMs on the larger surface offer more material for wear prevention.

Table 2-1 Summary of experiments designed to elucidate wear behavior of PEM constructs on different substrates (dry state)

	Pin	Slider	(PAH 7.5/PAA 3.5) PEM Characteristics[e]	Normal Stress[b] (MPa)	Evolution in Friction Profile[c]?	Wear of Slider?	μ (or range)
1	Tool steel	SS[a]	-	1	Yes	Yes	0.09-0.57
2	SS	SS	-	1	Yes	Yes	0.13-0.34
3	Tool steel	SS	On slider, 500 nm	1	No	No	0.58
4	SS	SS	On pin, 500 nm	1	Yes	No	0.14-0.35
5	SS	SS	On slider and pin, 500 nm	1	No	No	0.81
6	Tool steel	Si <111>	-	4	Yes	Yes	0.1-0.58
7	Tool steel	Si <111>	On slider, 20 nm	4	No[d]	No[d]	0.23
8	Tool steel	Si <111>	On slider, 80 nm	4	No	No	0.49

(a) Stainless steel type 316

(b) Based on the diameter of the pin

(c) Over the duration of a 30-cycle test, unless otherwise specified

(d) After 20 cycles, however, wear of the silicon substrate was observed

(e) PAH last adsorbed layer in all cases

Further evidence for the important role of PEM fragments in wear reduction is shown in Figures 2-9 and 2-10. Figure 2-9 presents optical micrographs of a wear-free track on the slider for the case in which both the stationary steel pin and the sliding steel substrate were coated with 500 nm thick PEMs. At a normal stress of 1 MPa, no wear of the steel substrate was observed; the friction coefficient remained at a steady value of approximately 0.8 during the length of the test (Table 2-1, line 5). The PEM on the steel

slider was removed along the 3 mm path length. When the same pin was subsequently tested against an uncoated stainless steel slide, a profile similar to that depicted in Figure 2-8 was obtained. The original film on the pin, in conjunction with some fragments transferred from the coated original steel slide, was successful in preventing wear of the substrate over 30 cycles. Optical micrographs of the test region on the steel slide and the pin, at the end of the test, are presented in Figure 2-10. This configuration is recommended for make-and-break type of contact situations, in which contact may not always be reestablished at the point of severance, where the advantageous PEM-fragments lie on the wear track. The PEM constructs on the pin will, however, still be available to prevent substrate wear during the second run.

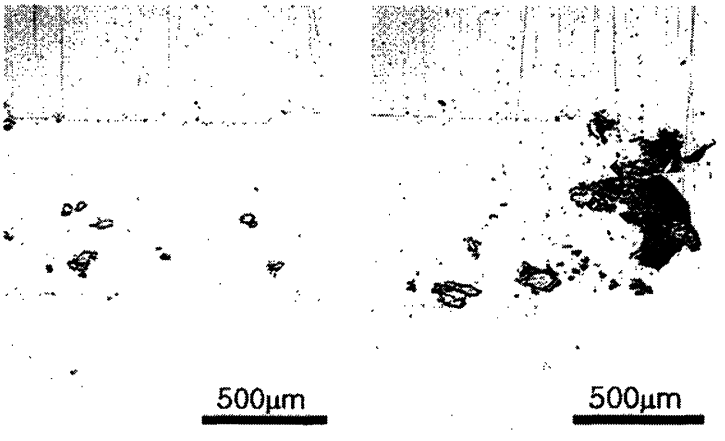

Figure 2-9 Optical micrographs of the wear track when a PEM-coated steel pin was articulated against a PEM-coated steel slide at a normal stress of 1 MPa; both PEMs were assembled at the (PAH 7.5/PAA 3.5) combination and were 500 nm thick.

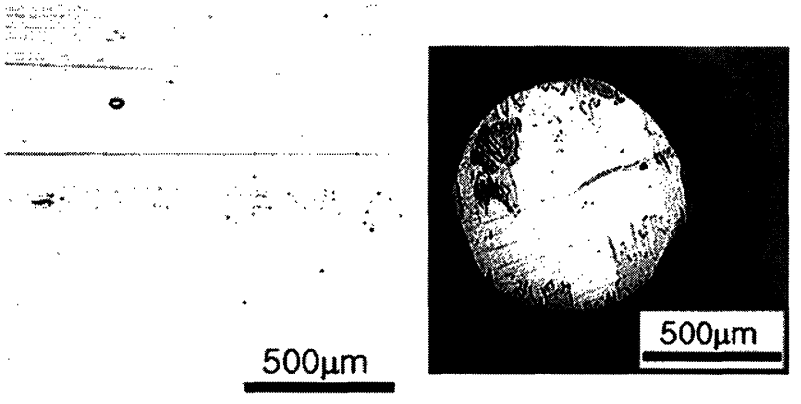

Figure 2-10 Optical micrographs of the test region on the bare steel slider (left) and the steel pin (right, used for the test depicted in Figure 9) after 30 cycles of reciprocating motion at a normal stress of 1 MPa. There is negligible wear of the steel slider; PEM fragments from the slider in Figure 2-9 can be seen on the PEM-coated pin.

A trade-off exists between lowering the friction coefficient and avoiding early initiation of substrate wear when the slider is PEM-coated. Films on the slider must have a certain minimum thickness to supply the desirable wear-reducing properties. Slightly higher thicknesses are required for steel substrates compared to silicon, owing to the higher associated surface roughness.

To examine the efficacy of the films with respect to wear reduction over a larger number of cycles and normal pressures, tests were carried out on a macroscale pin-on-disk wear tester. The configuration is described in Section 2.2.3.2. Assuming elastic contact between the steel pin and the glass substrate, the maximum contact stress for the 3.5 N load was calculated to be 450 MPa using Hertzian analysis. Optical micrographs and surface profiles of the wear tracks after 2000 cycles of reciprocating motion, on coated and uncoated glass substrates, are presented in Figure 2-11. In the case of the

uncoated glass slide, steel deposition from the pin onto the wear track was observed within the first few cycles. Cross-sectional profiles indicated wear track depths up to 7 μm. Conversely, for glass coated with a (PAH 3.5/PAA 3.5) 70 nm film, no steel deposition was seen, and a clean wear track was obtained at the end of 2000 cycles. The wear-track profile indicated film removal over the width of the wear track, but absence of substrate wear.

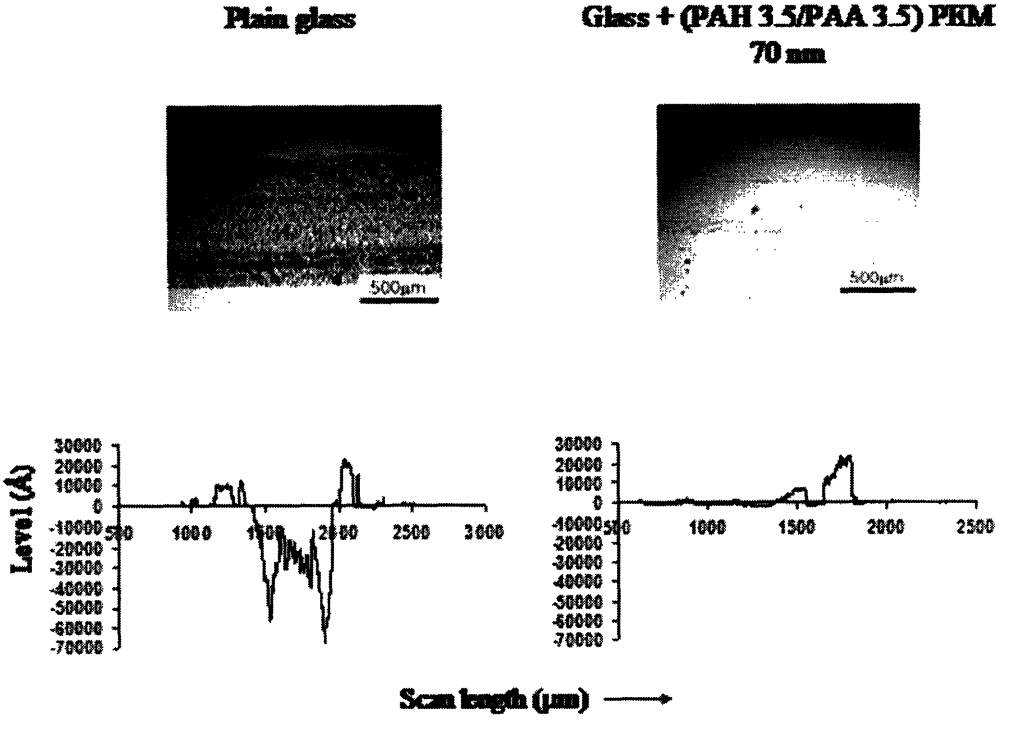

Figure 2-11 Optical micrographs and cross-sectional surface profiles of wear tracks after macroscale pin-on-disk tests (2000 cycles).

At thicknesses of about 500 nm, the pH values of the assembly solutions do not play a significant role in the wear reducing power of PEM fragments. At lower thicknesses, however, the differences in the degrees of ionic-crosslinking in the (PAH

7.5/PAA 3.5) and (PAH 3.5/PAA 3.5) constructs [3] could have an effect on the load bearing capacity of these films. Nanoindentation (see Chapter 5) has been used to characterize the mechanical behavior of PEMs assembled at varying pH combinations.

Surface modification has received a large amount of attention in the case of micromotors, gear trains, mechanical relays, valves, and other devices in MEMS [22]. The factors impeding reliable operation of these devices include wear of the silicon-based materials, high friction forces, and stiction between the mating surfaces [23]. A number of organic coatings have been studied with respect to friction, stiction, and wear reduction in these devices, including Langmuir-Blodgett monolayers [24], self-assembled monolayers [5,22,25], and polymer films with layered architectures [26,27]. Most of these coatings require either an intricate protocol for assembly, or a large density of functional groups by which they can covalently bind to the substrate. Release of corrosive by-products, and polymerization of precursor molecules leading to particulate formation, are some examples of other problems encountered during processing of these films [5]. These issues are not encountered during processing of PEMs. The films obviate the need for elaborate pretreatment steps, and can be assembled on a wide variety of materials. In addition, no corrosive by-products are formed during processing. Hence, PEMs may present a facile solution to the tribological issues facing MEMS. At stresses causing wear of unprotected silicon, 20-80 nm thick PEMs exhibited low friction forces coupled with an absence of substrate wear (Table 2-1, lines 6,7, and 8). The friction coefficients of PEM-coated substrates, however, are higher than the value of 0.1 exhibited by the bare silicon substrate, prior to the onset of wear. Adhesion of the hydrophilic films to the counterface, some asperity penetration, and resistance to orientation in the direction of

sliding are the likely causes for the higher friction forces. Strategies that have been explored in an effort to reduce the friction coefficients include surface capping of these films with block co-polymers, and the introduction of metallic nanoclusters into the PEMs (see Chapter 4).

2.3.2 Characterization in a Liquid Medium

Table 2-2 outlines the results of preliminary experiments to elucidate the wear behavior of PEM-coated stainless steel in the presence of water. A (PAH 3.5/PAA 3.5) 70 nm construct was assembled on the steel slider; the tool steel pin was uncoated. The pin-slider interface was submerged in water. Analogous to the dry state tests, PEM fragments inhibited wear particle generation, and hence evolution of the friction curve over the 30-cycle duration of the test. Again, adhesion to the counterface and dragging of the hydrated fragments at the interface contributed to a friction force that was higher than the control experiment.

Table 2-2 Wear behavior of PEM-coated substrates in water.

	Pin	Slider	(PAH 3.5/PAA 3.5) PEM Characteristics	Normal Stress[(b)] (MPa)	Evolution in Friction Profile[(c)]?	Wear of Slider?	μ (or range)
1	Tool steel	SS[(a)]	-	1	Yes	Yes	0.12-0.32
2	Tool steel	SS	On slider, 70 nm	1	No	No	0.50

(a) Stainless steel type 316

(b) Based on the diameter of the pin

(c) Over the duration of a 30-cycle test

PAH-PAA PEMs are being investigated for wear reduction in orthopedic implants; wear debris induces bone resorption in a normal implant leading to its loosening [28]. Surface modification of the commonly used metal-on-plastic or metal-on-metal configurations to reduce the wear rates, without compromising the bulk mechanical properties, offers a potential solution to this problem; this route has already attracted some interest in the literature [29]. Bovine calf serum is routinely used as the lubricant to simulate the presence of joint synovial fluid. The lubricant solution normally contains EDTA as an antichelating agent [30]; sodium azide serves as an antibacterial agent. The pH of this solution is at physiological levels, around 7. In addition to inorganic salts, calf serum primarily contains two proteins: albumin and γ-globulin. It is known that the PEM structure is responsive to the ionic strength and pH of the surrounding medium [13]. Hence careful consideration needs to be given to the choice of polyelectrolyte assembly pH when calf serum is used as a lubricant. We have found that (PAH 7.5/PAA 3.5) PEMs exhibit very little structural rearrangement at physiological pH conditions; the uniformity and thickness of these films remains essentially unaltered (see Chapter 3 for details). Thermally-induced chemical crosslinking at 130 °C for 3 hours [31] further stabilizes these films.

Tribological tests on the crosslinked films in bovine calf serum were conducted using the biaxial apparatus; a tool steel pin was made to articulate against a PEM-coated stainless steel slide at a normal stress of 2 MPa. Physiological stress levels in the human hip joint are in the 3-6 MPa range [19]. Figure 2-12 depicts wear track analysis for the PEM-coated and uncoated steel slides, submerged in the calf serum-containing lubricant, after 30 cycles of reciprocating motion; both substrates were immersed in the lubricant

for 24 hours prior to testing. The serum served as a lubricant for the uncoated steel slide by reducing the wear track depth to approximately 0.3 μm at a normal stress of 2 MPa, compared to 1.5 μm at 1 MPa stress when water was used as the surrounding medium. The friction profile exhibited minimal evolution with an average friction coefficient of about 0.3. When the steel slide was coated with a 100 nm PEM, no wear of the substrate was observed. Surface profiles (Figure 2-12) pointed to the role of PEM fragments in wear reduction. The friction coefficient remained at 0.3, close to that of the uncoated substrate. These tests suggest the potential merit of PEM-induced surface modification for metallic substrates when bovine calf serum is used as the lubricant.

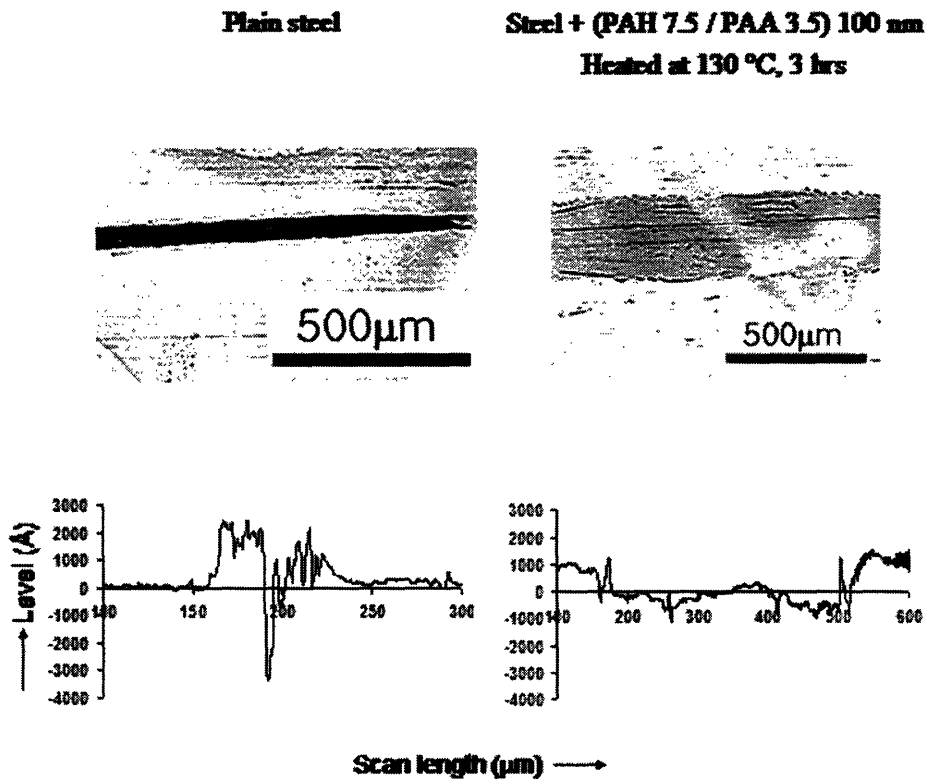

Figure 2-12 Optical micrographs and surface profiles of wear tracks on a plain stainless steel slide, and steel coated with 100 nm PEM. Tests conducted in calf serum lubricant at a normal stress of 2 MPa. Original metal surface is at level zero.

It must be noted, however, that the tests on the biaxial apparatus were conducted over only 30 cycles, using reciprocating motion. Multidirectional wear tests over millions of cycles to simulate motion in a human hip joint, using substrates with clinically relevant surface roughness values, are discussed in Chapter 3 in the effort to investigate the efficacy of these films for wear reduction in total joint replacements.

2.4 Conclusions

PEMs provide conformal nanocoatings for a variety of substrates with little or no pretreatment. The tribological properties of PAH-PAA PEMs were investigated using a meso/micro-scale biaxial apparatus and a pin-on-disk tester. The "true" values of friction coefficient for PEM constructs (on steel) against glass, in the absence of substrate wear, were higher than those exhibited by the bare substrates; an entangled structure, adhesion, slight asperity penetration, and deformation of the films were the principal causes. The coefficient of friction decreased with increasing normal stress, as expected for polymeric materials.

PEM constructs demonstrated a significant capacity for substrate wear prevention. A certain minimum thickness of the film, depending on the substrate roughness, is required on the slider for consistent wear prevention without a significant increase in friction force. Tests on a macroscale revealed that wear of glass substrates was prevented even after 2000 cycles. We have proposed that the film fragments absorb the stresses at the interface, preventing contact between and deformation of the mating surfaces, when PEMs are assembled on the larger surface. Deformation and dragging of these

fragments, in conjunction with adhesion to the contacting surfaces, are the principal causes of friction forces at these higher stresses. Evidence of the role of PEM fragments in wear reduction was gleaned when PEMs were built on both mating surfaces. In this case, the film fragments from the slider adhered to the film on the stationary pin leading to wear prevention when contact was re-established during a second run. This assembly is especially useful for intermittent contact type situations, where contact may not be re-established at the point of severance. When assembled only on the pin, these films prevented wear of the substrate; the friction coefficient also remained close to that of the bare substrate (prior to the onset of its wear).

Preliminary experiments using reciprocating motion revealed that the films served to prevent wear of steel substrates in the presence of water and bovine calf serum, used to simulate joint synovial fluid. The choice of assembly pH needs careful consideration when the lubricant is calf serum at physiological pH.

PEMs provide a facile means of surface modification for a variety of substrates. Their tribological behavior also shows promise for two diverse applications. Further work is needed before this new class of materials can be exploited with success for their friction and wear behavior in areas with tribological concerns.

2.5 References

(1) Decher, G. *Science* **1997**, *277*, 1232-1237.

(2) Yoo, D.; Shiratori, S. S.; Rubner, M. F. *Macromolecules* **1998**, *31*, 4309-4318.

(3) Shiratori, S. S.; Rubner, M. F. *Macromolecules* **2000**, *33*, 4213-4219.

(4) Joly, S.; Kane, R.; Radzilowski, L.; Wang, T.; Wu, A.; Cohen, R. E.; Thomas, E. L.; Rubner, M. F. *Langmuir* **2000**, *16*, 1354-1359.

(5) Maboudian, R.; Ashurst, W. R.; Carraro, C. *Tribology Letters* **2002**, *12*, 95-100.

(6) Hidber, P. C.; Helbig, W.; Kim, E.; Whitesides, G. M. *Langmuir* **1996**, *12*, 1375-1380.

(7) Hiller, J. A.; Mendelsohn, J. D.; Rubner, M. F. *Nature Materials* **2002**, *1*, 59-63.

(8) Decher, G.; Schlenoff, J.B., Eds. *Multilayer thin films: Sequential assembly of nanocomposite materials*; Wiley-VCH Verlag GmbH & Co. KGaA: Weinheim, 2003.

(9) Hammond, P. T. *Current Opinion in Colloid and Interface Science* **2000**, *4*, 430-442.

(10) Bertrand, P.; Jonas A.; Laschewsky, A.; Legras, R. *Macromol. Rapid Commun.* **2000**, *21*, 319-348.

(11) Wang, T. C.; Cohen, R. E.; Rubner, M. F. *Abstr. Pap. Am. Chem. Soc.* **2002**, *223: 275-POLY.*

(12) Wang, T. C.; Rubner, M. F.; Cohen, R. E. *Langmuir* **2002**, *18*, 3370-3375.

(13) Wang, T. C.; Cohen, R. E.; Rubner, M. F. *Adv. Mater.* **2002**, *14*, 1534-1537.

(14) Hiller, J. A.; Mendelsohn, J. D.; Rubner, M. F. *Abstr. Pap. Am. Chem. Soc.* **2002**, *223:157-COLL.*

(15) Graul, T.; Schlenoff, J. B. *Anal. Chem.* **1999**, *71*, 4007-4013.

(16) Tryoen-Toth, P.; Vautier, D.; Haikel, Y.; Voegel, J.; Schaaf, P.; Chluba, J.; Ogier, J. *J. Biomed. Mater. Res.* **2002**, *60*, 657-667.

(17) Mendelsohn, J. D.; Yang, S. Y.; Hochbaum, A. I.; Colson, C. D.; Rubner, M. F. *Abstr. Pap. Am. Chem. Soc.* **2002**, *223: 397-COLL.*

(18) Shuiying, G.; Laigui, Y. *Chinese Journal of Chemical Physics* **2002**, *15*, 132-136.

(19) Wang, A.; Essner, A.; Polineni, V. K.; Sun, D. C.; Stark, C.; Dumbleton, J. H. In *New Directions in Tribology*; Hutchings, I. M., Ed.; Mechanical Engineering Publications Limited: Bury St Edmunds, UK, 1997; pp 443-458.

(20) Gearing, B. P.; Anand, L. In *2001 ASME International Mechanical Engineering Congress and Exposition*: New York, New York, USA, 2001.

(21) Suh, N. P. *Tribophysics*; Prentice-Hall, Inc.: Englewood Cliffs, New Jersey, 1986.

(22) Sundararajan, S.; Bhushan, B. In *NATO advances study institute on fundamentals of tribology and bridging the gap between the macro- and micro/nano scales*;

Bhushan, B., Ed.; Kluwer Academic Publishers: Keszthely, Hungary, 2000; Vol. 10, pp 821-850.

(23) Komvopoulos, K. *Wear* **1996**, *200*, 305-327.

(24) Tsukruk, V. V.; Bliznyuk, V. N.; Hazel, J.; Visser, D.; Everson, M. P. *Langmuir* **1996**, *12*, 4840-4849.

(25) DePalma, V.; Tillman, N. *Langmuir* **1989**, *5*, 868-872.

(26) Julthingpiput, D.; Ahn, H.; Kim, D.; Tsukruk, V. V. *Tribology Letters* **2002**, *13*, 35-40.

(27) Sidorenko, A.; Ahn, H.; Kim, D.; Yang, H.; Tsukruk, V. V. *Wear* **2002**, *252*, 946-955.

(28) Ingham, E.; Fisher, J. *Proc. Instn. Mech. Engrs. Part H-Journal of Engineering in Medicine* **2000**, *214 (H1)*, 21-37.

(29) Widmer, M. R.; Heuberger, M.; Voros, J.; Spencer, N. D. *Tribology Letters* **2001**, *10*, 111-116.

(30) Liao, Y.; Benya, P. D.; McKellop, H. A. *J. Biomed. Mater. Res. (Appl. Biomater.)* **1999**, *48*, 465-473.

(31) Harris, J. J.; DeRose, P. M.; Bruening, M. L. *J. Am. Chem. Soc.* **1999**, *121*, 1978-1979.

Chapter 3 Polyelectrolyte Multilayers for Wear Reduction in Orthopedic Implants

3.1 Introduction

Wear particle-induced aseptic loosening of hip replacement prostheses remains a major cause of revision surgeries for the commonly used metal/ultra-high molecular weight polyethylene (UHMWPE) [1] and metal/metal[2] articulating pair configurations. In addition to osteolytic loosening, metal/metal articulations are plagued by concerns of electrochemical corrosion [2], and carcinogenesis, owing to the dissemination of wear particles to other parts of the body [2,3]. Surface modification, through the application of coating materials, offers the potential to reduce the wear rates without compromising the bulk mechanical behavior of the implant material. A variety of hard coatings have been investigated for metallic bearing surfaces (for a review, see reference 4); examples include diamond-like carbon [5-9], amorphous diamond [10], and titanium nitride [9]. By comparison, there is a distinct lack of literature on materials for coating UHMWPE for the purpose of wear reduction. In one reported study [11], the surface hydrophilicity of UHMWPE was increased using oxygen-plasma treatment. Improved boundary lubrication, through protein adsorption from serum, was attributed to the observed decrease in dynamic friction. The effect of the plasma treatment, however, was short-lived. In addition, no experiments were carried out to establish the effect of change in surface properties on wear of UHMWPE.

The recent introduction of polyelectrolyte multilayers (PEMs) [12] offers a facile means of modifying the surfaces of various metallic, ceramic, plastic, and glass substrates. PEMs are assembled by the layer-by-layer adsorption of oppositely charged polyelectrolytes, leading to film architectures that are tuned as a function of the processing conditions and the choice of polyelectrolyte pair. The utility of these films is enhanced by their ease-of-fabrication (aqueous-based automated assembly proceeds at ambient conditions), in addition to large-scale conformity and uniformity of coverage. Unlike most coating materials, strongly adherent PEM films can be constructed on a wide variety of substrates with little or no pretreatment; films are generally resistant to scotch-tape peel tests [13]. Current research (see reference 14 for a comprehensive review) has focussed on PEM application in the areas of biomaterials [15-18], photonic structures [19,20], separation membranes [21], and electrochemical devices [22-24].

In Chapter 2, the friction-and-wear behavior of PEM-coated substrates was studied, both at ambient conditions and in the presence of a liquid medium. Poly(acrylic acid) (PAA) and poly(allylamine hydrochloride) (PAH) were used to assemble the PEMs. Significant wear prevention of steel, glass, and silicon substrates was observed, when coated with PEMs, during tests up to 2000 cycles of reciprocating motion in the dry state; applied normal stresses up to 450 MPa were employed. The delaminated film fragments prevented contact between the mating surfaces, avoiding substrate wear. The friction forces for the PEM-coated substrates, however, were marginally higher than the bare substrates in the absence of wear due to deformation and dragging of the film fragments at the interface. PEMs assembled on both mating surfaces were shown to be suitable for intermittent contact situations. Preliminary experiments conducted using a

meso/microscale-testing device, in the presence of bovine calf serum and at physiological levels of normal load, revealed that wear of underlying steel substrates was avoided over 30 cycles of reciprocating motion when coated with a 100 nm-thick film.

This chapter evaluates, in detail, the friction-and-wear behavior of PEM-coated metal/metal and metal/UHMWPE systems at two scales of testing, and under physiological conditions of loading, motion, number of cycles, and surrounding medium. PAA and PAH were used to assemble the films. This is the first study devoted to the wear behavior of electrostatic layer-by-layer films in prosthetic systems. Further optimization will be needed before the orthopedic community can capitalize on this new class of materials.

3.2 Experimental Details

PAH (M_W = 70000) was purchased from Sigma-Aldrich (Milwaukee, WI). PAA (M_W = 90000) was obtained from Polysciences (Warrington, PA). Both the polymers were used without further purification. Deionized water (>18 MΩ cm, Millipore Milli-Q) was used for preparation of all aqueous solutions, and during rinsing procedures. Stainless steel sheets (type 316, #8 mirror finish), with an average roughness of approximately 0.006 μm measured using a Tencor P-10 surface profiler, were purchased from McMaster-Carr (Dayton, NJ). UHMWPE GUR 1050 rod stock was purchased from Poly Hi Solidur Inc. (Fort Wayne, IN). Bars were machined out of the rod stock, and heated to 150 °C in a hydraulic press (Carver, Inc.). They were pressed between two mirror-finish steel plates to obtain sheets of 1 mm thickness; the associated average roughness was in the 0.15 μm range. Glass microscope slides from VWR Scientific Inc.

(West Chester, PA) were used. Stainless steel, UHMWPE, and glass were some of the substrates used for PEM assembly.

PAH/PAA PEMs were assembled on these substrates as previously described [25,26]. Materials were degreased in a detergent solution, via ultrasonication, for 15 minutes, followed by ultrasonication in water for 10 minutes. After further rinsing in water, and drying by flushing with air, the substrates were subject to air-plasma treatment (5 minutes at 100 W-Harrick Scientific PDC-32G plasma cleaner/sterilizer). PAH and PAA aqueous solutions (0.01 M based on molecular weights of the repeat unit) were adjusted to the desired pH using 1 M sodium hydroxide or 1 M hydrochloric acid. Films were assembled by immersing the plasma-treated materials into the PAH solution for 15 minutes, followed by three rinsing steps in water for 2,1, and 1 minute respectively. They were then immersed in the PAA solution, followed by identical rinsing steps. The cycle was repeated to build PEMs of the desired thickness. The immersion and rinsing steps were automated using a Zeiss HMS programmable slide stainer [25]. Finally, the film-coated substrates were dried in a stream of air, and stored at ambient conditions for several hours before testing. The films were assembled at a pH of 7.5 or 3.5 for the PAH solution, and a pH of 3.5 for PAA, referred to as (PAH 7.5/PAA 3.5) or (PAH 3.5/PAA 3.5). A profilometer was used to measure thicknesses of PEM films on glass substrates.

Bovine calf serum (77-79 g/l total protein, JRH Biosciences, Lenexa, KS) was used to simulate joint synovial fluid. The stability of PEMs in bovine calf serum was studied by immersing films, on glass substrates, in the lubricant solution for varying lengths of time. The lubricant solution was prepared by diluting the bovine calf serum to a protein concentration of 23 g/l, following literature recommendations [27]. The solution

also contained 20 mM of the sodium salt of ethylenediaminetetraacetic acid (EDTA) and 0.2 % sodium azide (by weight). Both these chemicals were obtained from Sigma-Aldrich (Milwaukee, WI). EDTA is normally used as an antichelating agent during tribological testing, while sodium azide serves as an antibacterial agent [28]. Physiological conditions were maintained-pH approximately 7 and a temperature of approximately 37 °C. After immersion, the slides were subject to two 1-minute rinsing steps in water before drying thoroughly. The average thickness and roughness values were calculated after measurements at several locations across the substrate using a profilometer.

Friction-and-wear behavior, on steel and UHMWPE slides, was studied on a meso/micro-scale using a flexure-based biaxial apparatus as described in reference 29. Bovine calf serum lubricant solution, described above, was used as the surrounding medium. A flat/flat configuration was used for all tests. The upper cylindrical pin with a flat surface, 1 mm in diameter, was made of D2 hardened tool steel. It is held stationary in the apparatus, while the lower, larger surface is subject to reciprocating motion. A schematic of the mating surfaces has been already depicted in Figure 2-3. In all experiments, uncoated and film-coated steel and UHMWPE substrates were mounted on the lower slider using double-coated paper scotch tape. The interface region was immersed in the lubricant solution. Between tests, the pin was polished using 1 μm-aluminum oxide film-coated disks; a specially designed holder ensured a flat surface during polishing. The pin was subsequently cleaned with acetone, and dried in a blast of air. A sliding speed of 200 μm/s and a path length of 3 mm were used in all tests. The test was confined to 30 cycles, corresponding to an accumulated sliding distance of 180 mm. Wear tracks were examined using an optical microscope and a profilometer; in all

cases, surface profiles, examined at three points along the track, closely resembled each other.

Macroscale wear tests were carried out on a custom-made pin-on-disk wear testing machine. The six-station machine, capable of bi-directional motion, is described in detail in reference 30. UHMWPE pins, 9 mm in diameter, and 15 mm long, were machined from the rod stock. They were made to articulate against 33 mm diameter cobalt-chrome disks, polished to implant grade (average roughness 0.05 μm). The pins and disks were either uncoated, or both coated with PEMs using the procedure described earlier. 100 % bovine calf serum, with EDTA and sodium azide additives, was used as the surrounding medium. A double peak, Paul type loading curve with a peak load of 1865 N, and a preload of 265 N, was employed. Each pin experiences a peak contact stress of 4.8 MPa [30] when the load curve is applied evenly across the 6 stations. Motion of the disks was designed to have the pins trace a rectangular articulation path 0.5 cm x 1 cm. The tests were run for 500, 000 cycles at a frequency of 2 Hz. Figure 3-1 is a pictorial representation of the articulating combination. Prior to testing, the pins were weighed and then immersed in calf serum for 24 hours. Subsequently, they were rinsed with water and briefly dried before being weighed again. At the end of the test, the pins were vigorously rinsed with water, and dried by flushing with air. Finally, they were weighed to determine the weight loss due to wear.

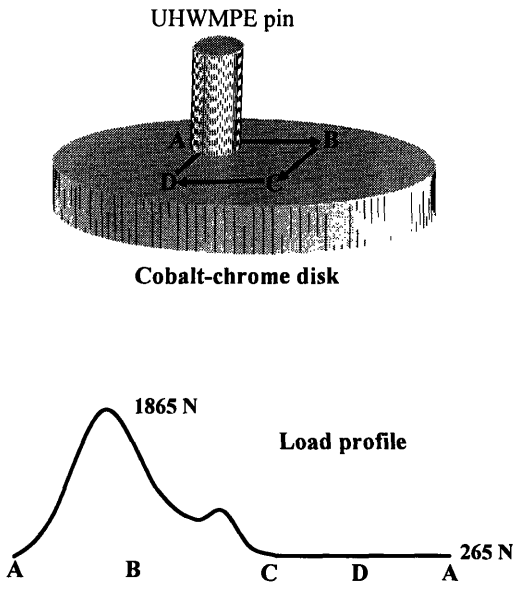

Figure 3-1 Pictorial representation of articulating surfaces and loading cycle in bi-directional pin-on-disk wear tester.

3.3 Results

For weak polyelectrolytes like PAH and PAA, the degree of ionization is a function of the pH, relative to the pKa values. Manipulation of the pH of the assembly solutions offers precise control over the physico-chemical architectures of the resulting PEM films [25,26]; spatial control over parameters like film thickness and organization, and nature of functional groups at the film surface can be achieved. At ambient conditions, it was observed that the assembly pH combination did not influence wear behavior of PEM-coated substrates above a certain critical film thickness (see Chapter 2). This critical value of thickness, required to allow for enough film material at the interface to

prevent contact between the mating surfaces, was a function of substrate roughness. When immersed in a liquid, however, PAH/PAA PEMs behave like hydrogels [20]; the films are responsive to the pH and ionic strength of the surrounding medium. The bovine calf serum lubricant solution is associated with a pH around 7, primarily two proteins, and inorganic salts [31]. Hence the PEM assembly pH needs careful consideration in the presence of the lubricant.

(PAH 3.5/PAA 3.5) and (PAH 7.5/PAA 3.5) architectures, with PAA as the last adsorbed polyelectrolyte, were chosen for the study. For the latter structure, a film with PAH as the last adsorbed layer was also investigated. These films were immersed in the lubricant solution for different periods of time as explained in Section 3.2. The average thickness-immersion time profile is depicted in Figure 3-2. (PAH 3.5/PAA 3.5) PEMs constitute an interpenetrated structure with a certain degree of unionized carboxylic acid groups i.e., not all the –COOH groups of PAA are electrostatically linked with PAH. The surface of the film exhibits a proportion of these –COOH groups irrespective of the last adsorbed layer [26]. On the other hand, (PAH 7.5/PAA 3.5) combinations result in thick, loopy structures with a high degree of ion-pairing between PAH and PAA (and almost no free –COOH groups) in the bulk of the film. While the bulk structure of these films, like other PEM constructs, consists of an interpenetrated network, the surface is dominated by functional groups from the last adsorbed polyelectrolyte [26]; hence both PAH and PAA-topped films were investigated. A 20-25 nm decrease in thickness was observed for the (PAH 3.5/PAA 3.5) PEMs within 15 minutes of immersion in the calf serum lubricant. This was accompanied by a loss of structural integrity and uniformity of coverage. The remnant film-covered regions exhibited some subsequent rise in thickness and roughness.

The average roughness was 25 nm after 6 hours (600 min) of immersion compared with an initial value of approximately 1.5 nm. Film coverage was not recovered after 24 hours. Conversely, the (PAH 7.5/PAA 3.5) architectures demonstrated a high degree of bulk structural robustness even after 24 hours (1440 min) of immersion. For the PAA-topped film, a slight decrease in thickness was observed initially, but without any adverse effect on the uniformity or interfacial roughness. The thickness of the same PEM architecture, but with PAH adsorbed last, remained almost constant over the test periods.

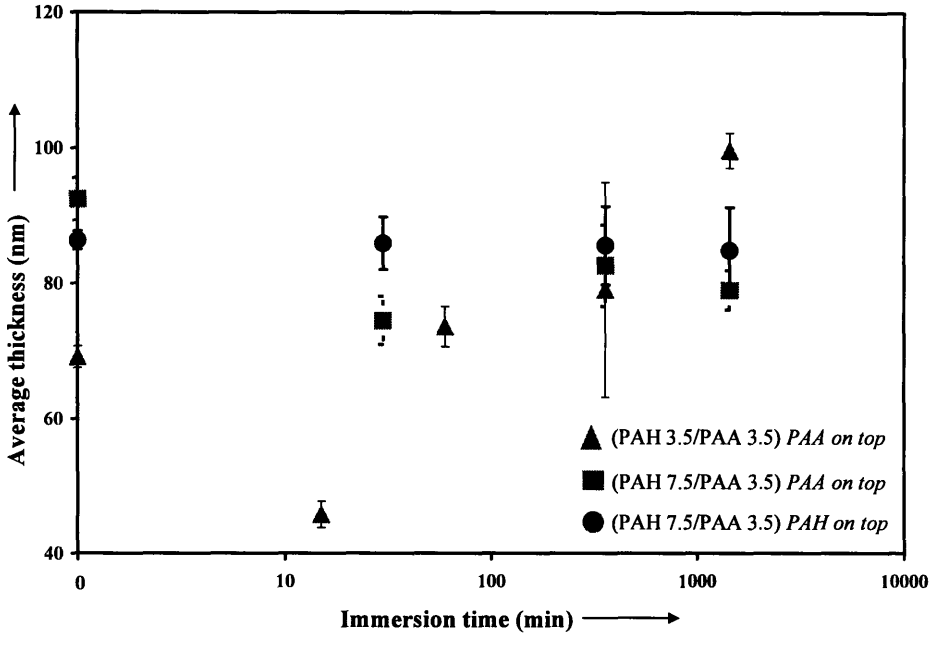

Figure 3-2 Average PEM thickness after immersion in bovine calf serum lubricant; films were rinsed in water and dried thoroughly before thickness measurements

Corresponding friction coefficients for the above studied PEM architectures, on UHMWPE substrates, were evaluated using the biaxial apparatus. All films were soaked in the serum solution for 24 hours prior to testing. The applied stress was 4 MPa based on the diameter of the pin. The steady state friction coefficients are reported in Table 3-1. The value of normal stress was chosen to mimic physiological stress levels in the hip joint, which are reported to be between 3 and 6 MPa [27]. The film-coated substrates exhibited higher friction forces than bare UHMWPE. The (PAH 7.5/PAA 3.5) architectures were associated with the lowest friction forces among the film-coated substrates, with no discernable dependence of the coefficient of friction on the last adsorbed polyelectrolyte.

Table 3-1 Steady state friction coefficients for uncoated and PEM-coated UHMWPE in the presence of bovine calf serum-containing lubricant solution. Normal stress: 4 MPa.

Substrate	Film thickness (nm)*	Friction Coefficient
UHMWPE	-	0.08
UHMWPE + (PAH 3.5/PAA 3.5)	62	0.20
UHMWPE + (PAH 7.5/PAA 3.5) *PAH on top*	82	0.10
UHMWPE + (PAH 7.5/PAA 3.5) *PAA on top*	102	0.10

*Prior to 24-hour soak in bovine calf serum-containing lubricant solution; films assembled on glass substrates were used for thickness measurements.

The (PAH 7.5/PAA 3.5) assembly combination, with PAH adsorbed last, was chosen for subsequent wear studies owing to its structural robustness in bovine calf serum (see Figure 3-2 and Table 3-1). A conservative film thickness value of 500 nm (~ 45 bilayers) was employed following promising results in the dry state (Chapter 2). Uncoated and coated stainless steel slides were used as substrates in the meso/micro-scale biaxial apparatus at a normal stress of 2 MPa. To preclude interaction with calf serum, a fraction of the ionic linkages between PAH and PAA were converted to covalent amide bonds through thermal treatment [32]; the film was heated at 130 °C for 3-5 hours in vacuum. Nanoindentation studies in water (pH adjusted to 7), reported in Chapter 5, revealed that the chemically crosslinked films, obtained after thermal treatment, were also associated with a hardness value 8 times as high as their electrostatically crosslinked counterparts; a higher hardness value reflects a higher load-bearing capacity for the thermally treated films. Figure 3-3 depicts optical micrographs and cross-sectional surface profiles of the wear tracks on bare and PEM-coated steel after the test. For the

latter case, an optical micrograph of the 1 mm-diameter pin surface at the end of the test is depicted in Figure 3-4.

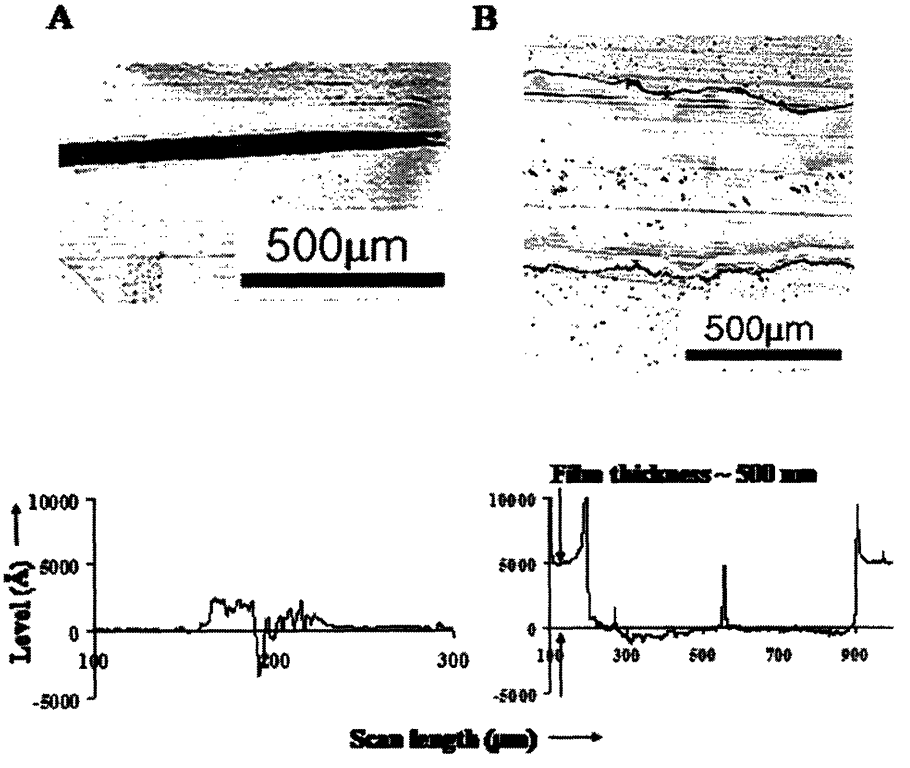

Figure 3-3 Optical micrographs and cross-sectional surface profiles of wear tracks on A. plain stainless steel slide, and B. steel coated with 500 nm PEM. It is evident that PEMs prevented wear of the steel surface. Remnant film fragments contribute to spike at the center of the surface profile. Original metal surface is at level zero in both cases. Tests conducted in calf serum lubricant at a normal stress of 2 MPa. Film was assembled at the (PAH 7.5/PAA 3.5) combination, with PAH adsorbed last.

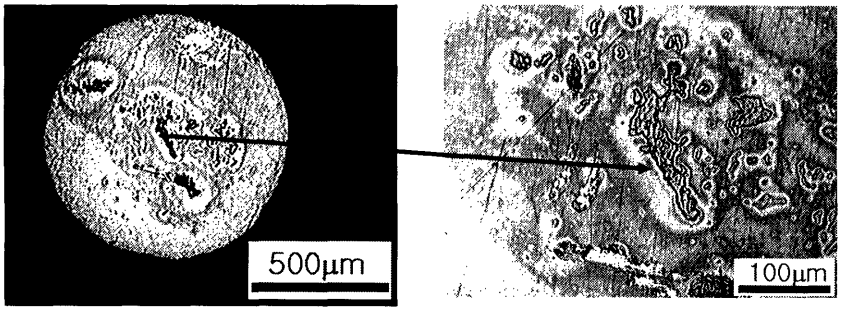

Figure 3-4 Optical micrograph of pin counterface after the test from Figure 3-3 (B); PEM fragments transferred from the slider can be seen adhered to the pin surface. Test was conducted in calf serum lubricant at a normal stress of 2 MPa.

It is obvious from Figure 3-3 that the PEMs prevented wear of the steel surface. The friction coefficients for the uncoated and coated systems were comparable, around 0.3. The delaminated PEM-fragments were responsible for absorbing the interfacial stresses and preventing contact between the pin and the slider, thus avoiding substrate wear. This is verified by examination of the cross-sectional surface profile of the wear track (Figure 3-3), where the 500 nm film is removed across the width of the track, but the steel surface is untouched. The protective fragments aggregated at the ends of the wear track or occasionally on the pin as seen in Figure 3-4. Previous work, in Chapter 2, has demonstrated wear prevention of steel substrates in calf serum with films as thin as 100 nm.

Results from tests on the macroscale pin-on-disk tester are presented in Figure 3-5. These tests, in calf serum lubricant, were conducted using clinically relevant bearing surface materials and number of cycles (500,000), in addition to using bi-directional motion to simulate motion of the hip joint [30]. Both the cobalt-chrome disks and the UHMWPE pins were coated with (PAH 7.5/PAA 3.5) 500 nm-thick PEMs (PAH on top). The weight loss due to wear was consistently lower for the film-coated systems; two

separate runs, each over three stations, were carried out to establish reproducibility of wear reduction. The calculated weight of the film was negligible compared with the measured loss in weight; wear of UHMWPE contributed solely to the weight loss. In the best case, the weight loss due to wear was reduced by 45 % when the films were thermally treated after assembly. Surface profiles confirmed that the films had delaminated over the area of contact. These delaminated PEM fragments, loosely adhered to the pin surface, were subsequently detached when the pins were rinsed with water after the test, and before weighing.

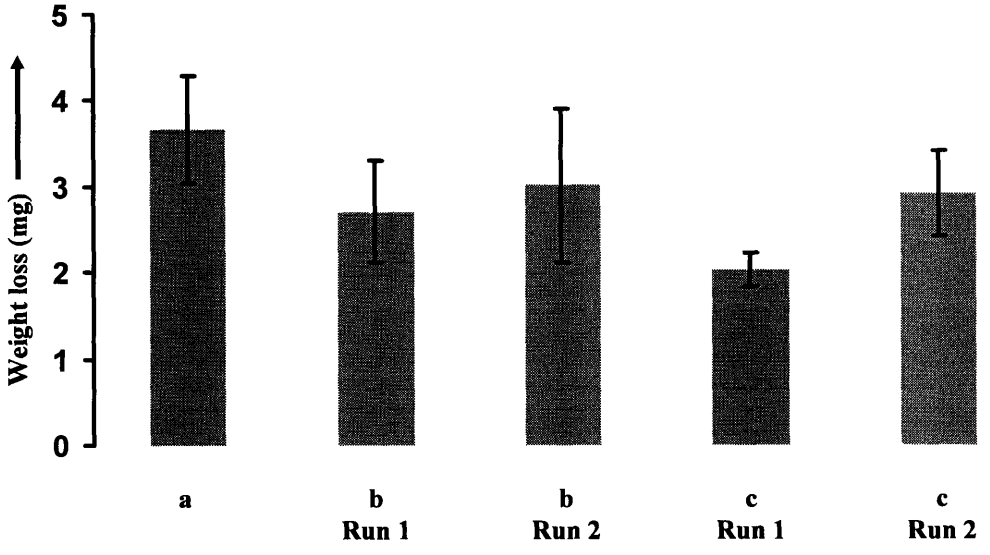

Figure 3-5 Weight loss due to wear after 500,000 cycles of bi-directional motion in a macroscale pin-on-disk wear tester. Average weight losses are depicted for (a) uncoated UHMWPE (average of 10 results), (b) 500-600 nm-thick PEM-coated UHMWPE, and (c) 500-600 nm-thick, and thermally treated PEM-coated UHMWPE. For film coated systems (b and c), both the pins and disks were coated with (PAH 7.5/PAA 3.5) PEMs; each bar represents average weight loss exhibited by a 3-station test.

3.4 Discussion

PEM structures with free carboxylic acid groups interact unfavorably with bovine calf serum lubricant. Exposure to pH values above the pKa of PAA (approximately 5) causes ionization of, and repulsion between the unionized -COOH groups leading to straightening out of the chains. If, in addition, the polymer-polymer linkages are substituted by polymer-inorganic ion interactions, film disintegration could occur in extreme cases [33]. This might explain the behavior of the (PAH 3.5/PAA 3.5) combination in calf serum (see Figure 3-2). For the (PAH 7.5/PAA 3.5) structures, almost all the acid groups are ion-paired with PAH. This reduces the degree of interaction with the surrounding serum. The decrease in thickness for the (PAH 7.5/PAA 3.5) films (Figure 3-2), with PAA as the last adsorbed layer, might be attributed to reorganization of the surface layer (containing free –COOH groups). The integrity of the bulk structure, with a high degree of ionization of PAA, is retained. Change in film structure can be precluded by thermally-induced chemical crosslinking. The resulting covalent bonds are not susceptible to changes in ambient pH or ionic strength.

Spotty coverage by rough PEM fragments manifests as high friction coefficients for the (PAH 3.5/PAA 3.5) film (Table 3-1, line 2). Conversely, retention of structural uniformity results in lower forces for the (PAH 7.5/PAA 3.5) architectures (lines 3 and 4). In all cases, the friction forces for coated UHMWPE are at least marginally higher (1.25-2.5 times) than the bare substrate. Adhesion to the pin counterface, deformation, and dragging of the delaminated film fragments contribute to the higher coefficient values. The delaminated PEM fragments, however, serve to prevent contact between the

mating surfaces, leading to wear reduction at both scales of testing, and for metal/metal and metal/UHMWPE systems (see Figures 3-3 and 3-5).

Radiation-induced crosslinking is the currently accepted method for reducing the wear of UHMWPE bearing surfaces in the hip joint [1,34,35]. The treatment has been found, however, to adversely affect the mechanical properties of the polymer [36]; these properties might be important for the overall mechanical stability of the hip implant, but are especially crucial in the knee joint where the contact stresses are much higher. Surface modification through PEMs offers the potential for wear reduction without compromising the bulk properties of UHMWPE.

There is promising preliminary evidence of the biocompatibilty of PEMs. PAH/PAA films have been used for tailoring cell-surface interactions [15,18]. In addition, Ogier and co-workers [37] have successfully investigated various PEM combinations in the effort to improve integration efficiencies of implants with the surrounding tissue. That work, in combination with ours, could potentially pave the way for PEM-coatings on the entire prosthesis, serving the dual purposes of wear prevention and bone integration. The problems of electrochemical corrosion associated with metal/metal implants might also be circumvented through the use of PEMs; references 38 and 39 relate to rendering metallic surfaces corrosion resistant by coating with PEMs. Finally, we have used only two assembly pH combinations in this study. By tuning the pH of the polyelectrolyte solutions, or even the choice of polyelectrolyte pair, it might be possible to construct films that demonstrate some degree of protein (polyelectrolyte) uptake from joint fluid. A design of this nature could manifest as a film with material renewal characteristics if film coverage is periodically diminished at certain locations.

3.5 Conclusions

Surface modification through polyelectrolyte multilayer films offers a facile means of wear reduction in metal/UHMWPE and metal/metal joint replacement prostheses. The wear-reducing efficacy of these films, composed of weak polyelectrolytes PAH and PAA, was demonstrated on a meso/microscale testing device over 30 cycles, and corroborated over 500,000 cycles of bi-directional motion on a macroscale pin-on-disk wear tester. The assembly pH of these films must be carefully chosen to preclude any adverse effects on film structure at physiological conditions of pH and ionic strength.

We believe that this is the first clinically relevant demonstration of the tribological potential of PEMs for orthopedic applications. Further work, including investigating the biological response to PEM fragments that might leave the interface, is needed. It is likely that the wear-preventing properties of the PAH/PAA combination will also extend to other PEM combinations, though experimental verification will be required. In addition to the choice of polyelectrolyte pair satisfying the constraints of structural stability in joint fluid, biocompatibility, corrosion resistance, and wear prevention, other parameters that can be the subject of optimization studies include adhesion of the PEMs to the surface and degree of conversion of ionic attachments to covalent bonds.

3.6 References

(1) Kurtz, S. M.; Muratoglu, O. K.; Evans, M.; Edidin, A. A. *Biomaterials* **1999**, *20*, 1659-1688.

(2) Savarino, L.; Granchi, D.; Ciapetti, G.; Cenni, E.; Pantoli, A. N.; Rotini, R.; Veronesi, C. A.; Baldini, N.; Giunti, A. *J. Biomed. Mater. Res. (Appl. Biomater.)* **2002**, *63*, 467-474.

(3) Ingham, E.; Fisher, J. *Proc. Instn. Mech. Engrs. Part H-Journal of Engineering in Medicine* **2000**, *214 (H1)*, 21-37.

(4) Dearnley, P. A. *Proc. Instn. Mech. Engrs. Part H-Journal of Engineering in Medicine* **1999**, *213 (H)*, 107-135.

(5) Hauert, R. *Diamond and Related Materials* **2003**, *12*, 583-589.

(6) Platon, F.; Fournier, P.; Rouxel, S. *Wear* **2001**, *250*, 227-236.

(7) Saikko, V.; Ahlroos, T.; Calonius, O.; Keranen, J. *Biomaterials* **2001**, *22*, 1507-1514.

(8) Kiuru, M.; Alakoski, E.; Tiainen, V.; Lappalainen, R.; Anttila, A. *J. Biomed. Mater. Res. Part B: Appl. Biomater.* **2003**, *66B*, 425-428.

(9) Onate, J. I.; Comin, M.; Braceras, I.; Garcia, A.; Viviente, J. L.; Brizuela, M.; Garagorri, N.; Peris, J. L.; Alava, J. I. *Surface and Coatings Technology* **2001**, *142-144*, 1056-1062.

(10) Lappalainen, R.; Selenius, M.; Anttila, A.; Konttinen, Y. T.; Santavirta, S. S. *J. Biomed. Mater. Res. Part B: Appl. Biomater.* **2003**, *66B*, 410-413.

(11) Widmer, M. R.; Heuberger, M.; Voros, J.; Spencer, N. D. *Tribology Letters* **2001**, *10*, 111-116.

(12) Decher, G.; Hong, J. D.; Schmitt, J. *Thin Solid Films* **1992**, *210*, 831-835.

(13) Hidber, P. C.; Helbig, W.; Kim, E.; Whitesides, G. M. *Langmuir* **1996**, *12*, 1375-1380.

(14) Decher, G.; Schlenoff, J. B., Eds. *Multilayer thin films: Sequential assembly of nanocomposite materials*; Wiley-VCH Verlag GmbH & Co. KGaA: Weinheim, 2003.

(15) Mendelsohn, J. D.; Yang, S. Y.; Hiller, J.; Hochbaum, A. I.; Rubner, M. F. *Biomacromolecules* **2003**, *4*, 96-106.

(16) Mendelsohn, J. D.; Yang, S. Y.; Hochbaum, A. I.; Colson, C. D.; Rubner, M. F. *Abstr. Pap. Am. Chem. Soc.* **2002**, *223: 397-COLL.*

(17) Hochbaum, A.; Mendelsohn, J. D.; Rubner, M. F. *Abstr. Pap. Am. Chem. Soc.* **2002**, *223:184-COLL.*

(18) Berg, M. C.; Mendelsohn, J. D.; Yang, S. Y.; Hammond, P. T.; Rubner, M. F. *Abstr. Pap. Am. Chem. Soc.* **2002**, *223:158-COLL.*

(19) Wang, T. C.; Cohen, R. E.; Rubner, M. F. *Abstr. Pap. Am. Chem. Soc.* **2002**, *223: 275-POLY.*

(20) Wang, T. C.; Cohen, R. E.; Rubner, M. F. *Adv. Mater.* **2002**, *14*, 1534-1537.

(21) Graul, T.; Schlenoff, J. B. *Anal. Chem.* **1999**, *71*, 4007-4013.

(22) DeLongchamp, D. M.; Hammond, P. T. *Abstr. Pap. Am. Chem. Soc.* **2002**, *223:286-POLY.*

(23) DeLongchamp, D. M.; Hammond, P. T. *Abstr. Pap. Am. Chem. Soc.* **2002**, *223: 114-COLL.*

(24) DeLongchamp, D. M.; Kastantin, M.; Hammond, P. T. *Chem. Mater.* **2003**, *15*, 1575-1586.

(25) Yoo, D.; Shiratori, S. S.; Rubner, M. F. *Macromolecules* **1998**, *31*, 4309-4318.

(26) Shiratori, S. S.; Rubner, M. F. *Macromolecules* **2000**, *33*, 4213-4219.

(27) Wang, A.; Essner, A.; Polineni, V. K.; Sun, D. C.; Stark, C.; Dumbleton, J. H. In *New Directions in Tribology*; Hutchings, I. M., Ed.; Mechanical Engineering Publications Limited: Bury St Edmunds, UK, 1997; pp 443-458.

(28) Liao, Y.; Benya, P. D.; McKellop, H. A. *J. Biomed. Mater. Res. (Appl. Biomater.)* **1999**, *48*, 465-473.

(29) Gearing, B. P.; Anand, L. In *2001 ASME International Mechanical Engineering Congress and Exposition*: New York, New York, USA, 2001.

(30) Bragdon, C. R.; O'Connor, D. O.; Lowenstein, J. D.; Jasty, M.; Briggs, S. A.; Harris, W. H. *Journal of Arthroplasty* **2001**, *16*, 658-665.

(31) Kitano, T.; Ateshian, G. A.; Mow, V. C.; Kadoya, Y.; Yamano, Y. *Journal of Biomechanics* **2001**, *34*, 1031-1037.

(32) Harris, J. J.; DeRose, P. M.; Bruening, M. L. *J. Am. Chem. Soc.* **1999**, *121*, 1978-1979.

(33) Dubas, S. T.; Schlenoff, J. B. *Macromolecules* **2001**, *34*, 3736-3740.

(34) McKellop, H.; Shen, F.; Lu, B.; Campbell, P.; Salovey, R. *J. Orthop. Res* **1999**, *17*, 157-167.

(35) Lewis, G. *Biomaterials* **2001**, *22*, 371-401.

(36) Gomoll, A.; Bellare, A.; Wanich, T. In *Deformation, yield, and fracture of polymers: 11th International conference*, 2000; p 254.

(37) Tryoen-Toth, P.; Vautier, D.; Haikel, Y.; Voegel, J.; Schaaf, P.; Chluba, J.; Ogier, J. *J. Biomed. Mater. Res.* **2002**, *60*, 657-667.

(38) Farhat, T. R.; Schlenoff, J. B. *Electrochemical and Solid-State Letters* **2002**, *5*, B13-B15.

(39) Dai, J.; Sullivan, D. M.; Bruening, M. L. *Ind. Eng. Chem. Res.* **2000**, *39*, 3528-3535.

Chapter 4 Engineering the Friction-and-wear Behavior of Polyelectrolyte Multilayer Nanoassemblies through Block Copolymer Surface Capping, Metallic Nanoparticles and Multi-wall Carbon Nanotubes[2]

4.1 Introduction

Surface modification, via soft organic coatings, has been employed extensively in the effort to alleviate the tribological problems associated with micromechanical device operation. Stiction, high friction forces, and wear remain the dominant issues [1], particularly in those microelectromechanical systems (MEMS) with moving components subject to intermittent or continuous contact. Examples include motors, turbines, gear trains, actuators, valves, accelerometers, and display-device mirror assemblies [2]. Langmuir-Blodgett monolayers [3], self-assembled thiol-based [2], silane-based [4-6], and alkene-based [7] monolayer films, and polymer films with layered architectures [8-11] have been investigated in this regard. The coatings demonstrate low friction forces; only some provide wear reduction of underlying substrates at higher normal stresses [9-11].

These films require, however, either an intricate protocol for assembly [3], or a functionalized surface to which they can bind covalently [2,4-11]. The substrate, which in most cases is silicon, thus requires some level of pretreatment to present the desired functional groups. Generally, the pretreatment leads to the formation of a thin layer of oxide on the surface [5]; charge trapping by this insulating layer can potentially lead to device failure. Chlorosilane-based monolayers are also associated with release of corrosive by-products, and the precursor molecules have the potential for bulk

[2] Portions of this chapter appear in the Journal of Applied Polymer Science **2004**, *92*, 439-448

polymerization which leads to considerable particulate formation. Additionally, reproducibility and scale-up of the fabrication procedures for these surface modification techniques have proved challenging [5].

Chapter 2 studies the tribological properties of polyelectrolyte multilayers (PEMs), formed by the layer-by-layer adsorption of oppositely charged polyelectrolytes. Weak polyelectrolytes--poly(acrylic acid) (PAA) and poly (allylamine hydrochloride) (PAH), were used in the investigation. The structures of the repeat units of the polyelectrolytes are depicted in Figure 2-1. The PEM assembly provides films that are easy-to-fabricate; assembly is automated [12], and proceeds at ambient conditions from aqueous solutions. The process is not associated with release of by-products. Unlike other surface engineering techniques, PEMs can be assembled on a wide variety of substrates with little or no pretreatment. Strongly adhering PAH/PAA films, resistant to scotch-tape peel tests [13], have been formed on metallic, plastic, glass, and silicon-based materials. Devices with complex architectures can be coated uniformly over large areas. PEMs are thus ideally suited to combat the tribological challenges in MEMS operations.

At low normal stresses, friction coefficients of PAH/PAA PEM-coated surfaces were higher than those exhibited by their uncoated counterparts (see Chapter 2). These films, however, demonstrated a significant capacity for wear prevention of underlying stainless steel, glass, and silicon substrates at normal stresses up to 450 MPa and 2000 cycles of reciprocating motion. Delaminated film fragments prevented contact between the mating surfaces, avoiding wear. When assembled on the larger surface, a certain minimum film thickness (approximately 20-30 nm for silicon substrates), depending on the substrate roughness, was required for consistent wear reduction without a substantial

increase in the friction force. At higher thicknesses (above about 70 nm for silicon), PEMs provided reliable wear reduction; however, for the thicker films, adhesion to the counterface, deformation, and dragging of the fragments increased the friction forces over those observed for thinner films and the bare substrate (see Chapter 2).

The objective of this chapter is to discuss and evaluate strategies for engineering the PEM structure to reduce the friction coefficient (at lower normal stresses) without compromising its wear-preventing ability (at higher loads). The friction coefficient of the film (or its fragments) can be varied by altering its hardness, shear strength, or its adhesion to the counterface. In one strategy, we addressed these issues through surface capping of the PEM structure. Amphiphilic block copolymers were used to modify the surface properties of PEMs. By using one block to bind to the PEM surface, the other block can be chosen to decrease the adhesive component of friction of the PAH/PAA PEM surface, increase its hardness, or lower its resistance to orientation in the sliding direction. We selected polystyrene-block-poly(acrylic acid) (PS-PAA) to modify the surface of the PEM, noting that Choi and Rubner [14] successfully adsorbed PS-PAA onto PAH/PAA PEM surfaces. The PAA block was used for anchoring to the multilayer, thus exposing the PS block to the surface. Water contact angles as high as 85° after the treatment were reported [14] for films where the contact angle, prior to modification, was about 45 °.

For a second strategy, we note that polymer composites with nanometer-sized metallic and ceramic filler particles have been investigated for their tribological properties; for references see 15-19. The composites exhibit increased wear resistance compared with the unfilled polymer. Mixed results, however, have been reported about

the effects of nano-fillers on friction forces. PAH/PAA PEMs can serve as nanoreactors for the *in-situ* synthesis of metallic and semiconducting particles [20]. At certain assembly pH values, the unpaired (free) carboxylic acid functional groups in PAA can be utilized to bind various inorganic ions through an ion-exchange process; these ions are converted into nanoparticles by reduction or substitution chemistry. The process of incorporating nanoclusters in PAH/PAA PEMs can be repeated multiple times, systematically increasing both the mean particle size and volume fraction in the polymer matrix [21]. This technique offers a unique method of creating polymer nanocomposite coatings, with a variety of filler particles, that may demonstrate interesting friction and wear properties. We have chosen to study the effect of silver nanoclusters incorporated in PAH/PAA PEMs.

Finally, this chapter also discusses the friction-and-wear behavior of PEM structures that contain multi-wall carbon nanotubes (MWNTs). Cumings and Zettl [22] demonstrated the reversible extension of a MWNT and suggested that these novel materials might serve as low-friction nanoscale linear bearings. Kotov and co-workers [23] constructed multilayer assemblies of negatively charged single-wall nanotubes and a cationic polyelectrolyte; tensile tests revealed enhanced mechanical properties for these structures. There is no reported literature on the friction and wear behavior of PEMs containing MWNTs.

In addition to tribological characterization of the modified PEM structures, nanoindentation was employed to correlate the friction-and-wear behavior of the films with their mechanical properties.

4.2 Experimental Details

PAH (M_W = 70000), silver acetate, octadecyltrichlorosilane (OTS), toluene, and tetrahydrofuran (THF) were purchased from Sigma-Aldrich (Milwaukee, WI). PAA (M_W = 90000) was obtained from Polysciences (Warrington, PA). PS-PAA (M_W of PS block = 16500, M_W of PAA block = 4500, M_W/M_N = 1.05) was purchased from Polymer Source Inc.(Dorval, Canada). MWNTs, 1-5 μm in length and 20-50 nm in diameter, were obtained from NanoLab (Brighton, MA). 70% nitric acid and 30% hydrogen peroxide were purchased from EM Science (Gibbstown, NJ). Sulfuric acid was obtained from Mallinckrodt Baker, Inc. (Paris, KY), and BOC Gases (Murray Hill, NJ) supplied hydrogen (grade 4.7) and nitrogen (grade 5). All these materials were used without further purification. Deionized water (>18 MΩ cm, Millipore Milli-Q) was used for preparation of all aqueous solutions, and during rinsing procedures.

Stainless steel sheets (type 316, #8 mirror finish), with an average roughness of approximately 6 nm, were purchased from McMaster-Carr (Dayton, NJ). Polished single-crystal silicon wafers of <100> orientation were obtained from Nestec, Inc. (New Bedford, MA). Glass microscope slides from VWR Scientific Inc. (West Chester, PA) were used. The average roughness for the glass and silicon substrates did not exceed 1 nm. These materials were all used as substrates for PEM assembly.

PAH/PAA PEMs were assembled on these substrates as previously described [12]. The films were assembled at a pH of 7.5 or 3.5 for the PAH solution,and a pH of 3.5 for PAA, referred to as (PAH 7.5/PAA 3.5) or (PAH 3.5/PAA 3.5). The films were flushed with air at room temperature and stored at ambient conditions for several hours prior to further processing.

(PAH 7.5/PAA 3.5) films, constructed with PAH as the last adsorbed layer, were immersed in PS-PAA solution in THF (0.001 M based on the molecular weight of the PAA repeat unit, pH unadjusted) for 15 min, following reported protocol [14]. They were then rinsed twice in pure THF for 1 minute, before drying in air.

(PAH 3.5/PAA 3.5) films, with PAA adsorbed last, were used as matrices for silver nanocluster synthesis. The experimental procedure has been described in detail in references 20 and 21. Films, originally 70 nm thick, with 1,3, and 5 silver ion load (via an exchange process) and reduction cycles were prepared following the literature procedure.

PAH/MWNT multilayer composites were constructed using a protocol adapted from reference 23. A suspension of MWNTs was refluxed in 70% nitric acid for 6 hours. The acid was subsequently removed using centrifugation, and replaced with deionized water. The treatment with nitric acid leads to partial oxidation of the carbon nanotubes [24]. Sonication of the suspension resulted in a stable aqueous dispersion of the MWNTs. For multilayer assembly, a (PAH 2.5/PAA 2.5) bilayer was first deposited on the substrate to promote film adhesion. This was followed by 5 layers of (PAH 2.5/MWNT 2.5). After every fifth layer of PAH/MWNT, a PAH/PAA bilayer was deposited to promote stable film growth, as recommended by Kotov and co-workers [23]. The resulting structure is represented as $[(\text{PAH 2.5/PAA 2.5})_1/(\text{PAH 2.5/MWNT 2.5})_5]_x$, where x (see Table 4-1) denotes the number of times the cycle was repeated. Dipping times of 15 minutes for PAH and PAA, and 60 minutes for the MWNT dispersion were used. After exposure to each solution, the substrate was subject to three rinsing steps in water for 2, 1, and 1 minute respectively. The MWNTs were the last adsorbed material in all cases.

Self-assembled monolayer films of OTS were assembled on silicon substrates to compare their performance with PEMs. Silicon slides were treated with piranha solution (3:1 volume ratio of sulfuric acid and 30% hydrogen peroxide) for 30 min at 90 °C. After washing with water and ethanol, the substrate was dried in a stream of nitrogen. Subsequently, it was immersed in a solution of OTS in toluene (0.001 M) for 60 minutes. The resulting monolayer was rinsed with acetone and ethanol, and dried by flushing with nitrogen.

Thicknesses of PEM films on glass substrates were measured using a Tencor P-10 surface profiler. For films less than 10 nm thick, a Gaertner L116 ellipsometer was used to measure thickness; silicon was used as the substrate. Contact angle measurements were carried out using a Rame-Hart goniometer. In all cases, average values were obtained after measurements at 3-5 locations at ambient conditions.

For transmission electron microscopy (TEM) of MWNT multilayer composites, films were deposited on silicon nitride membrane window grids obtained from Structure Probe, Inc. (West Chester, PA); details about the grid structure are given in reference 25. Imaging was performed on a JEOL 200CX operated at 200 kV.

Friction and wear behavior was studied using a flexure-based biaxial apparatus as described in reference 26. Flat-on-flat configurations were used for all tests. The upper cylindrical pin with a flat surface, 1 or 2 mm in diameter, is held stationary and the lower, larger surface is subject to reciprocating motion over a 3 mm path length. In all the experiments, uncoated and film-coated substrates were mounted on the lower slider using double-coated paper scotch tape. The 1 mm diameter pin, used for wear studies at large normal stresses, was made of D2 hardened tool steel, while the 2 mm diameter

counterface, for friction tests at 250 kPa, was made of type 316 stainless steel. Between tests, these pins were polished against 1 μm aluminum film-coated disks using a specially designed pin-holder to maintain a flat surface. The polished pins were subsequently cleaned with acetone, and dried in a blast of air. A sliding speed of 200 μm/s was used in all tests. The number of cycles was confined to 20-30, corresponding to an accumulated sliding distance between 120-180 mm. The humidity in the test area was not controlled; it varied in the 15-55 % range over the duration of the test period.

Wear tracks, obtained during the tribological tests, were examined using an optical microscope. Wear was also characterized by examining the cross-section of the wear track with a profilometer. The wear track was examined at three different points; in all cases, the surface profiles closely resembled each other.

Mechanical behavior of PEMs, assembled on glass substrates, was characterized using a nanoindenter (TriboIndenter®, Hysitron, Inc.); a diamond Berkovich tip, with a tip radius between 100 and 200 nm, was used in most cases. Maximum loads between 75 and 1000 μN were applied using a trapezoidal load function consisting of a 5s loading segment, 2s hold time, and 5s unloading segment. For the ~ 6000 nm-thick (PAH 7.5/PAA 3.5) film (600 bilayers), the load and unload segments were of a 33s duration. Penetration depths varied between 50-300 nm for films 1000-6000 nm in thickness. To achieve penetration depths less than 10 nm, a NorthStar 90° cube-corner diamond indenter tip was employed; the tip radius was approximately 40-50 nm. A maximum load of 4 μN was applied using the 5s-2s-5s load function described above. In all cases, the unloading segments of the indentation curves were utilized to elicit values of film hardness and effective modulus (E_r), as suggested by Oliver and Pharr [27] (detailed

analysis procedure in Chapter 5). Both the indenter tip and indented materials contribute to E_r, given by the following equation:

$$\frac{1}{E_r} = \frac{\left(1-\nu_s^2\right)}{E_s} + \frac{\left(1-\nu_i^2\right)}{E_i} \quad (1)$$

The subscripts *s* and *i* refer to the sample and the indenter; E and ν denote the elastic modulus and Poisson's ratio. For the cube-corner indenter, the relation between the contact area and the distance (of the surface) from the indenter tip was accurately calibrated using a fused quartz sample of known mechanical properties (see Chapter 5). An approximate relation, based on ideal tip geometry [27], was used for the Berkovich tip. The temperature was maintained in the 20-25 °C range; the ambient humidity was approximately 50 %.

4.3 Results

Two levels of normal stress were investigated to elucidate the tribological merit of the PEM modification strategies. Films assembled on glass substrates were tested at a low normal stress of 250 kPa (based on the diameter of the pin) to elicit their frictional response without a dominating influence of substrate wear on the results; higher stresses in the 1-4 MPa range were used to study wear behavior of coated silicon and steel substrates. Table 4-1 depicts the average values of the steady-state friction coefficients μ exhibited by film-coated glass slides over 20 cycles of reciprocating motion, for the unmodified PEMs, and for the surface capping and MWNT composite strategies.

Table 4-1 Average coefficients of friction (μ) for surface capped PAH/PAA PEMs and PAH/MWNT multilayer composites, assembled on glass substrates; normal stress 250 kPa.

No.	Type of Film	Film Thickness (nm)	Average μ
1	*-(Glass substrate)*	---	0.44±0.24
2	(PAH 7.5/PAA 3.5)	5.5	0.45±0.07
3	(PAH 7.5/PAA 3.5)	72	0.67±0.04
4	(PAH 7.5/PAA 3.5) + PS-PAA	9.5	0.39±0.01
5	(PAH 7.5/PAA 3.5) + PS-PAA	75	0.75±0.16
6	$[(PAH\ 2.5/PAA\ 2.5)_1(PAH\ 2.5/MWNT\ 2.5)_5]_2$[3]	140	0.21±0.01
7	$[(PAH\ 2.5/PAA\ 2.5)_1(PAH\ 2.5/MWNT\ 2.5)_5]_6$[iii]	940	0.33±0.05
8	$[(PAH\ 2.5/PAA\ 2.5)_1(PAH\ 2.5/MWNT\ 2.5)_5]_6$ Heated at 150 °C, 6 hrs	940	0.26±0.04

Choi and Rubner [14] recommend the (PAH 7.5/PAA 3.5) system, with PAH adsorbed last, for enhanced adsorption of the PS-PAA block copolymer. At this pH combination, the surface of the PEM structure is enriched with functional groups from the last adsorbed polyelectrolyte [28]. The amine groups of PAH offer anchoring sites for the acid-containing PAA blocks of the copolymer. The advancing contact angle with water increased from 42° for the PAH/PAA film to 86° after adsorption of PS-PAA, in agreement with previously reported work [14]. Two thicknesses for surface capped PEMs were studied-9 nm and approximately 70 nm. Friction coefficients μ for the PAH/PAA PEM, prior to surface modification, are also reported in Table 4-1. For both thicknesses,

[3] These structures are electrically conducting in areas where the nanotube density is high. When this film was subject to a silver ion loading and reduction cycle, the average resistances (2-point measurements) exhibited a 50-fold decrease from 12 MΩ to 250 k Ω; the resulting film was electrically conducting in all areas. Also see Appendix C for friction coefficients of more MWNT-containing PEM structures.

the friction forces were only slightly affected after the capping (compare lines 2, 4 and 3, 5 of Table 4-1).

Figure 4-1 depicts a plan-view TEM image of a 140 nm thick multilayer composite containing MWNTs. The MWNTs are well dispersed in the multilayer; only a few large aggregates were seen. Table 4-1 (lines 6 and 7) reports friction coefficients for this film and for its 940 nm thick counterpart. The latter film was also chemically crosslinked by heating at 150 °C for 6 hours [29]; line 8 shows its associated μ value. The 140 nm PAH/MWNT film exhibited the lowest friction force, with a coefficient only slightly above 0.2.

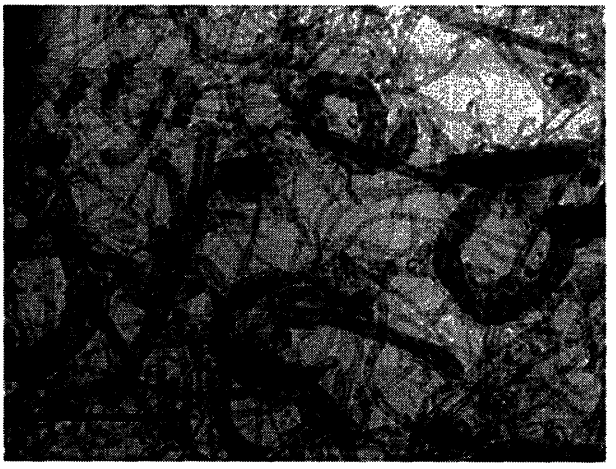

Figure 4-1 Plan view TEM image of a $[(PAH\ 2.5/PAA\ 2.5)_1(PAH\ 2.5/MWNT\ 2.5)_5]_2$ 140 nm-thick multilayer composite. Scale bar depicts 500 nm.

(PAH 3.5/PAA 3.5) films, 70 nm in thickness, were chosen as the matrix for the *in-situ* introduction of silver nanoclusters. This assembly pH combination is associated with free (unpaired) carboxylic acid groups (from PAA) that may be utilized for silver

ion loading [21]; subsequent reduction using hydrogen gas results in 3-4 nm diameter silver nanoparticles. This process may be repeated to increase the size and volume fraction of the silver clusters. Figure 4-2 depicts friction coefficients for PEMs after 1, 3, and 5 cycles of silver loading and reduction; the friction coefficient for the unfilled 70 nm-thick PEM is also depicted. The film with 3 load-and-reduction cycles exhibited the lowest average coefficient of friction of 0.3 in this series of specimens.

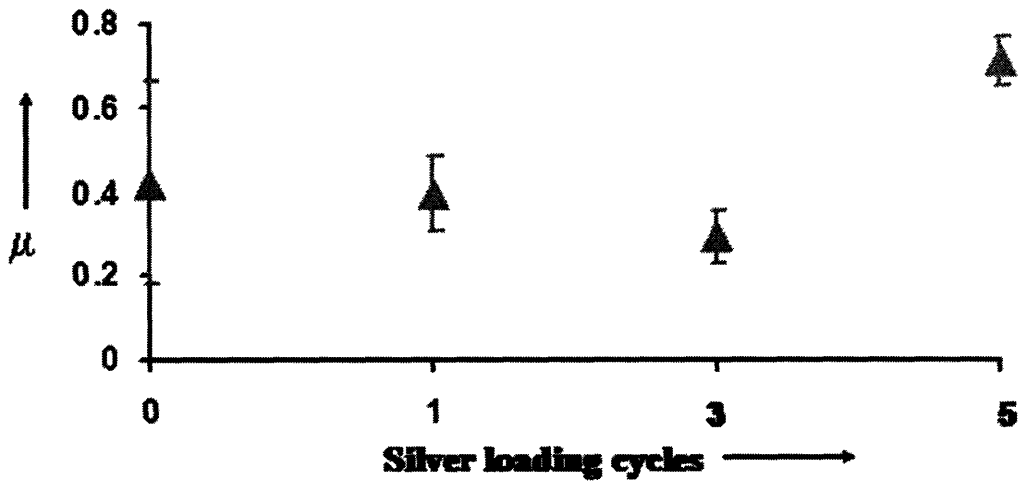

Figure 4-2 Average friction coefficients for silver-containing PAH/PAA PEMs assembled on glass. In all cases, native film was assembled at the (PAH 3.5/PAA 3.5) combination and was approximately 70 nm thick. Normal stress: 250 kPa.

Wear behavior of surface capped PAH/PAA PEMs is presented in Figure 4-3; these experiments were carried out at values of normal stresses causing wear of the bare system. Silicon substrates were used for these tests, carried out at a normal stress of 4 MPa. Figure 4-3 depicts the maximum and minimum steady-state friction coefficients observed over 2-3 tests for each configuration, over 20 cycles of reciprocating motion. For the case of bare silicon, mixed results were observed. In the absence of system wear, the friction was confined to a low value of 0.12; wear particles raised the value to as high

as 0.7. A self-assembled monolayer of OTS, currently the preferred surface modification technique in MEMS devices [1], was tested for comparison; this 1.5-2 nm film exhibited an advancing water contact angle of 101°. In the best case, the film lowered the friction coefficient to 0.07 without system wear. For two of the three experiments, however, system-wear occurred within the first few cycles, leading to high friction coefficients. By comparison, a 6 nm PAH/PAA PEM was unable to prevent system wear, resulting in friction coefficients in the 0.4-0.7 range. When the same film was surface-capped with the block copolymer, no wear was observed in all three experiments. The friction coefficient was restricted to a narrow window between 0.22 and 0.26. 70 nm-thick films prevented system wear in both the native and capped forms; the associated friction coefficients were comparable.

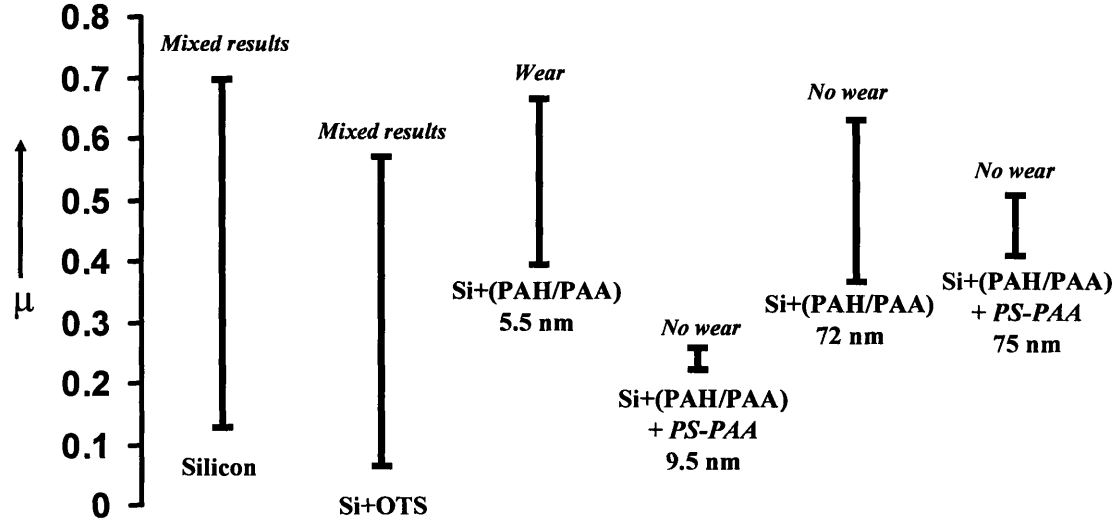

Figure 4-3 Maximum and minimum steady-state friction coefficients, and wear behavior of native and surface capped PAH/PAA PEMs on silicon substrates at a normal stress of 4 MPa.

Wear tests on stainless steel substrates were conducted at a normal stress of 1 MPa. 70 nm-thick PEMs, unfilled and containing one loading cycle of silver nanoparticles, and a 200-250 nm PAH/MWNT composite were tested. The average friction coefficients and wear results are presented in Table 4-2. Except for the bare substrate, wear prevention of the steel slider was observed in all cases. Figure 4-4 shows optical micrographs and cross-sectional surface profiles of the wear tracks, for the case of the bare substrate, and the unfilled and silver-containing PEM-coated slider; in the latter two cases, the wear of the steel substrate has been significantly reduced. The optical micrograph and cross-sectional profile for the MWNT multilayer composite-coated steel surface, after the test, are depicted in Figure 4-5.

Table 4-2 Wear Behavior of Silver Nanoparticle- and MWNT-containing PEMs on steel substrates; normal stress 1 MPa.

No.	Type of Film	Thickness (nm)	Substrate Wear?	Average μ
1	---	---	Yes	0.57
2	(PAH 3.5/PAA 3.5)	70	No	0.76
3	(PAH 3.5/PAA 3.5) + Silver (1 Loading)	70	No	0.60
4	$[(PAH\ 2.5/PAA\ 2.5)_1(PAH\ 2.5/MWNT\ 2.5)_5]_2$	200-250	No	0.27

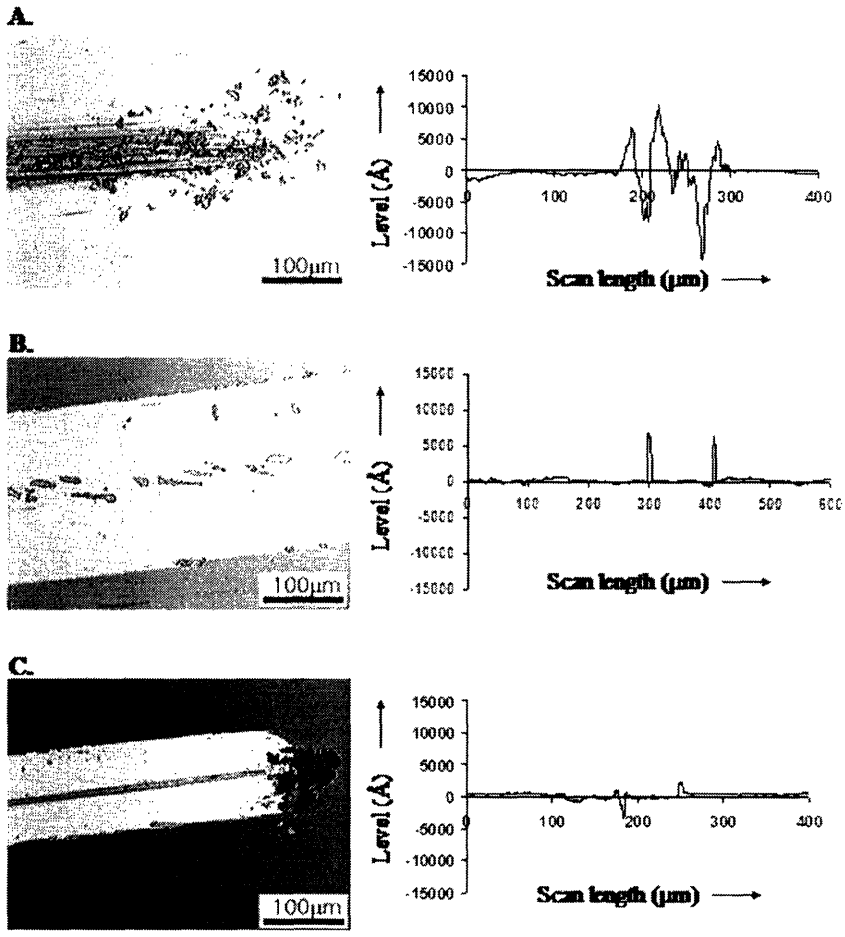

Figure 4-4 Optical micrographs and cross-sectional wear track profiles on A. bare steel, B. 70nm (PAH 3.5/PAA 3.5) PEM-coated steel, and C. 70 nm thick PEM-coated steel containing one silver loading cycle. Test was carried out at 1 MPa normal stress and 30 cycles of reciprocating motion. PEMs prevent wear of underlying steel. In all cases, steel substrate is at level zero

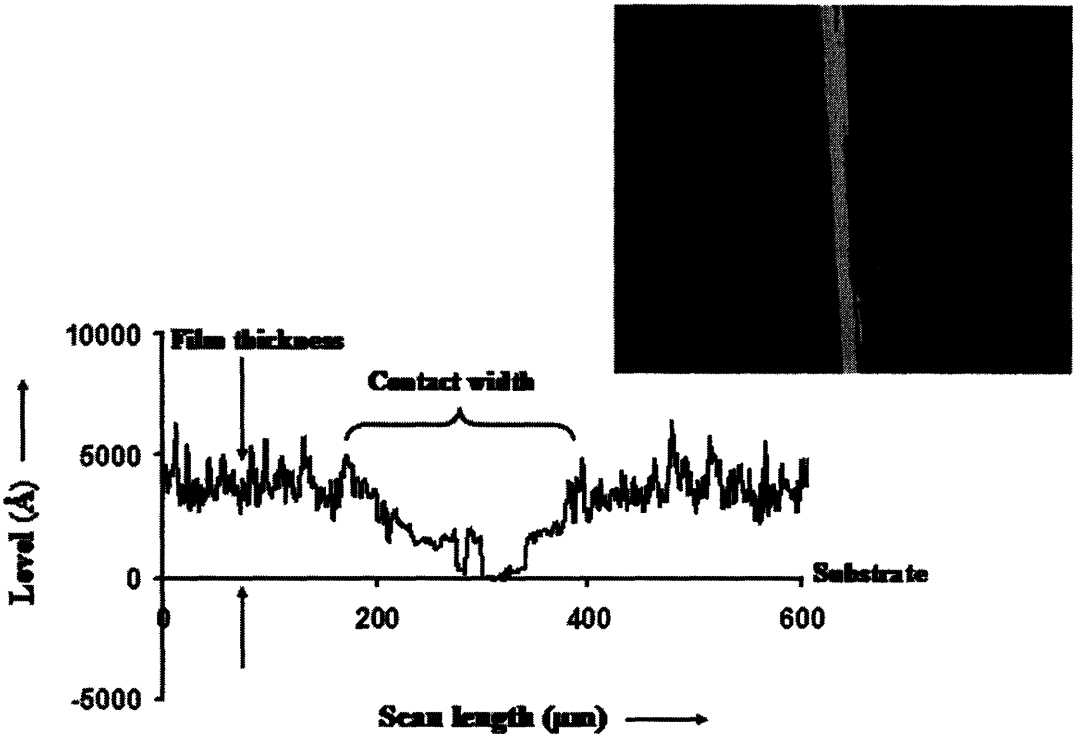

Figure 4-5 Optical micrograph and cross-sectional surface profile of wear track on PAH/MWNT composite-coated steel after 30 cycles of reciprocating motion at a normal stress of 1 MPa; substrate is at level zero. Scale bar in optical micrograph depicts 200 μm.

Results from nanoindentation studies on the modified PEM structures are presented in Table 4-3. Since the indenter tip was diamond, E_i=1140 GPa, and ν_i=0.07 (see Equation 1). For most materials E_i>>Es, and the contribution of the second term in the equation is negligible. The Poisson's ratio for a range of polymeric materials lies between 0.25 and 0.45; E_s is thus 80-95 % of the value of E_r. Tip penetration was quantified by the contact depth, which corrects the penetration depth at peak load for the deflection of the surface at the contact perimeter [27]. Based on literature recommendations [30], contact depths were limited to 10-15 % of the film thickness to eliminate contributions from the glass substrate, associated with an elastic modulus of 70 GPa [27]. Detailed

analysis, reported in Chapter 5, was carried out to confirm the validity of this recommendation. To establish that the choice of indenter geometry did not affect results significantly, 6000 nm-thick (PAH 7.5/PAA 3.5) films were indented to approximately the same contact depths with the Berkovich and cube-corner indenter tip. Table 4-3, lines 1 and 2, reveals only a 13 % difference in the values of E_r.

Table 4-3 Mechanical Properties of PEM Assemblies through Nanoindentation

No.	Type of Film	Approx. Film Thickness (nm)	Indenter Tip	Contact Depth (nm)	Reduced Modulus E_r (GPa)	Hardness (GPa)
1	(PAH 7.5/PAA 3.5)	6000	Berkovich	316±10	12.6±0.5	0.39±0.03
2	(PAH 7.5/PAA 3.5)	6000	Cube-corner	312	10.9	0.36
3	(PAH 7.5/PAA 3.5)	100	Cube-corner	8.4 ± 1.0	7.9 ± 1.0	0.76 ± 0.09
4	(PAH 7.5/PAA 3.5) +PS-PAA	100	Cube-corner	8.9 ± 0.7	12.9 ± 2.4	1.23 ± 0.18
5	(PAH 7.5/PAA 3.5) + PS-PAA	6000	Berkovich	124±9	10.8±0.7	0.35±0.06
6	(PAH 3.5/PAA 3.5)	1300	Berkovich	55±10	19.2±2.6	0.96±0.26
7	(PAH 3.5/PAA 3.5) + Silver (1 loading)	1300	Berkovich	56±3	20.2±1.0	0.86±0.15
8	$[(PAH\ 2.5/PAA\ 2.5)_1(PAH\ 2.5/MWNT\ 2.5)_5]_6$	940	Berkovich	196±24	1.1±0.3	0.04±0.02
9	$[(PAH\ 2.5/PAA\ 2.5)_1(PAH\ 2.5/MWNT\ 2.5)_5]_6$ *Heated at 150 °C, 6 hrs*	940	Berkovich	181±35	1.5±0.7	0.06±0.04

NOTE: The measurement in line 9 was corroborated using a cube-corner indenter tip. Film thickness in this case was 1250 nm. Measured values of E_r: 1.64±0.41 GPa, H: 0.16±0.03 GPa, for contact depth of 79 nm.

4.4 Discussion

The flat pin-on-slider geometry used here, and previously (Chapter 2), introduces a degree of plowing at both the kPa and MPa stress levels, causing delamination of the

film. In the absence of substrate wear, adhesion of the PEM fragments to the counterface, their deformation, and dragging at the interface raise the friction forces above those exhibited by the bare substrate (Table 4-1, lines 1 and 3). We hypothesized that tuning the hardness, adhesive friction component, or shear strength of the PEM fragments would alter the friction coefficients. Adsorption of the PS-PAA block copolymer lowers the hydrophilicity of the PAH/PAA PEM as reflected by an increase in the water contact angle. The 3-4 nm-thick PS block [14], below its glass transition temperature, is not expected to be amenable to orientation in the sliding direction and thereby alter the shear strength of the film. At a normal stress of 250 kPa, the friction force for a 9 nm-capped film was only marginally lower than the uncapped film (Table 4-1, lines 2 and 4). At higher stresses, however, the effect of the surface capping was more pronounced (see Figure 4-3). The 9 nm-thick film prevented system wear repeatedly, accompanied by friction coefficients in the 0.20-0.25 range. The uncapped control did not demonstrate wear prevention capability. The improved friction-and-wear behavior, at higher stresses, can be explained, not by a decrease in the adhesion friction component owing to the reduced hydrophilicity, but by improved mechanical behavior for the capped structure. At thicknesses less than 10 nm, the block copolymer contributes to 40-50 % of the total film thickness, and hence significantly to the mechanical response. Indentation studies, employing contact depths of 8-9 nm, revealed that the modulus and hardness of the capped structure was 60 % higher than its uncapped counterpart (Table 4-3, lines 3 and 4). This translates into a larger load-bearing capacity and a lower degree of asperity penetration for the capped film, during sliding. The improved tribological performance

was especially evident at higher stresses. By comparison, monolayers of OTS (Figure 4-3) do not demonstrate wear prevention at these high loads.

At higher thicknesses around 70 nm, the block copolymer contributes to only about 5 % of the film thickness. The underlying PEM matrix thus dominates the mechanical properties. Table 4-3, lines 1 and 5, depicts the hardness and modulus values of the native and capped structure after indenting to contact depths much greater than the thickness of the block copolymer; essentially, no difference was observed between the capped and uncapped films. There is enough film material at the interface, in both systems, to prevent wear of the system at 4 MPa (see Figure 4-3), and the friction coefficients (approximately 0.6-0.7, see Table 4-1) depend mainly on the conformation of the fragments at the sliding interface.

At stresses causing system wear, 10 nm PS-PAA capped PAH/PAA PEMs demonstrate consistent low values of friction coupled with substrate wear prevention. With an increase in film thickness, however, the efficacy of the block copolymer-capped PEM with respect to friction reduction is lost.

Silver nanoclusters, introduced *in-situ* into PAH/PAA PEMs, are expected to facilitate sliding, at lower normal stresses, by transferring contact off the polymer matrix (onto themselves). An optimum number of loading cycles are needed to reduce the friction coefficient reliably; larger particles or an excess of silver can increase friction through a third body effect. This trend is reflected in Figure 4-2. Three loading cycles of silver exhibited the lowest coefficient, while a substantial increase in friction was observed after 5 loading cycles. Nanoindentation studies on an unfilled and once loaded, silver-containing PEM revealed comparable mechanical properties-see Table 4-3, lines 6

and 7; mechanical reinforcement of the film structure due to the silver particles was not observed. The nanoparticles occupy 5.5 % of the film, by volume, after one loading and reduction cycle [21]. After 5 loading cycles, the value increases to 17 %. In the absence of a substantially high volume fraction of silver, the polymer matrix will determine wear behavior of the film at higher stresses. The friction coefficient for a once loaded, silver-containing film, at a normal stress of 1 MPa, is slightly lower than the unfilled PEM (Table 4-2, compare lines 2 and 3). The values of μ, however, are mainly governed by the conformation of the interface film fragments at these stresses. Optical micrographs and surface profiles (Figure 4-4) depict significant prevention of substrate wear for PEM-coated systems, in accordance with previous work (see Chapter 2).

Silver-containing PEMs offer the advantage of a wear preventing PEM matrix at high normal loads, and a low friction surface (compared to the native film) at lower stresses. It is unclear if the choice of nanoparticle will affect the friction coefficient. The general nanocluster incorporation scheme [20] like the one presented by PAH/PAA PEMs offers the possibility of introducing a wide variety of nanoparticles of metals and metallic compounds into the polymer matrix, and studying their effect on tribological behavior.

From Table 4-3, it is clear that the assembled PAH/MWNT composites were significantly softer than their PAH/PAA counterparts. Nanoindentation studies, reported in Chapter 5, revealed that the mechanical properties of the composites were comparable to those of thin films of PAH. The individual MWNTs, used as the anionic material, can be displaced easily during indentation, leading to modulus and hardness values that are close to that of the surrounding polyelectrolyte matrix.

Both Table 4-1 and 4-2 reflect the tribological merit of this easy-to-shear carbon nanotube-containing material. The friction coefficients are the lowest observed in this study, even for a 940 nm film. Thermally converting the ionic PAH-MWNT surface attachments to covalent amide bonds does little to reinforce the PAH polymer matrix; the friction coefficient (Table 4-1, lines 7 and 8) and hardness (Table 4-3, compare lines 8 and 9) values are comparable. The nature of surface bonds may play a role in the presence of a liquid, where the films behave as hydrogels [32], responsive to the pH and ionic strength of the surrounding medium. The PAH/MWNT composites also exhibit values of μ as low as 0.27 at higher stresses, as depicted in Table 4-2; this is in addition to substrate wear prevention. From Figure 4-5 it is clear that a considerable portion of the film remains attached to the wear track. MWNT multilayer composites thus show merit for friction and wear reduction at both levels of stress. The multilayer assembly technique offers a facile way to create low friction surfaces by exploiting the properties of MWNTs.

4.5 Conclusions

This chapter has evaluated three strategies for tuning the friction forces exhibited by polyelectrolyte multilayers, while sustaining (or enhancing) their wear-retarding properties. PAH/PAA PEMs, less than 10 nm thick and capped with the PS-PAA block copolymer, exhibited enhanced substrate wear prevention at high stresses compared with the uncapped counterpart; this was in addition to maintaining low friction forces. These films are ideally suited for devices where wear particle generation leads to high friction forces and hinders smooth operation. The introduction of silver nanoparticles into PEMs has a beneficial tribological effect at low normal stresses; an optimum amount (and

particle size) of surface silver is required for low friction coefficients. At higher stresses, the tribological behavior of these composites is dominated by the surrounding PEM matrix. The general scheme of nanoparticle synthesis offered by these films makes it possible to study the effect of various nanoparticle types on friction. Finally, novel PEM-MWNT composites, demonstrating low friction-and-wear at all levels of stress, have been assembled. These multilayer composite coatings exhibited the lowest values of friction forces among the strategies studied. Nanoindentation was successfully used to correlate the mechanical properties of these structures with their observed tribological behavior.

In all cases, these polyelectrolyte multilayer films provide a wear-preventing coating associated with a well-defined friction force. PEM-based coatings are ideally suited to combat the tribological challenges in a number of applications employing different bearing materials.

4.6 References

(1) Komvopoulos, K. *Wear* **1996**, *200*, 305-327.

(2) Sundararajan, S.; Bhushan, B. In *NATO advances study institute on fundamentals of tribology and bridging the gap between the macro- and micro/nano scales*; Bhushan, B., Ed.; Kluwer Academic Publishers: Keszthely, Hungary, 2000; Vol. 10, pp 821-850.

(3) Tsukruk, V. V.; Bliznyuk, V. N.; Hazel, J.; Visser, D.; Everson, M. P. *Langmuir* **1996**, *12*, 4840-4849.

(4) DePalma, V.; Tillman, N. *Langmuir* **1989**, *5*, 868-872.

(5) Maboudian, R.; Ashurst, W. R.; Carraro, C. *Tribology Letters* **2002**, *12*, 95-100.

(6) Srinivasan, U.; Howe, R. T.; Maboudian, R. In *Tribology Issues and Opportunities in MEMS*; Bhushan, B., Ed.; Kluwer Academic Publishers: AA Dordrecht, The Netherlands, 1998; pp 597-605.

(7) Ashurst, W. R.; Yau, C.; Carraro, C.; Lee, C.; Kluth, G. J.; Howe, R. T.; Maboudian, R. *Sensors and Actuators A* **2001**, *91*, 239-248.

(8) Tsukruk, V. V.; Nguyen, T.; Lemieux, M.; Hazel, J.; Weber, W. H.; Shevchenko, V. V.; Klimenko, N.; Sheludko, E. In *Tribology Issues and Opportunities in MEMS*; Bhushan, B., Ed.; Kluwer Academic Publishers: AA Dordrecht, The Netherlands, 1998; pp 607-614.

(9) Tsukruk, V. V. *Tribology Letters* **2001**, *10*, 127-132.

(10) Julthingpiput, D.; Ahn, H.; Kim, D.; Tsukruk, V. V. *Tribology Letters* **2002**, *13*, 35-40.

(11) Sidorenko, A.; Ahn, H.; Kim, D.; Yang, H.; Tsukruk, V. V. *Wear* **2002**, *252*, 946-955.

(12) Yoo, D.; Shiratori, S. S.; Rubner, M. F. *Macromolecules* **1998**, *31*, 4309-4318.

(13) Hidber, P. C.; Helbig, W.; Kim, E.; Whitesides, G. M. *Langmuir* **1996**, *12*, 1375-1380.

(14) Choi, J.; Rubner, M. F. *J. Macromol. Sci.-Pure Appl. Chem.* **2001**, *A38*, 1191-1206.

(15) Yu, L.; Yang, S.; Wang, H.; Xue, Q. *J. App. Polym. Sci.* **2000**, *77*, 2404-2410.

(16) Sawyer, W. G.; Freudenberg, K. D.; Bhimaraj, P.; Schadler, L. S. *Wear* **2003**, *In press*.

(17) Voort, J. V.; Bahadur, S. *Wear* **1995**, *181*, 212-221.

(18) Wang, Q.; Xue, Q.; Shen, W.; Zhang, J. *J. App. Polym. Sci.* **1998**, *69*, 135-141.

(19) Petrovicova, E.; Knight, R.; Schadler, L. S.; Twardowski, T. E. *J. App. Polym. Sci.* **2000**, *78*, 2272-2289.

(20) Joly, S.; Kane, R.; Radzilowski, L.; Wang, T.; Wu, A.; Cohen, R. E.; Thomas, E. L.; Rubner, M. F. *Langmuir* **2000**, *16*, 1354-1359.

(21) Wang, T. C.; Rubner, M. F.; Cohen, R. E. *Langmuir* **2002**, *18*, 3370-3375.

(22) Cumings, J.; Zettl, A. *Science* **2000**, *289*, 602-603.

(23) Mamedov, A. A.; Kotov, N. A.; Prato, M.; Guldi, D. M.; Wicksted, J. P.; Hirsch, A. *Nature Materials* **2002**, *1*, 190-194.

(24) Mawhinney, D. B.; Naumenko, V.; Kuznetsova, A.; Yates, J. T.; Liu, J.; Smalley, R. E. *Chem. Phys. Lett.* **2000**, *324*, 213-216.

(25) Boontongkong, Y.; Cohen, R. E. *Macromolecules* **2002**, *35*, 3647-3652.

(26) Gearing, B. P.; Anand, L. In *2001 ASME International Mechanical Engineering Congress and Exposition*: New York, New York, USA, 2001.

(27) Oliver, W. C.; Pharr, G. M. *J. Mater. Res.* **1992**, *7*, 1564-1583.

(28) Shiratori, S. S.; Rubner, M. F. *Macromolecules* **2000**, *33*, 4213-4219.

(29) Harris, J. J.; DeRose, P. M.; Bruening, M. L. *J. Am. Chem. Soc.* **1999**, *121*, 1978-1979.

(30) Fischer-Cripps, A. C. *Nanoindentation*; Springer-Verlag New York, Inc.: New York, 2002.

(31) Wang, T. C.; Cohen, R. E.; Rubner, M. F. *Adv. Mater.* **2002**, *14*, 1534-1537.

Chapter 5 Mechanical Characterization of Polyelectrolyte Multilayers through Quasi-static Nanoindentation[3]

5.1 Introduction

The electrostatic layer-by-layer assembly of polyelectrolytes has attracted much interest over the last decade [1]. This simple methodology leads to the deposition of architectures that can be precisely tuned by manipulation of the processing conditions or polyelectrolyte pair. The resulting ultra-thin polyelectrolyte multilayer (PEM) films have been investigated for a wide range of applications, including drug delivery [2-4], tailoring cell-surface interactions [5,6], photonic structures [7,8], electrochemical devices [9-11], wear-retarding coatings [12,13], and separation membranes [14]. Critical to the success of these applications is the structural integrity and robustness of PEMs in various environments; the mechanical properties of these films have thus been heavily relied upon. Not much is known,a however, about the mechanical properties of the polyelectrolyte multilayers, particularly in the dry state, and the effect of processing conditions on mechanical behavior.

One of the primary reasons for the lack of literature data on the mechanical properties of the ionically stitched multilayer systems is the small amount of material available for testing. Deposited as thin films (incremental thicknesses [15] range from 0.5 nm to 14 nm per adsorbed bilayer), the elucidation of mechanical properties, independent

[3] This chapter was submitted to Macromolecules **2004**, *37(13)*, 4865-4871.

of influences from the supporting material, is rendered difficult using conventional testing. The indirect measurement of elastic moduli of PEM films, through tensile tests on coated fibers, has been attempted [16]. These tests require the deconvolution of substrate contribution from the measurements. Atomic Force Microscopy (AFM) has been used to study the deformation of PEM microcapsules[17-19] filled with aqueous and organic solvents and polymer solutions. Modulus values for the walls of PEM microcapsules have been estimated from osmotic pressure induced deformations[20,21]. Plastic deformation in PEM microcapsules has been studied[22]. Recently a direct AFM study of the wet-state mechanical properties of PEMs in flat film geometry has been reported[23].

Nanoindentation is a useful tool that allows the direct measurement of mechanical properties of thin films[24], including polymer films[25-28] By indenting a material to a desired force (or depth) followed by retraction of the tip, a force-displacement (*P-h*) curve, characteristic of the material being tested, is obtained. Various properties, including the elastic modulus and hardness, can be elicited by analysis of this curve. Proper use of this method facilitates the mechanical probing of thin films without a significant influence of the mechanical properties of the underlying substrate.

This paper focuses on the elucidation of mechanical behavior of PEMs through quasi-static nanoindentation. Poly(acrylic acid) (PAA) and poly(allylamine hydrochloride) (PAH) were used for film assembly. The degree of ionization of the functional groups of these weak polyelectrolytes is a function of solution pH, thus offering intricate control over the molecular organization and composition of the assembled PEM structures. The pH conditions employed in the processing of PEMs from

the PAH/PAA pair govern important structural parameters like layer organization and thickness, surface roughness, and nature of functional groups at the surface (contact angle) [15,29] . The objective of this study is to examine the effect of film thickness and PAH/PAA assembly conditions on the elastic modulus and hardness of the PEMs, elicited through analyses of the *P-h* curves. The mechanical properties of the films are compared with those of the parent polyelectrolytes and a few other commercially available polymers that have been examined in nanoindentation tests. While most of the results reported here were obtained on dry PEMs equilibrated in ambient air, a few hydrated PEMs were studied after immersion in pH neutral water.

5.2 Experimental Details

5.2.1 Materials

PAH (M_W = 70000) and tetrahydrofuran (THF) were purchased from Sigma-Aldrich (Milwaukee, WI). PAA (M_W = 90000) was obtained from Polysciences (Warrington, PA). Poly(methyl methacrylate) (PMMA, M_w=35000) from Scientific Polymer Products, Inc. (Ontario, NY) was used. All the materials were used without further purification. Deionized water (>18 MΩ cm, Millipore Milli-Q) was used for preparation of all aqueous solutions, and during rinsing procedures. Glass microscope slides from VWR Scientific, Inc. (West Chester, PA) were used as substrates for PEM assembly.

5.2.2 Film Assembly and Thickness Measurements

PAH/PAA PEMs were assembled on the glass substrates as previously described [15,29] . The glass slides were degreased in a detergent solution, via ultrasonication, for 15 minutes, followed by ultrasonication in water for 10 minutes. After further rinsing in water and drying in air, the substrates were subject to air-plasma treatment (5 minutes at 100 W-Harrick Scientific PDC-32G plasma cleaner/sterilizer). PAH and PAA aqueous solutions (0.01 M based on molecular weights of the repeat unit) were adjusted to the desired pH using 1 M NaOH or 1 M HCl. PEM films were assembled by immersing the plasma-treated slides into the PAH solution for 15 minutes, followed by three rinsing steps in water for 2, 1, and 1 minute respectively. They were then immersed in the PAA solution, followed by identical rinsing steps. This process built a PAH/PAA bilayer. The cycle was repeated to build PEMs of the desired thickness. The immersion and rinsing steps were automated using a Zeiss HMS programmable slide stainer [29]. Finally, the film-coated substrates were dried by flushing with air, and stored at ambient conditions for several hours before testing. The film constructions will be represented as (PAH x/PAA y)$_z$, where x and y denote the pH of the PAH and PAA solutions used for PEM assembly, and z denotes the number of PAH/PAA bilayers. Thickness of PEM films on glass substrates was measured using a Tencor P-10 surface profiler; the films were scored at 3-5 locations and the step heights were measured.

Films of PAH, PAA, and PMMA homopolymers were prepared by spin coating (Specialty Coating Systems, Inc.) onto glass substrates. Aqueous solutions of PAH and PAA at pH values of approximately 7.5 and 3-3.5, respectively, were used. A solution of PMMA in THF was used for spin coating. The PAH and PAA films were dried by

flushing with air and stored at ambient conditions. The spin-coated PMMA film was dried in a vacuum oven at 25-30 °C for 2-3 hours. The surface profiler was used to measure film thickness in all cases.

5.2.3 Mechanical Characterization

Nanomechanical testing was carried out using a Triboindenter® from Hysitron Inc.. The instrument is a load-controlled, displacement-sensing device. NorthStar cube-corner and Berkovich diamond indenter tips were employed. The total included angle for the three-sided cube-corner indenter shape is 90°; the tip radius was 40-50 nm. The tip radius for the Berkovich indenter was in the 100-200 nm range (included angle 142.3°); this flatter indenter tip was used for films greater than 500 nm thick. A trapezoidal loading pattern consisting of a 5 second loading segment, a 2 second hold period, and a 5 second unloading segment was used for most tests. The maximum applied load was based on the thickness of the film. The hold time was incorporated to minimize the effects of specimen creep on the estimated values of modulus and hardness [30]. Prior to indentation, the tip was made to scan the specimen surface in a contact mode of engagement. This allowed the instrument to stabilize and a thermal drift rate to be estimated; the reported penetration depth readings were corrected for drift. For measurements at ambient conditions, the temperature was maintained in the 20-25 °C range; the relative humidity was approximately 50 %.

The unloading segment of the P-h curve was utilized for the extraction of mechanical properties, based on the method of Oliver and Pharr [31]; a sample P-h curve is shown in Figure 5-1.

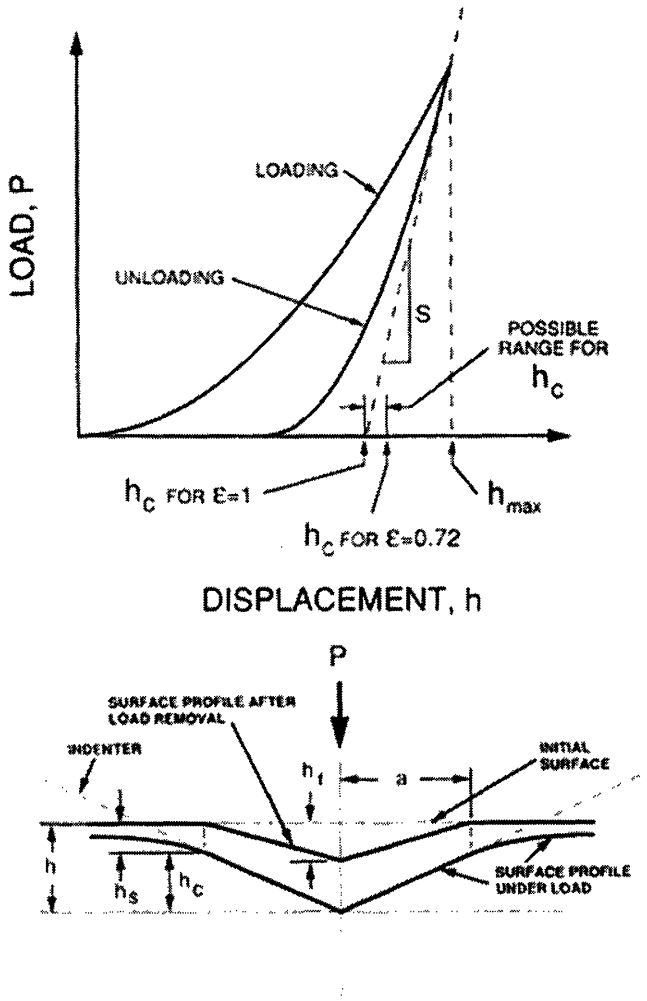

Figure 5-1 Sample P-h curve and indent profile (figure adapted from reference 31)

The effective modulus E_r, a combination of the properties of the indenter and indented materials, and the sample hardness H are defined by the following equations:

$$\frac{1}{E_r} = \frac{\left(1-\nu_s^2\right)}{E_s} + \frac{\left(1-\nu_i^2\right)}{E_i} = \frac{2}{S}\sqrt{\frac{A}{\pi}} \tag{1}$$

$$H = \frac{P_{\max}}{A} \tag{2}$$

A prefactor, numerically equal to 1.034 for both the Berkovich and the cube corner indentors[24], has been neglected in Equation 1. The symbols ν and E denote the Poisson's ratio and elastic modulus for the indenter material (subscript *i*) and the sample (subscript *s*). A is the projected area of contact at peak load P_{max}, and S is the unloading stiffness. S is defined as the slope of the unloading curve at the maximum penetration depth h_{max}. To calculate S, the unloading curve was fitted to a power law equation of the form

$$P = B(h - h_f)^m \tag{3}$$

B, h_f, and m were arbitrary fitting parameters. S is thus mathematically defined as

$$S = \frac{dP}{dh}(h_{\max}) = mB(h_{\max} - h_f)^{m-1} \tag{4}$$

The contact depth h_c, used to calculate A, is given by the equation

$$h_c = h_{\max} - \varepsilon\frac{P_{\max}}{S} \tag{5}$$

The latter term accounts for the deflection of the surface at the contact perimeter [31]. The geometric constant ε, based on the geometry of the indenter tip[31], was taken as 0.75. A tip calibration function was used for relating A to h_c using a polynomial expression.

$$A = C_0 h_c^2 + C_1 h_c + C_2 h_c^{1/2} \tag{6}$$

The constants C_0, C_1, and C_2 for the cube-corner indenter were empirically determined using a fused quartz sample of known modulus and hardness.

$$C_0 = 4.397$$

$$C_1 = 158.2$$

$$C_2 = 1083.2$$

For the Berkovich tip, a value of 24.5 was used for C_0 in Equation (6) based on ideal tip geometry[31]; C_1 and C_2 were taken as zero.

In this study, the indenter tip material was diamond with E_i=1140 GPa and ν_i=0.07. For materials with an elastic modulus of the order of 10 GPa, the contribution of the indenter tip material to E_r (see Equation 1) is negligible. Because Poisson's ratio for most polymeric materials lies in the 0.25-0.45 range, the elastic modulus (E_s) of the sample is numerically equal to 80-95 % of the measured effective modulus value (E_r).

To study the behavior of PEM films in the hydrated state, water (pH adjusted to 7 using 1 M NaOH) was used as the surrounding medium. After adding a few drops of water, the film was allowed to stand for 15 minutes before testing. A cube-corner diamond fluid cell indenter tip was used for these measurements. P-h curves were analyzed in a manner identical to that described for measurements at ambient conditions.

5.3 Results

5.3.1 Effect of Film Thickness

To investigate the effect of film thickness on mechanical response, PEM films were subject to eighty indentations, beginning at a maximum load of 12000 μN for the first indent; the load was decreased by 10% for each subsequent indent, reaching a value of 3 μN for the final load level. The effective modulus and hardness profiles for the approximately 80 nm, 500 nm and 6000 nm-thick films are depicted in Figures 5-2 and 5-3; all films were assembled at the (PAH 7.5/PAA 3.5) combination, with PAA as the last adsorbed polyelectrolyte.

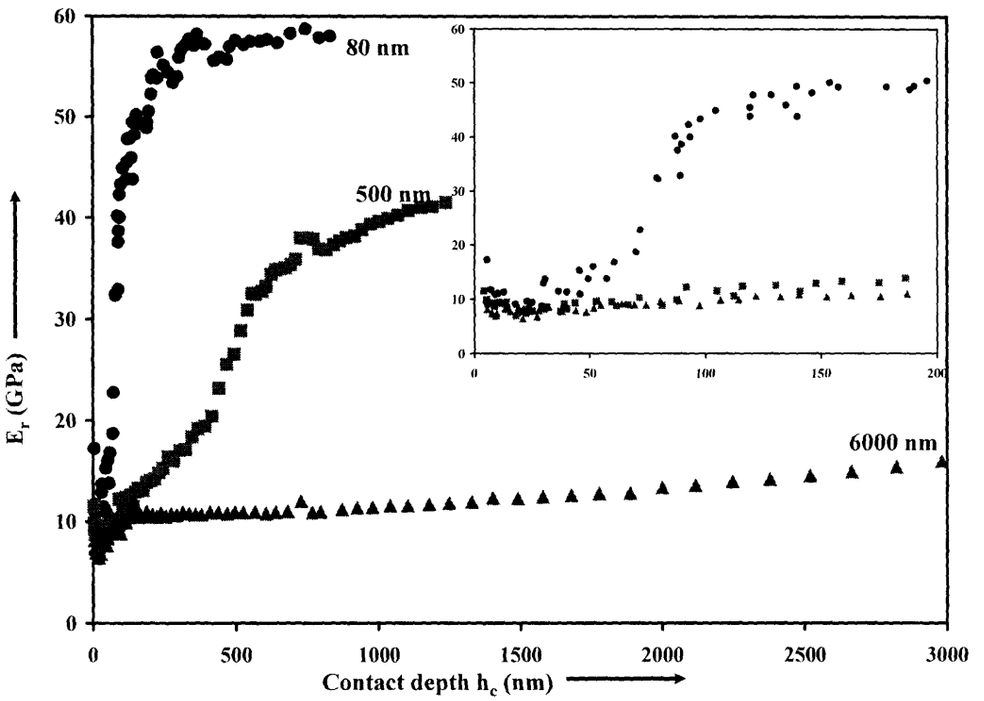

Figure 5-2 Effective modulus (Er)-contact depth profile for 80 nm (8 bilayers, circles), 500 nm (45 bilayers, squares), and 6000 nm (600 bilayers, triangles)-thick PEMs. Inset depicts magnified profile at lower h_c values. All films were assembled on glass at the (PAH 7.5/PAA 3.5) combination. The cube-corner indenter tip was used for these measurements at ambient conditions.

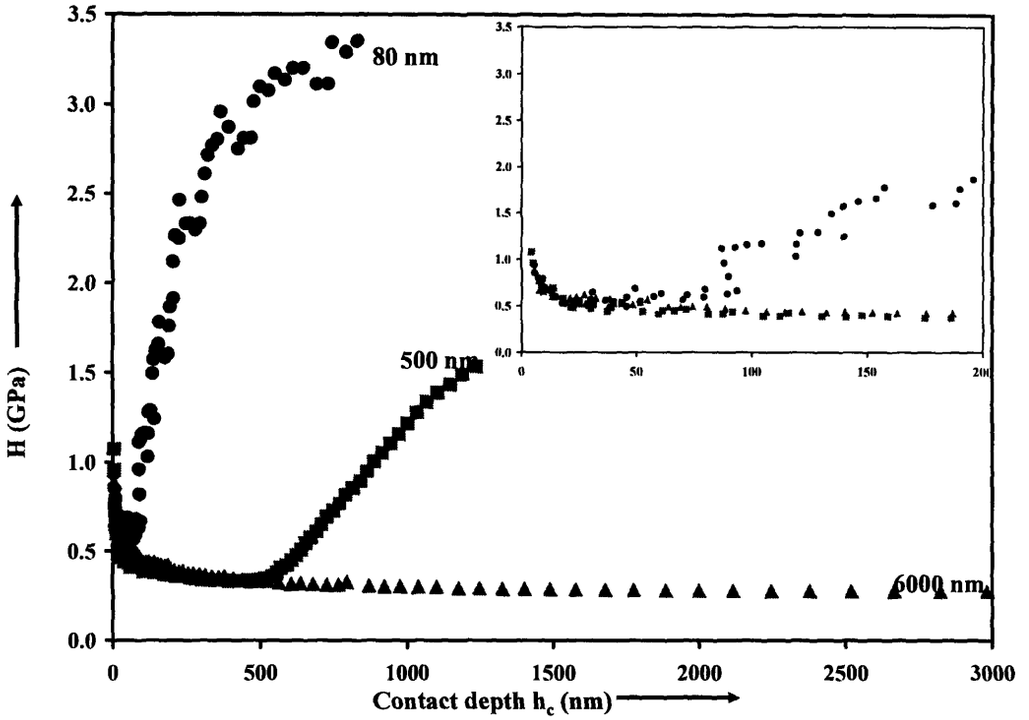

Figure 5-3 Hardness (H)-contact depth profile for 80 nm (8 bilayers, circles), 500 nm (45 bilayers, squares), and 6000 nm (600 bilayers, triangles)-thick PEMs. Inset depicts magnified profile at lower hc values. All films were assembled on glass at the (PAH 7.5/PAA 3.5) combination. The cube-corner indenter tip was used for these measurements at ambient conditions.

For all films, the modulus and hardness profiles exhibited a U-shaped curve, with an initial decrease, a plateau region, and a subsequent rise in values as contact depths approached the film thickness; this behavior is in agreement with previously reported work on nanoindentation of thin polymer films [25,26]. The values in the plateau region are considered representative of the mechanical behavior of the sample. At values of h_c approaching the thickness of the film, the stress fields are affected by the underlying glass substrate, as reflected by an increase in the values of E_r and H; glass is associated with an elastic modulus slightly greater than 70 GPa [31]. It has been recommended in the past that indentation depths be confined to no more than 10 % of the film thickness to

preclude any influence of the underlying substrate on the P-h curve [24]. The initial decrease in E_r and H at very low contact depth below 10 nm is attributed to surface effects and/or impurities, but not to substrate influence. The modulus profiles exhibit negligible substrate effects up to contact depths approaching 20-40 % of the thickness of the film; the hardness profiles, on the other hand, do not reveal significant influence from the glass substrate up to contact depths comparable with the film thickness. Table 5-1 compares the E_r and H values for the three films at a contact depth of 20 nm where both the surface and the substrate effects are not appreciable. To ensure that the measured mechanical properties were not an artifact of the cube corner tip geometry and the corresponding induced stress fields, a (PAH 7.5/PAA 3.5) film was indented using a Berkovich indenter. The results, compared with data from the cube-corner indenter tip at comparable contact depths (Table 5-1 lines 4 and 5), reveal a 7 % difference in hardness and a 16 % difference in modulus values; the measurements using the Berkovich and cube-corner indenter tips were also performed on different Triboindenter® machines.

Table 5-1 Effective modulus (E_r) and hardness (H) values for various (PAH 7.5/PAA 3.5) constructs and the parent polyelectrolytes.

	Film	Approx. Thickness (nm)	Type of Indenter*	h_c (nm)	H (GPa)	E_r (GPa)
1	$(PAH\ 7.5/PAA\ 3.5)_8$	80	Cube-corner	21.5	0.483	7.96
2	$(PAH\ 7.5/PAA\ 3.5)_{45}$	500	Cube-corner	22.5	0.479	8.12
3	$(PAH\ 7.5/PAA\ 3.5)_{600}$	6000	Cube-corner	21.2	0.486	7.83
4	$(PAH\ 7.5/PAA\ 3.5)_{600}$	6000	Cube-corner	312.2	0.363	10.87
5	$(PAH\ 7.5/PAA\ 3.5)_{600}$**	6000	Berkovich	316.3 ± 9.9	0.389 ± 0.025	12.64 ± 0.47
6	$(PAH\ 7.5/PAA\ 3.5)_{600}$ *Heated at 150 °C, 6 hrs*	6000	Cube-corner	459.5 ± 2.8	0.432 ± 0.006	11.2 ± 0.37
7	PAH#	600	Berkovich	130 ± 31.5	0.036 ± 0.006	1.35 ± 0.58
8	PAA	4500	Berkovich	128.3 ± 3.8	0.35 ± 0.023	9.51 ± 0.28

*A trapezoidal load function with a 5 s loading segment, 2 s hold time, and 5 s unloading segment (5s-2s-5s) was used, unless otherwise specified. All measurements at ambient conditions.

**Trapezoidal 33s-2s-33s loading function was used

#Trapezoidal 5s-4s-5s loading function was used

The nature of the linkages between the PAH and PAA chains can be changed via thermal treatment[32]. By heating the PEMs, a fraction of the ionic attachments between the carboxyl groups of PAA and the amine groups of PAH are converted to covalent amide bonds. Table 5-1 (lines 4 and 6) shows that there is almost no difference in the dry state mechanical properties between the ionically stitched film and those that also contain some amide crosslinks. The latter structure is associated with a marginally higher value of hardness while the modulus values are identical within error; this observation was confirmed through dynamic nanomechanical analysis[33], presented in Appendix B.

Table 5-1 also presents the mechanical properties of spin-coated films of PAH and PAA. The data of Table 5-1 indicate that some of the PAH/PAA PEM structures are mechanically superior to either parent polyelectrolyte. The modulus and hardness of PAA were 7-10 times the values for PAH. Some representative P-h curves are depicted in Figure 5-4.

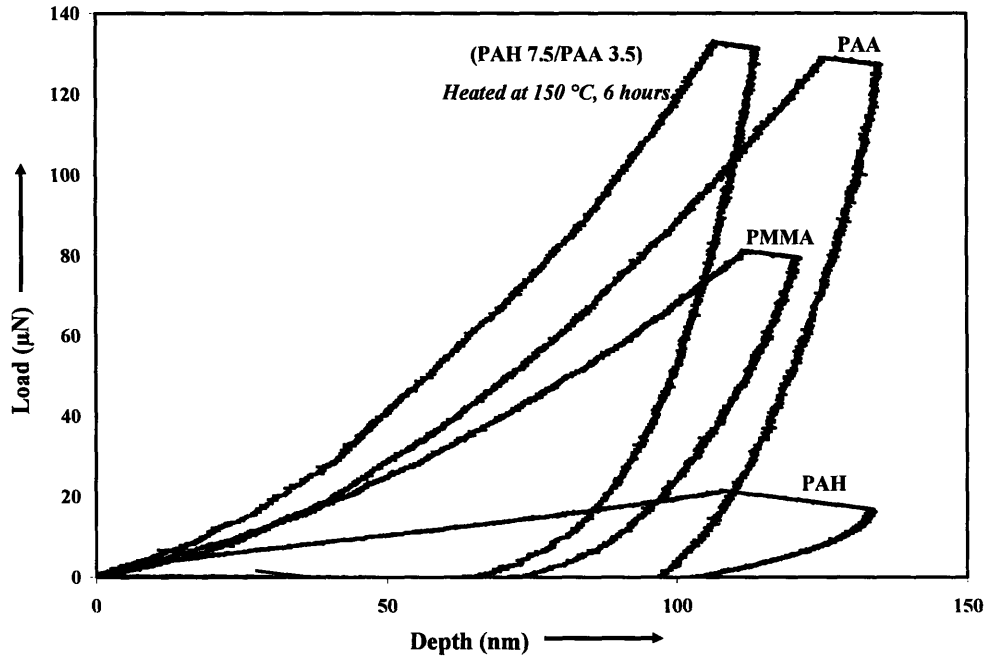

Figure 5-4 Sample load (P) - depth (h) curves for some thin-film specimens. A trapezoidal 5s-2s-5s loading function was used in most cases. For PAH, a hold time of 4 s was used to minimize the effects of sample creep on the unloading curve.

5.3.2 Effect of Assembly pH Combination

Figure 5-5 compares measured hardness and effective modulus values for three different PAH/PAA pH assembly combinations along with previously reported incremental thicknesses per deposited bilayer. Contact depths of 7-9 nm were employed for these 80-100 nm-thick films. Thicker films of the (PAH 3.5/PAA 3.5) combination were indented to contact depths of 50-60 nm, and values of modulus and hardness identical to those shown in Figure 5-5 were obtained. Similarly the results on the 7.5/3.5 and 6.5/6.5 PAH/PAA PEM systems were cross-checked and corroborated using dynamic nanomechanical tests (Appendix B).

For PEMs constructed from weak polyelectrolytes like PAH and PAA, the molecular-level architectures are intimately connected with the pH of the polyelectrolyte assembly solutions, relative to their pKa values. The pKa values for PAH and PAA are approximately 9 and 5, respectively [5]. For the case of (PAH 6.5/PAA 6.5), the PEM films are assembled from solutions containing both polyelectrolytes in their fully charged state. The resulting film has a high density of ion-paired linkages [15]. Furthermore, at pH 6.5, both polyelectrolytes adsorb as highly charged, flattened and extended chains resulting in low incremental thicknesses of about 5 Å per adsorbed bilayer. The (PAH 7.5/PAA 3.5) architecture is formed by adsorption from solutions of partially charged polyelectrolytes; the selected pH values are close to the pKa value for both PAH and PAA. The deposited layers are relatively thick and loopy (thickness per bilayer ~ 80 Å), and the resulting internal structure is highly interpenetrated. PAH and PAA chains are both highly ionized in the interior of the film structure. For details about the formation of these structures, see references[15,33]. Finally, the (PAH 3.5/PAA 3.5) multilayer represents

the intermediate bilayer thickness regime (approximately 55 Å per adsorbed bilayer), with PAH being fully charged and PAA partially ionized at this combination [15]. To produce an approximately 100 nm-thick film, 20 bilayers were required at the 3.5/3.5 pH combination, compared with 140 bilayers for the case of PAH 6.5/PAA 6.5, and 8 for the PAH 7.5/PAA 3.5 assembly conditions. In all cases in Figure 5-5, PAA was the last adsorbed polyelectrolyte.

The hardness of a sample is defined as its resistance to plastic deformation. From Figure 5-5, it is evident that the hardness is highest for the (PAH 6.5/PAA 6.5) architectures, with a value of 1.5 GPa. The (PAH 7.5/PAA 3.5) films exhibit the least resistance to plastic deformation with a hardness of 0.76 GPa (See Figure 5-3 for the detailed hardness profile of this film). The modulus values for (PAH 3.5/PAA 3.5) and (PAH 6.5/PAA 6.5) assemblies are comparable within error; the loopy coil configurations of the (PAH 7.5/PAA 3.5) films are associated with the lowest values of modulus.

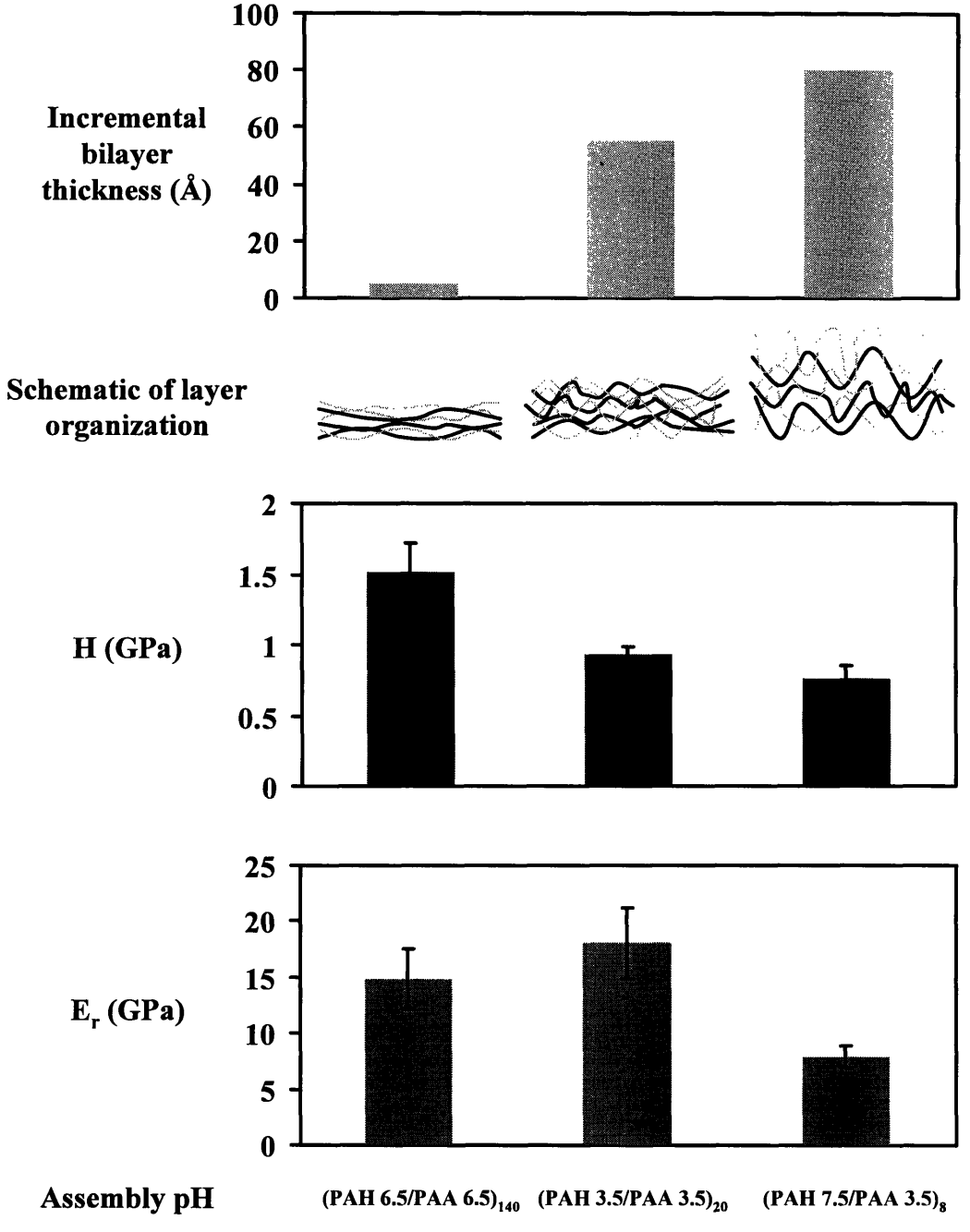

Figure 5-5 Incremental bilayer thicknesses [29], schematic structures, and measured hardness and effective modulus values for three assembly pH combinations; cube-corner indenter tip used for this study. Film thicknesses were 80-100 nm.

5.3.3 Comparison with Other Polymeric Systems

Table 5-2 compares the mechanical properties of the (PAH 7.5/PAA 3.5) PEM structures with those measured for thin spin-coated PMMA films. In addition, some literature values for elastic moduli and hardness of polystyrene (PS) [27], polycarbonate (PC) [27], and polytetrafluoroethylene (PTFE) [25] spin-coated films are presented. The comparisons in Table 5-2 are made with respect to the (PAH 7.5/PAA 3.5) system, which is associated with the lowest modulus and hardness values among the PAH/PAA pH combinations studied (see Figure 5-5).

Table 5-2 Comparison of mechanical properties of PEMs with those measured for spin-coated PMMA films and reported values for other polymer thin-films.

	Film	Approx. Thickness (nm)	h_c (nm)	H (GPa)	E_r (GPa)	Elastic Modulus (GPa)
1	$(PAH\ 7.5/PAA\ 3.5)_{600}$[#]	6000	316.3 ± 9.9	0.389 ± 0.025	12.64 ± 0.47	10.08-11.85[*]
2	PMMA[##]	2700	104 ± 4.5	0.30 ± 0.04	5.91 ± 0.2	5.23[**]
3	PC (ref. [28])					2.2
4	PS (ref. [28])					2.6
5	PTFE (ref. [24])			0.058		2.3

[#]A trapezoidal 33s-2s-33s loading function and a Berkovich indenter were used.

[##]A trapezoidal 5s-2s-5s loading function and a Berkovich indenter were used

[*]Calculated using a 0.25-0.45 range for Poisson's ratio

[**]Using a value of 0.34 for Poisson's ratio

5.3.4 Mechanical Behavior in Water

It is well known that the PEM structure swells in the presence of a hydrating or plasticizing medium. In the case of aqueous systems, the degree of swelling depends on pH and ionic strength. The amount of swelling for PAH/PAA films also depends

strongly on the assembly pH conditions [5,34,35] . To investigate the mechanical behavior of PEM films swollen in a liquid medium, (PAH 7.5/PAA 3.5) architectures were subjected to indentation while immersed in pH neutral water. The results are presented in Table 5-3. Rubner and co-workers [5] have reported thickness increases of 130% for this PEM architecture upon exposure to phosphate buffered saline at physiological pH. The hydrated structures exhibit modulus values that are about two orders of magnitude lower than the identical film in the dry state at ambient conditions (compare lines 1 and 3 of Table 5-3). This film architecture does not lose polyelectrolyte material (no soluble chains) at pH 7 so the observed reduction in modulus is not a result of network deterioration, but instead reflects the expected reduction in modulus associated with plasticization by a low molecular weight diluent. When covalent bonds replace some of the ionic crosslinks between PAH and PAA, the swollen structure exhibits a modulus that is significantly larger than the ionically crosslinked precursor film in pH 7 water, as seen from lines 3 and 4 of Table 5-3.

Table 5-3 Comparison of mechanical properties of PEMs with those measured for PMMA and reported values for other polymer thin-films.

	Film[#]	Surrounding medium	h_c (nm)	H (GPa)	E_r (GPa)
1	(PAH 7.5/PAA 3.5)	Air[*]	312.2	0.363	10.87
2	(PAH 7.5/PAA 3.5) Heated at 150 °C for 6 hours	Air	459.5 ± 2.8	0.432 ± 0.006	11.2 ± 0.37
3	(PAH 7.5/PAA 3.5)	pH 7 water	512.3 ± 69.2	0.014 ± 0.003	0.07 ± 0.02
4	(PAH 7.5/PAA 3.5) Heated at 150 °C for 6 hours	pH 7 water	445.7 ± 37.7	0.109 ± 0.016	0.41 ± 0.04

[#]All films were 6000 nm thick (600 bilayers). A cube-corner indenter tip with a 5s-2s-5s loading function was used in all cases

[*]Relative humidity 50 %; temperature 20 – 25 °C

5.4 Discussion

The PEM system that most closely resembles our PAH/PAA films, and that has also been studied in the context of mechanical properties, is the PAH/polystyrene sulfonate polyelectrolyte pair. In those studies [17-20], the PEM moduli were estimated from various observations on microcapsules. AFM deformation[17,18] of microcapsules produced estimates of modulus in the range of 0.001 to 0.1 GPa, while osmotic swelling[19] of similar systems led to values between 0.20 and 0.24 GPa. Another osmotic pressure study[20] of PAH/PSS microcapsules led to modulus values between 0.50 and 0.75GPa. These previous estimates of wet-state PAH/PSS moduli are consistent with the rubbery/leathery modulus values (0.07 and 0.41GPa) measured directly in this study via flat-film nanoindentation of our PAH/PAA PEMs in pH 7 water. The wet-state, flat film AFM study[23] of a significantly different PEM system (PAH/azo-benzene-containing polyanion) showed lower modulus values, 0.007GPa and below, while a fifty fold variation in modulus was observed, depending on the pH conditions used in the film assembly.

To our knowledge, the results reported here are among the first direct measurements of the mechanical properties of dry PAH/PAA PEMs through quasi-static nanoindentation. By carefully mapping E_r and H as a function of contact depth for these films (Figures 5-2 and 5-3), the mechanical properties have been determined without significant influence from the underlying glass substrate . Consistent with the previously mentioned AFM study [23], we found that the mechanical properties of our PEMs, constructed from the weak polyelectrolyte pair PAH and PAA, can be tuned by varying

the processing conditions. Manipulation of the assembly polyelectrolyte pH influences the chain conformation and the degree of interchain ionic crosslinking in the PEM structure; a two-fold variation in the hardness and modulus results (Figure 5-5).

Both the (PAH 7.5/PAA 3.5) and (PAH 6.5/PAA 6.5) architectures are associated with interpenetrated structures and high degrees of ion pairing between the parent polyelectrolytes[1,15]. While the chains of the (PAH 6.5/PAA 6.5) constructs exist in highly stretched chain conformations leading to low incremental bilayer thicknesses of 5 Å (see Figure 5-5), the (PAH 7.5/PAA 3.5) structures are thicker and loop-rich. The latter configuration can deform to accommodate the moving indenter tip with greater ease than the (PAH 6.5/PAA 6.5) system; this is reflected in the lowest values of modulus and hardness for the (PAH 7.5/PAA 3.5) systems. The (PAH 6.5/PAA 6.5) film exhibits the most stretched-out chain conformation, and thus a great degree of resilience, leading to the highest hardness values, although not the highest modulus. For the latter parameter, chain orientation should lead to high values of in-plane modulus, whereas the nanoindentation experiment measures a modulus that is transverse to the plane of chain extension. This may explain the relatively lower than expected value of modulus for the 6.5/6.5 films. The (PAH 3.5/PAA 3.5) architecture may be viewed as intermediate between the above two conformations; PAA is partially ionized and PAH is fully charged. This structure is associated with a hardness value between the two extremes, while the modulus is, within error, the same as the (PAH 6.5/PAA 6.5) films. Noting the remarkably high value of modulus for the PAA homopolymer (Table 5-1), the higher than expected modulus for the 3.5/3.5 film might arise from PAA enrichment that results when partially charged PAA is incorporated into the PEM to compensate the fully

charged PAH. Clearly the overall set of results demonstrates a complex interplay of ionic crosslink density, chain orientation, and PEM composition on the anisotropy and the mechanical behavior of the PEM films.

The ultra-thin PAH/PAA PEM films exhibit mechanical properties that are superior to some commercial polymers in thin-film form (see Table 5-2). The spin-coated PMMA film had a hardness and modulus value of 0.3 GPa and 5.2 GPa, respectively, compared to the corresponding values of 0.39 GPa and approximately 11 GPa for the (PAH 7.5/PAA 3.5) system. For PMMA, the hardness and modulus values obtained in this investigation for a 2700 nm thick film are higher than those obtained for bulk PMMA samples, studied via indentation. Pruitt and co-workers [30] reported a hardness value of 0.05 GPa and an elastic modulus of 3.8 GPa through nanoindentation of bulk PMMA. The molecular level structure of a spin-coated film may be significantly different from that of the bulk sample[36] . Stronger associations, due to hydrogen bonding interactions, have also been reported for thin polymer films that might contain trace amounts of residual solvent [37]. For PMMA films, a decreasing glass transition temperature with increasing film thickness has been observed [25].

It is interesting that the values of modulus and hardness for the multilayer structures can be higher than those of either parent polyelectrolyte. The mechanical response of the PEMs builds on the contribution of the dominant PAA component (See Table 5-1, lines 4, 7, and 8). The mechanical integrity of the PEM films is enhanced over that of the parent materials by the interpenetration and ionic stitching of the polyelectrolyte chains, leading to an entangled and crosslinked network that resists movement of the indenter tip through the structure. The detailed nature of the bonds that

crosslink the PAH and PAA does not significantly affect the mechanical response of the films at ambient conditions; E_r and H values are comparable for the as-assembled film (ionic crosslinks) and post thermal treatment (covalent bonds); see Table 5-1, lines 4 and 6. The properties are strongly influenced, however, by the conformations of the polyelectrolyte chains in the construct, an inherent function of the assembly PAH/PAA pH combination.

Thermally treating the films after assembly, however, significantly affects the mechanical response of the swollen structure in the presence of water (See Table 5-3). Covalent linkages limit swelling more than their ionic precursors. The reduced uptake of water and smaller degree of swelling results in larger values of E_r and H for the chemically crosslinked films compared to the ionically crosslinked counterparts (Table 5-3, lines 3 and 4). When swollen, however, both the as-assembled and thermally treated films have modulus and hardness values that are much lower than their counterparts in the dry state; the modulus values for the swollen, ionically-crosslinked films are on the same order of magnitude as those for various rubber-like materials [38].

PAH/PAA PEMs have been used as nanoreactors for the *in-situ* synthesis of metallic and semiconducting nanoparticles [39]. Also it is known that surfaces of these PEMs can be modified through the use of block copolymer-capping agents [33] and that layer-by-layer assembly can be used to create nanocomposites containing clay particles, carbon nanotubes [40], nanocrystalline materials, graphite oxide and other nanocolloids.[41] . Advincula and co-workers[26] have studied the mechanical properties of polyelectrolyte/clay multilayer films through nanoindentation, and they reported modulus and hardness values of 9.5 GPa and 0.46 GPa, respectively, for their structures.

Nanoindentation studies on block copolymer-modified PEM structures, silver nanoparticle-containing PAH/PAA PEMs, and on PAH/carbon nanotube composites can be found in a previous publication (Chapter 4 and ref. 42), in which effective modulus values in the range of 1-20 GPa are reported.

5.5 Conclusions

The mechanical properties of layer-by-layer films composed of weak polyelectrolytes PAH and PAA were elucidated using quasi-static nanoindentation in a range of instrument operation and specimen thickness where the elastic modulus and hardness of the films were demonstrably free of the influence of the underlying supporting material. The mechanical properties of these ultra-thin PEM films can be altered significantly by varying the pH of the PAH and PAA assembly solutions. All of the PEM films exhibited modulus values that were larger than those of spin-coated films of commercial polymers, including PMMA.

Some of the PEMs are mechanically superior to either parent polyelectrolyte. In the dry state, the PEM properties are virtually unaffected by whether the linkages between the functional groups of the parent polyelectrolytes are ionic or covalent in nature. The essence of mechanical strength of PEMs lies in the high density of linkages in the film. The modulus values of these interpenetrated polyelectrolyte structures in the swollen state (in water) are about two orders of magnitude lower than the corresponding values in dry conditions; in the swollen state, chemical crosslinks do augment the modulus values owing to the smaller amount of water uptake in crosslinked films.

5.6 References

(1) Decher, G.; Schlenoff, J. B., Eds. *Multilayer thin films: Sequential assembly of nanocomposite materials*; Wiley-VCH Verlag GmbH & Co. KGaA: Weinheim, 2003.

(2) Caruso, F.; Sukhorukov, G. In *Multilayer thin films*; Decher, G.; Schlenoff, J. B., Eds.; Wiley-VCH Verlag GmbH & Co. KGaA: Weinheim, 2003.

(3) Mohwald, H.; Donath, E.; Sukhorukov, G. In *Multilayer thin films*; Decher, G.; Schlenoff, J. B., Eds.; Wiley-VCH Verlag GmbH & Co. KGaA: Weinheim, 2003.

(4) Caruso, F.; Trau, D.; Mohwald, H.; Renneberg, R. *Langmuir* **2000**, *16*, 1485-1488.

(5) Mendelsohn, J. D.; Yang, S. Y.; Hiller, J.; Hochbaum, A. I.; Rubner, M. F. *Biomacromolecules* **2003**, *4*, 96-106.

(6) Mendelsohn, J. D.; Yang, S. Y.; Hochbaum, A. I.; Colson, C. D.; Rubner, M. F. *Abstr. Pap. Am. Chem. Soc.* **2002**, *223: 397-COLL.*

(7) Wang, T. C.; Cohen, R. E.; Rubner, M. F. *Abstr. Pap. Am. Chem. Soc.* **2002**, *223: 275-POLY.*

(8) Wang, T. C.; Cohen, R. E.; Rubner, M. F. *Adv. Mater.* **2002**, *14*, 1534-1537.

(9) DeLongchamp, D. M.; Hammond, P. T. *Abstr. Pap. Am. Chem. Soc.* **2002**, *223:286-POLY.*

(10) DeLongchamp, D. M.; Hammond, P. T. *Abstr. Pap. Am. Chem. Soc.* **2002**, *223: 114-COLL.*

(11) DeLongchamp, D. M.; Kastantin, M.; Hammond, P. T. *Chem. Mater.* **2003**, *15*, 1575-1586.

(12) Pavoor, P. V.; Gearing, B. P.; Bellare, A.; Cohen, R. E. *Wear*, **2004**, *256*, 1196-1207.

(13) Pavoor, P. V.; Gearing, B. P.; Bellare, A.; Cohen, R. E. *Abstr. Pap. Am. Chem. Soc.* **2002**, *224:125-PMSE.*

(14) Graul, T.; Schlenoff, J. B. *Anal. Chem.* **1999**, *71*, 4007-4013.

(15) Shiratori, S. S.; Rubner, M. F. *Macromolecules* **2000**, *33*, 4213-4219.

(16) Hsieh, M. C.; Farris, R. J.; McCarthy, T. J. *Abstr. Pap. Am. Chem. Soc.* **1999**, *218: 59-PMSE.*

(17) Lulevich, V. V.; Radtchenko, I. L.; Sukhorukov, G. B.; Vinogradova, O. I. *Macromolecules* **2003**, 36, 2832 - 2837.

(18) Lulevich, V. V.; Radtchenko, I. L.; Sukhorukov, G. B.; Vinogradova, O. I. *J.Phys.Chem B* **2003**, 107, 2735-2740.

(19) Vinogradova, O. I.; Andrienko, D.; Lulevich, V. V.; Nordschild, S.; Sukhorukov, G. B. *Macromolecules* **2004** 37, 1113 - 1117.

(20) Gao, C.; Donath, E.; Moya, S.; Dudnik, V.; Mohwald, H. *Eur. Phys. J. E* **2001**, *5*, 21-27.

(21) Gao, C.; Leporatti, S.; Moya, S.; Donath, E.; Mohwald, H *Langmuir*, **2001**, 17, 3491-3495.

(22) Baumler, H.; Artmann, G.; Voigh, A.; Mitlohner, R.; Neu, B.; Kiesewetter, H, *J.Microencapsualtion* **2000** 17, 651-655

(23) Mermut, O.; Lefebvre, J.; Gray, D. G.; Barrett, C. J. *Macromolecules* **2003**, *36*, 8819-8824.

(24 Fischer-Cripps, A. C. *Nanoindentation*; Springer-Verlag New York, Inc.: New York, 2002.

(25) Wang, J.; Shi, F. G.; Nieh, T. G.; Zhao, B.; Brongo, M. R.; Qu, S.; Rosenmayer, T. *Scripta Mater.* **2000**, *42*, 687-694.

(26) Fan, X.; Park, M.; Xia, C.; Advincula, R. *J. Mater. Res.* **2002**, *17*, 1622-1633.

(27) Du, B.; Tsui, O. K. C.; Zhang, Q.; He, T. *Langmuir* **2001**, *17*, 3286-3291.

(28) VanLandingham, M.R.; McKnight, S.H.; Plamese, G.R.; Elings,J.R.; Huang,X.; Bogetti, T.A.; Eduljee, R.F.; Gillespe, Jr., J.W. *J. Adhesion* **1997**, 64, 31-59.

(29) Yoo, D.; Shiratori, S. S.; Rubner, M. F. *Macromolecules* **1998**, *31*, 4309-4318.

(30) Klapperich, C.; Komvopoulos, K.; Pruitt, L. *Journal of Tribology* **2001**, *123*, 624-631.

(31) Oliver, W. C.; Pharr, G. M. *J. Mater. Res.* **1992**, *7*, 1564-1583.

(32) Harris, J. J.; DeRose, P. M.; Bruening, M. L. *J. Am. Chem. Soc.* **1999**, *121*, 1978-1979.

(33) Choi, J.; Rubner, M. F. *J. Macromol. Sci.-Pure Appl. Chem.* **2001**, *A38*, 1191-1206.

(34) Dubas, S. T.; Schlenoff, J. B. *Langmuir* **2001**, *17*, 7725-7727.

(35) Hiller, J. A.; Mendelsohn, J. D.; Rubner, M. F. *Nature Materials* **2002**, *1*, 59-63.

(36) Prest, W. M.; Luca, D. J. *Journal of Applied Physics* **1980**, *51*, 5170-5174.

(37) Frank, C. W.; Rao, V.; Despotopoulou, M. M.; Pease, R. F. W.; Hinsberg, W. D.; Miller, R. D.; Rabolt, J. F. *Science* **1996**, *273*, 912-915.

(38) Wood, L. A. In *Polymer Handbook*; Brandrup, J.; Immergut, E. H., Eds.; John Wiley & Sons, Inc.: New York, 1989.

(49) Joly, S.; Kane, R.; Radzilowski, L.; Wang, T.; Wu, A.; Cohen, R. E.; Thomas, E. L.; Rubner, M. F. *Langmuir* **2000**, *16*, 1354-1359.

(40) Mamedov, A. A.; Kotov, N. A.; Prato, M.; Guldi, D. M.; Wicksted, J. P.; Hirsch, A. *Nature Materials* **2002**, *1*, 190-194.

(41) Kotov, N. A. In *Multilayer thin films*; Decher, G.; Schlenoff, J. B., Eds.; Wiley-VCH Verlag GmbH & Co. KGaA: Weinheim, 2003.

(42) Pavoor, P. V.; Gorga, R. E.; Gearing, B. P.; Bellare, A.; Cohen, R.E. *Journal of Appl. Polym. Sci.*, **2004**, *92*, 439 -448.

Chapter 6 Conclusions and Recommendations for Future Work

This thesis has explored the use of polyelectrolyte mutilayers (PEMs), composed predominantly of poly(allylamine hydrochloride) (PAH) and poly(acrylic acid) (PAA), for tribological applications. In addition to fundamental characterization of the friction-and-wear behavior of these conformal nanocoatings, the purpose of the work has been to evaluate the merit of their use in areas of practical tribological relevance–orthopedic implants and MEMS devices. The latter application motivated the modification of the native films to tune their frictional response. The thesis has also elucidated the mechanical properties of these multilayer structures through nanoindentation; the elicited values of modulus and hardness were successfully used to explain the observed tribological response of the films.

Chapter 2 discussed the friction-and-wear behavior of PEM-coated materials, primarily using a meso/micro-scale flexure-based apparatus. The friction coefficient of film-coated steel substrates against glass was higher than that exhibited by the bare substrates at all stresses; the average value decreased with an increase in the applied normal load, a trend predicted for polymeric materials. PEM constructs prevented wear of steel substrates in the dry state, and also in the presence of water and bovine calf serum, used to simulate synovial fluid in human joints. At these higher stresses, the delaminated film fragments prevented contact between, and deformation of, the mating surfaces, thus eliminating substrate wear. The adhesion, deformation, and dragging of the fragments caused the friction force to be higher than the bare substrates (prior to the onset of their

wear). Wear was prevented without a substantial increase in friction force by using thinner films on the larger slider surface or coating the smaller pin counterface. The capacity for PEM-induced wear reduction was corroborated at larger scales of testing in the dry state using a pin-on-disk tester.

The potential for wear reduction in total joint replacement prostheses was addressed in Chapter 3. PEM stability in joint fluid was demonstrated to be a key variable driving the choice of polyelectrolyte pair and film assembly conditions (pH combination). Wear tests, carried out at clinically-relevant conditions of loading, articulating bearing surfaces, surrounding medium, and number of cycles, revealed a 45 % reduction in weight loss, in the best case, for PEM-coated systems.

Chapter 4 evaluated three strategies for reducing the coefficients of friction associated with PEMs at low normal stress, while retaining their wear-retarding properties at high normal loads. Anchoring polystyrene-block-poly(acrylic acid) to the PAH surface of a multilayer film, less than 10 nm thick, enhanced the hardness, and hence the load-bearing capacity of these structures. The effect of surface capping was most pronounced at high normal stresses, where substantial wear prevention was observed, accompanied by low friction forces. The second strategy used the *in-situ* synthesis of silver nanoparticles in the PEM matrix for friction reduction. Optimum levels of silver loading were required (at the surface) to reduce the friction forces. Finally, multilayer composites were constructed using PAH and multi-wall carbon nanotubes. These assemblies exhibited the lowest values of friction among the strategies studied, at all levels of stress; in addition, substrate wear prevention was also achieved.

The tribological behavior of the PEM-modification strategies was correlated with the mechanical properties of the films, elicited via nanoindentation.

Fundamental mechanical characterization of PAH/PAA PEMs, and the effect of processing conditions on film modulus and hardness, was the object of Chapter 5. Nanoindentation was employed for the mechanical probing of PEM films, at penetration depths that precluded the influence of the stress fields associated with the underlying substrate. The mechanical properties of these films were shown to be readily tuned by manipulating the processing conditions (PAH/PAA pH combination) during assembly. The mechanical properties of PEMs were superior to the parent polyelectrolytes, and commonly used polymeric systems like PMMA, PTFE, and PC. This chapter studied the behavior of the as-assembled ionically-stitched films and their chemically crosslinked counterparts, at ambient conditions and also in the presence of a liquid medium.

To our knowledge, these are the first systematic and detailed measurements of these multilayer structures with respect to their tribological and mechanical properties. The work has attempted to lay the foundations and demonstrate the potential of these versatile polymeric systems in applications that might exploit their mechanical strength or their wear-retarding properties.

Recommendations for Future Research:

1. The adhesion of PEMs to the substrate deserves quantification. Nanoindentation and scratch testing are useful tools that allow the probing of the film-substrate interfacial response. Increasing film adhesion is likely to improve the tribological response through an enhanced resistance to delamination at high normal stresses; stronger plasma

treatments, or covalent bonding of the film to the substrate are possible methods to improve adhesion. Engineering film failure at a desired interface by introducing a "defect" into the film structure offers a means of avoiding delamination at the film-substrate interface. By introducing a weakly-bonded interface within the film bulk, delamination can be induced along a plane within the film instead of at the film-substrate interface. Such a system could be designed to have the remnant film take up polyelectrolytes from the surrounding medium (e.g. proteins from joint fluid), thus exhibiting material renewal characteristics. Introducing a single silver nanoparticle-containing PAH/PAA bilayer in a structure otherwise composed of strong polyelectrolytes is one idea for introducing such a "defect" (for reference, see Wang T.C., PhD Thesis, Chemical Engineering, MIT, p. 73)

2. This thesis has used the *in-situ* synthesis of silver nanoparticles in the PEM matrix as a model system to study the effect of embedded nanoclusters on friction and wear; it is not clear if the chemical nature of the particles plays a role. The general scheme of nanoparticle synthesis within PAH/PAA multilayers might be extended to incorporate commonly used Group V, VI dichalcogenide solid lubricants like molybdenum disulfide, tungsten disulfide, and calcium fluoride.

3. The PAH/carbon-nanotube composites in this thesis exhibited low modulus and hardness values, and subsequently less resistance to shear, leading to low friction coefficients. It might be interesting to assemble PAH/PAA films, with acid-treated nanotubes dispersed in PAA, instead of water (like those assembled for this thesis work). PAA has been shown to dominate the mechanical contribution to the multilayer system. A nanotube-containing PAH/PAA composite would be expected to demonstrate high

hardness values, thus resisting asperity penetration and plowing, in addition to exhibiting a carbon-containing surface; this system is likely to exhibit tribological merit (see preliminary results in Appendix C). The unused –COOH groups of PAA, depending on the assembly pH combination, might be further utilized for the loading of metallic nanoparticles, as discussed in Chapter 4 of this thesis. The resulting composite metal and carbon-nanotube-containing structure can be studied for its friction-and-wear and electrical properties (see footnote on Pg. 80). The layer-by-layer deposition can be extended to other dispersions to assemble structures containing clay platelets or graphite nanoparticles, which might exhibit tribological merit.

4. While this work has addressed surface capping of PAH/PAA PEM structures with the PS-PAA block copolymer to increase the hardness and reduce the wear rates, the choice of capping agent was not optimized. Other block copolymers might serve to provide higher increments of hardness when capped on to the multilayer structure. Further capping the block co-polymer with short hydrocarbon chains, possibly fluorinated, might serve to facilitate orientation during sliding, leading to further reduction in friction coefficients.

5. For all the above strategies, in addition to the friction-and-wear response, it is important to quantify film stiction. Stiction can be characterized using an atomic force microscope in contact mode. In addition, the AFM, and also the Triboindenter®, can be used for nano-wear experiments; potential alignment of the nanotube-containing composites during sliding, and the role of metallic nanoclusters synthesized in the PEM matrix with respect to friction, might be better understood using these instruments.

6. In the biological arena, further testing at clinically-relevant scales is recommended to establish the merit of these systems for wear reduction in total joint replacements. Potential variables for optimization are choice of polyelectrolyte pair, processing conditions, film thickness, film adhesion, and degree of chemical crosslinking. Finally, the biological response to PEM fragments that leave the interface during articulation might have to be addressed.

7. Future research in analyzing the mechanical behavior of PEMs should focus on obtaining a detailed modulus-hardness-PAH/PAA pH map (similar to Figure 5-5). This map will provide additional parameters to guide the choice of assembly conditions for a particular application. In addition to quasi-static and dynamic mechanical measurements on a nanoindenter, bulk tensile tests on thin film samples are recommended to corroborate the indentation measurements and elicit possible anisotropy in mechanical response. All these measurements could serve as inputs to (computer-aided) simulations of the mechanical response of PEMs, in the effort to enhance fundamental understanding about the assembled layer-by-layer structures.

Appendix A Scratch Tests on PEM-coated Polyethylene Substrates

Scratch testing on uncoated and polyelectrolyte multilayer (PEM)-coated polymer substrates was performed using a micro-scratch tester operated within a scanning electron microscope (SEM); the apparatus is described in detail in ref. 1. Ultra-high molecular weight polyethylene (UHMWPE) slides, 1 mm thick, were coated with 1.3 μm-thick (PAH 3.5/PAA 3.5) PEM films (245 bilayers); the nomenclature is defined in Chapter 2. A schematic of the test setup is depicted in Figure A-1. The surface being viewed (see Figure A-1) was coated with a 20-60 nm-thick gold film to facilitate conduction of electrons. The SEM was operated in high vacuum mode.

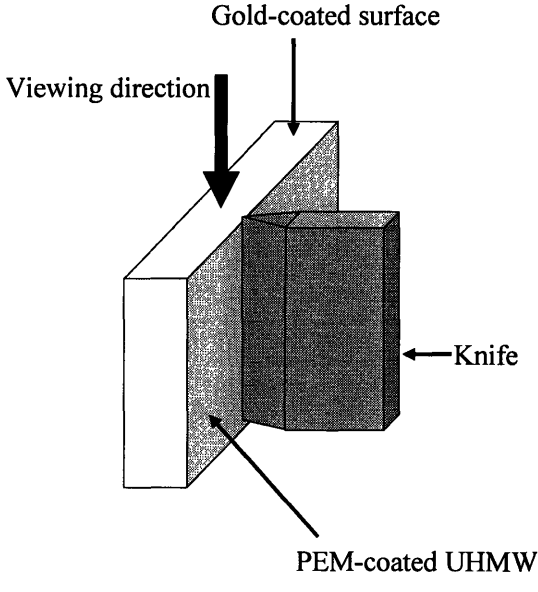

Figure A-1 Schematic of test setup in micro-scratch tester (adapted from ref. 1)

Figure A-2 compares force profiles for the bare and coated UHMWPE systems. Corresponding micrographs for the coated system, as the test proceeds, are depicted in Figure A-3. In both cases, the sample was indented with a stainless steel wedge-shaped knife (tip radius approximately 6 μm) up to a normal load of 5 N; this corresponded to an approximate indentation depth of 40 μm. The knife was subsequently moved tangentially to scratch the surface. A certain minimum tangential force is required to initiate scratching (material removal); the initiation point is represented as "A" in Figure A-2. This value of tangential force is characteristic of the system being tested. The negative value of force is the result of the sign convention system used. While the tangential force exhibits a rise prior to scratch initiation, the normal force, which is not controlled, decreases. Once material removal has begun, both the normal and tangential forces stabilize at slightly lower values. Finally, the knife is pulled back (not shown in Figure A-2).

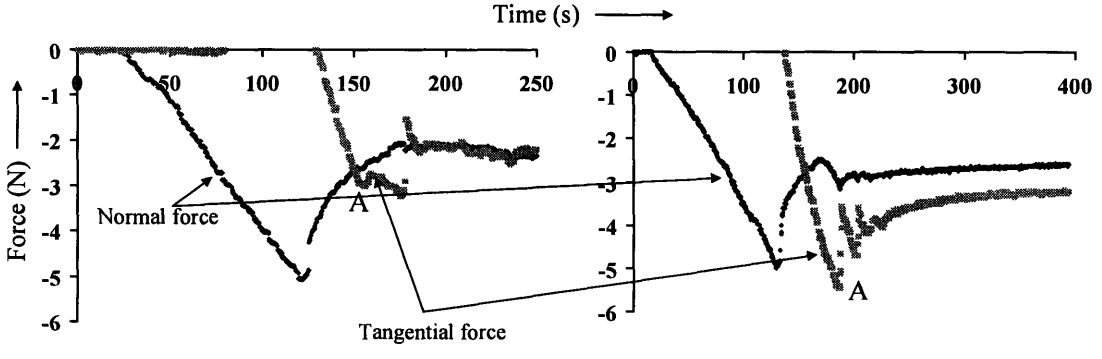

Figure A-2 Normal and tangential force profiles for uncoated UHMWPE (left) and 1 μm PEM-coated UHMWPE (right). "A" is point of scratch initiation (material removal).

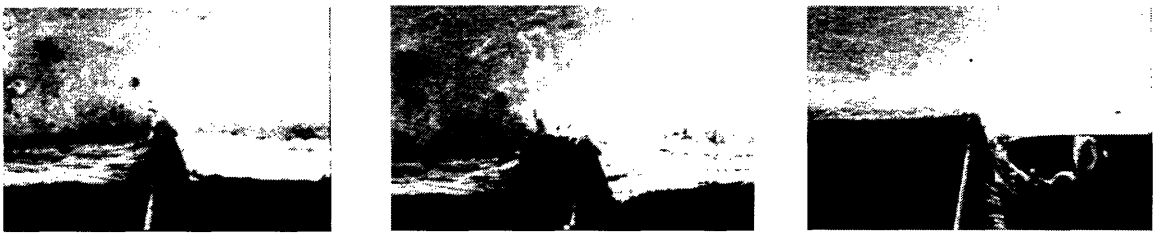

Figure A-3 SEM micrographs depicting evolution of the test for PEM-coated UHMWPE. Initial penetration depth is approximately 40 μm.

From Figure A-2 it is clear that the film-coated polymer required a tangential force almost 80% as high as that for the uncoated system to initiate material removal (point A), at identical values of normal forces (~ 3 N) and initial penetration depths (~ 40 μm). The larger tangential forces reflect a higher *scratch resistance* for the PEM-coated substrates.

References

1. Qi, H. *Mechanics of abrasive wear of elastomeric* materials, PhD Mechanical Engineering, MIT, 2003

Appendix B Dynamic Mechanical Analysis of Polyelectrolyte Multilayers

This appendix contains excerpts of a report from Hysitron, Inc. (Minneapolis, MN) on the dynamic mechanical analysis of polyelectrolyte multilayer (PEM) constructs. Three samples were tested; their thickness and assembly conditions are given below. In all cases, PAA was the last adsorbed polyelectrolyte.

Table B-1 List of samples subject to dynamic mechanical analysis

	Assembly conditions	Approx. thickness (nm)
Sample 1	(PAH 7.5/PAA 3.5)	6000
Sample 2	(PAH 6.5/PAA 6.5)	100-140
Sample 3	(PAH 7.5/PAA 3.5) *Heated at 150 °C, 6 hours*	6000

The Dynamic Mechanical Analysis (nanoDMA) technique is utilized for characterization of viscoelastic materials as a response to the insufficiencies in the legitimacy of quasistatic testing for materials that display significant time-dependant deformation and recovery. Figure B-1 shows the stiffness and damping from dynamic force and displacement. For viscoelastic materials, it is very difficult to obtain meaningful and accurate data using quasistatic testing due to the large effect that the choice of the loading function and the type of tip utilized will have on the measured properties due to creep and strain rate effects. Therefore, a dynamic method of characterizing materials on the nanoscale has been developed that provides the

augmented sensitivity for determining the stiffness and damping of a larger range of materials.

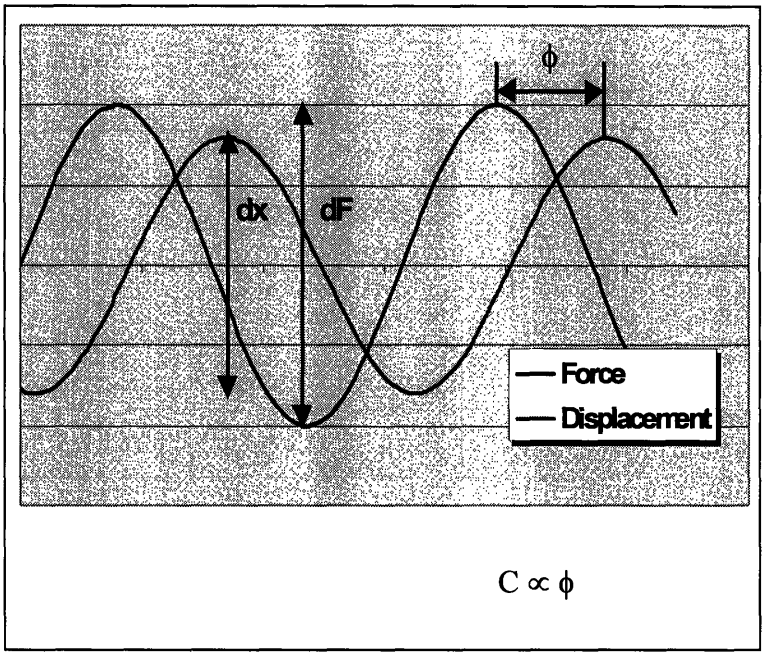

Figure B-1 Stiffness and damping from dynamic force/displacement

Additionally, in the case of viscoelastic materials, it is desirable to have the capability of characterizing both components of the complex modulus, the storage and the loss modulus. It is very challenging and time consuming to accurately quantify the complex modulus of polymeric materials using quasistatic techniques, requiring numerous tests and copious amounts of analysis. Standard analysis methods of quasistatic nanoindentation load/displacement data assume purely elastic/plastic material behavior, particularly during the loading and unloading portions of the test. This assumption ignores viscoelastic effects that exist throughout the entirety of the indentation test. The most commonly accepted quasistatic analysis, proposed by Oliver and Pharr (1992), measures stiffness by calculating the slope of the initial portion of the unloading curve. This analysis assumes that all recovery observed during the unloading

is elastic recovery, which is true for most ceramics and metals. However, most polymers show strongly viscoelastic behavior, which implies a time-dependant recovery. Therefore the unloading portion of the load/displacement data is a convolution of elastic and viscoelastic recovery, rendering it nearly impossible to calculate a true modulus.

Any dynamic system can be considered as a like the one observed in Figure B-2 that consists of elements that provide a means for storing potential energy –springs or elastic elements-, a means for storing kinetic energy-mass or inertia elements- and a means for dissipating energy-dampers or dash pots. When a dynamic test is being performed, the system that is effectively being measured is a total system of the mechanics of the indenter and the mechanical properties of the specimen. Therefore, in order to accurately measure the stiffness and damping properties of the specimen, one must have precise knowledge of the dynamic properties of the measurement system.

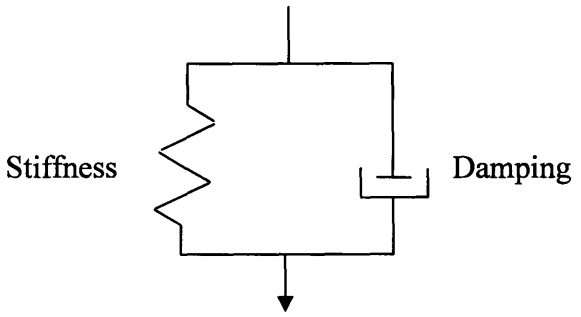

Figure B-2 Kelvin model for viscoelastic systems

If the tip is hanging free in the air and out of contact with a sample, the measured response from a dynamic test is indicative of the dynamic characteristics of the indenter. As seen in Figure B-3, a frequency sweep through the resonance peak of the system provides the necessary information to obtain the stiffness and damping of the system by

fitting the resonance curve to the response as predicted by the following derived equations.

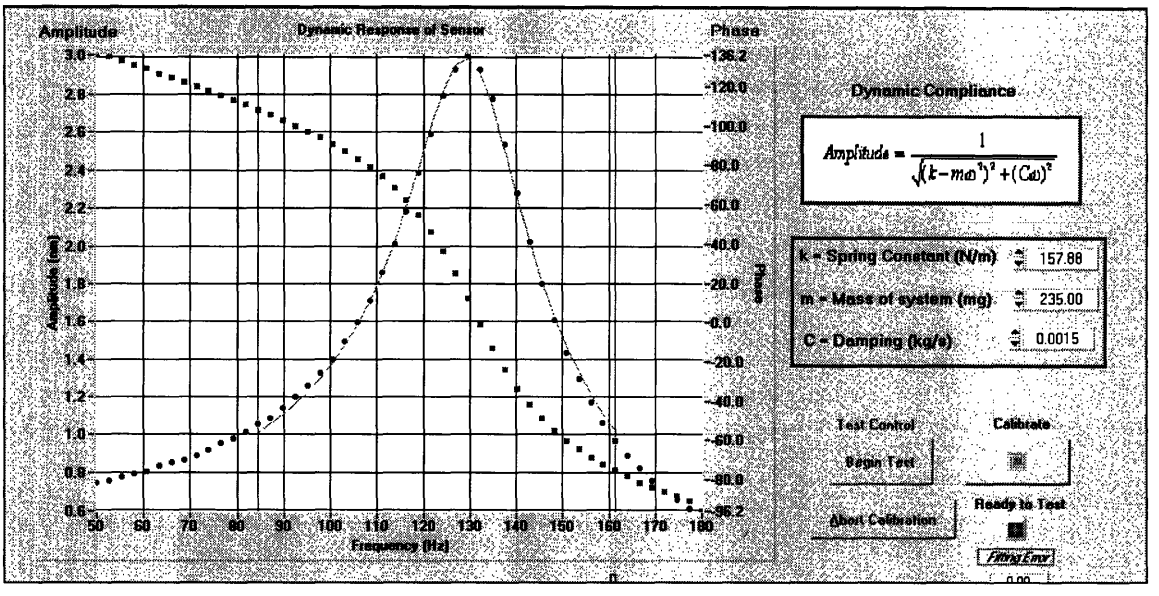

Figure B-3 Calibration of dynamic characteristics of transducer

The analysis of the dynamic test is derived from the classical equation for a single degree of freedom harmonic oscillator as given in equation 1 where F_0 is the magnitude of

Eq. 1. $$F_o \sin(\omega t) = \text{mx"} + C\text{x'} + k\text{x}$$

the sinusoidal force, ω is the frequency of the applied force, m is the mass, C is the damping coefficient and k is the stiffness of the system. The solution to this differential equation is seen as equation 2 where a displacement response is given for a given sinusoidal

Eq. 2.

$$X_o = \frac{F_o}{\sqrt{(k - m\omega^2)^2 + ((C_i + C_s)\omega)^2}}$$

force F_o, at a frequency ω, for a system with a given stiffness, mass and damping. The phase difference between the force and the displacement is given in equation 3.

Eq. 3.

$$\phi = \tan^{-1} \frac{(C_i + C_s)\omega}{k - m\omega^2}$$

The subscripts in Equations, i and s stand for indenter and sample respectively. By assuming a linear viscoelastic response, these equations can be used to calculate the stiffness and damping of a system from the displacement amplitude and phase lag. The stiffness and damping can in turn be used to calculate the storage modulus, loss modulus and tan delta using equations 4a-c.

Eq. 4 a)

$$E' = \frac{k_s \sqrt{\pi}}{2\sqrt{A_c}}$$

b)

$$E'' = \frac{\omega C_s \sqrt{\pi}}{2\sqrt{A_c}}$$

c)

$$\tan\delta = \frac{\omega C_s}{k_s}$$

The contact area that is used to calculate the moduli is obtained in a similar manner to the quasistatic testing technique, in that it is calculated from results from a test performed on a standard with a known modulus.

Samples 1, 2 and 3 were tested dynamically via the nano Dynamic Mechanical Analysis (nanoDMA) technique (results from quasistatic tests are presented in Chapter 5). On Sample 1 two frequency sweep tests were conducted over a frequency range of 10Hz to 250Hz, with a 30μN quasi-static (DC) load and a 2.0μN dynamic (AC) load;

based on quasistatic test data (Chapter 5), penetration depths are expected to be in the 20-30 nm range. Two load sweep tests were performed on sample 1 at a frequency of 40Hz with a quasi-static (DC) load from 5 to 50μN and a dynamic (AC) load of 1.5μN. This test was performed with a variable dynamic force in order to maintain an approximately constant displacement amplitude

On Sample 2 two frequency sweep tests were conducted over a frequency range of 10Hz to 250Hz, with a 4μN quasi-static (DC) load and a 0.25μN dynamic (AC) load; from Chapter 5, corresponding penetration depths are expected to be about 8-10 nm. Two load sweep tests were performed on sample 2 at a frequency of 40Hz with a quasi-static (DC) load from 5 to 50μN and a dynamic (AC) load of 4.5μN. This test was performed with a variable dynamic force in order to maintain an approximately constant displacement amplitude.

For Sample 3, two frequency sweep tests were conducted over a frequency range of 10Hz to 250Hz, with a 10μN quasi-static (DC) load and a 0.3μN dynamic (AC) load; penetration depths were about 20-30 nm. Two load sweep tests were performed at a frequency of 40Hz with a quasi-static (DC) load from 5 to 50μN and a dynamic (AC) load of 0.1μN. This test was performed with a variable dynamic force in order to maintain an approximately constant displacement amplitude.

Figure B-4 is a plot of the average storage and loss modulus versus frequency for the frequency sweep tests performed on Sample 1. Figure B-5 is a plot of the average tan delta versus frequency for the frequency sweep tests performed on Sample 1. Figure B-6 is a plot of the average storage and loss modulus versus displacement for the load sweep

tests performed on Sample 1. Figure B-7 is a plot of the average tan delta versus displacement for the load sweep tests performed on Sample 1.

Figure B-8 is a plot of the average storage and loss modulus versus frequency for the frequency sweep tests performed on Sample 2. Figure B-9 is a plot of the average tan delta versus frequency for the frequency sweep tests performed on Sample 2. Figure B-10 is a plot of the average storage and loss modulus versus displacement for the load sweep tests performed on Sample 2. Figure B-11 is a plot of the average tan delta versus displacement for the load sweep tests performed on Sample 2.

Figure B-12 is a plot of the average storage and loss modulus versus frequency for the frequency sweep tests performed on Sample 3. Figure B-13 is a plot of the average tan delta versus frequency for the frequency sweep tests performed on Sample 3. Figure B-14 is a plot of the average storage and loss modulus versus displacement for the load sweep tests performed on Sample 3. Figure B-15 is a plot of the average tan delta versus displacement for the load sweep tests performed on Sample 3.

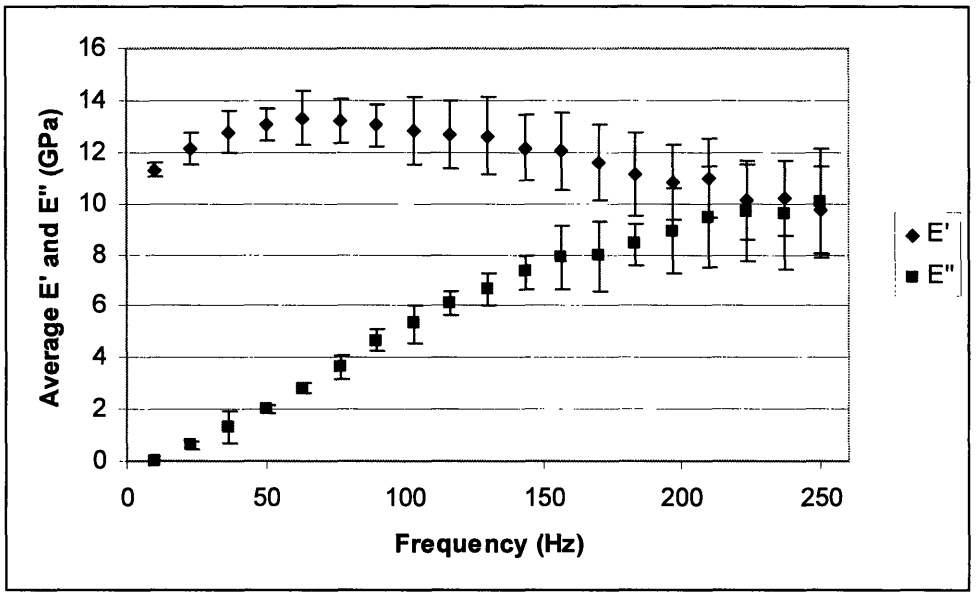

Figure B-4 Plot of average values of E' and E" vs. frequency for Sample 1.

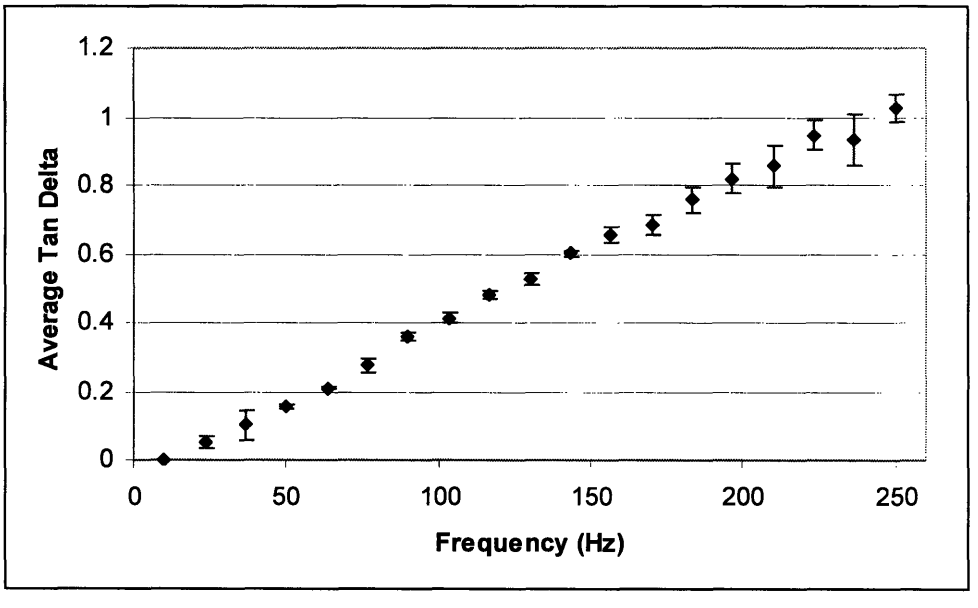

Figure B-5 Plot of average values of tan delta vs. frequency for Sample 1.

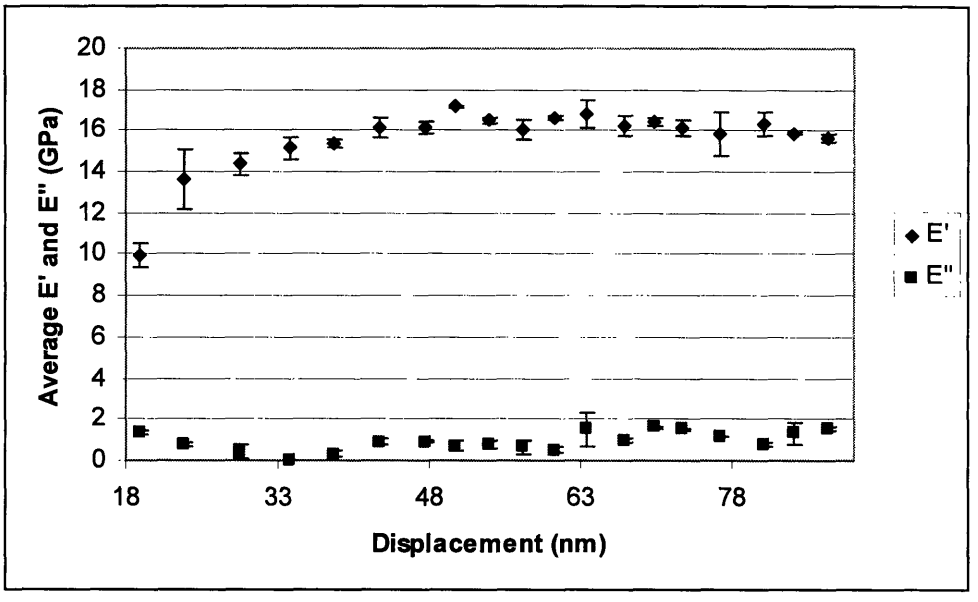

Figure B-6 Plot of average values of E' and E" vs. displacement for Sample 1.

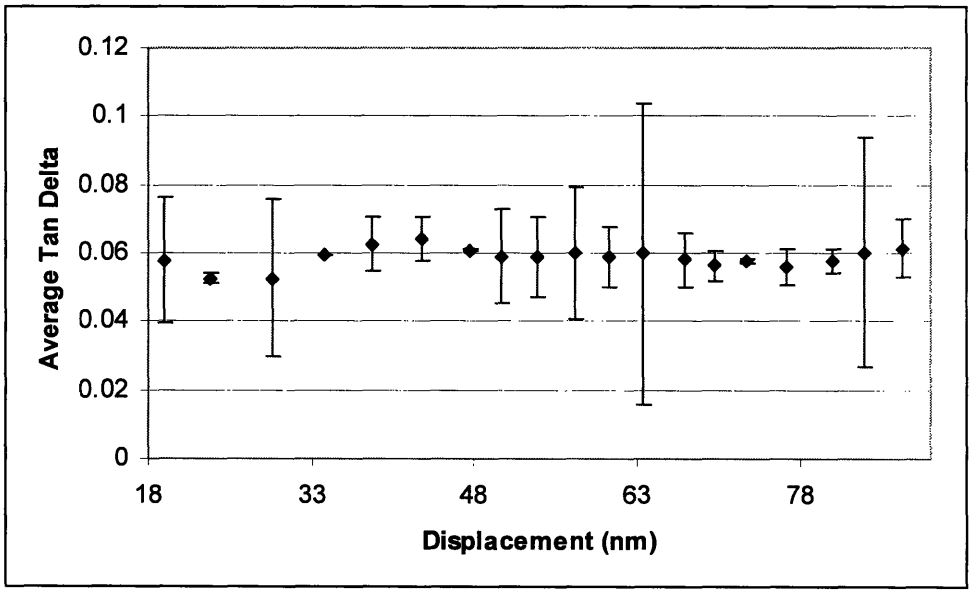

Figure B-7 Plot of average values of tan delta vs. displacement for Sample 1.

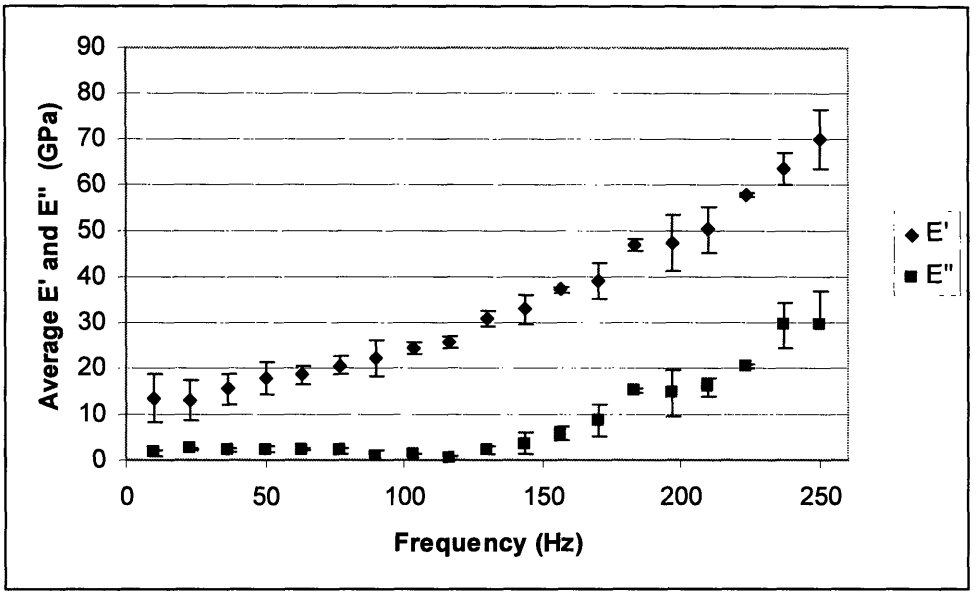

Figure B-8 Plot of average values of E' and E" vs. frequency for Sample 2.

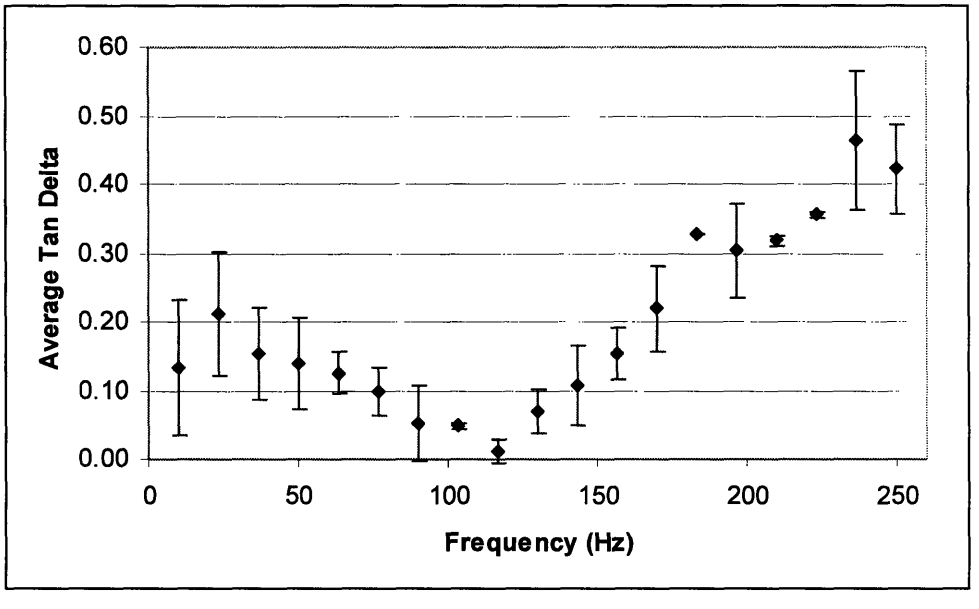

Figure B-9 Plot of average values of tan delta vs. frequency for Sample 2.

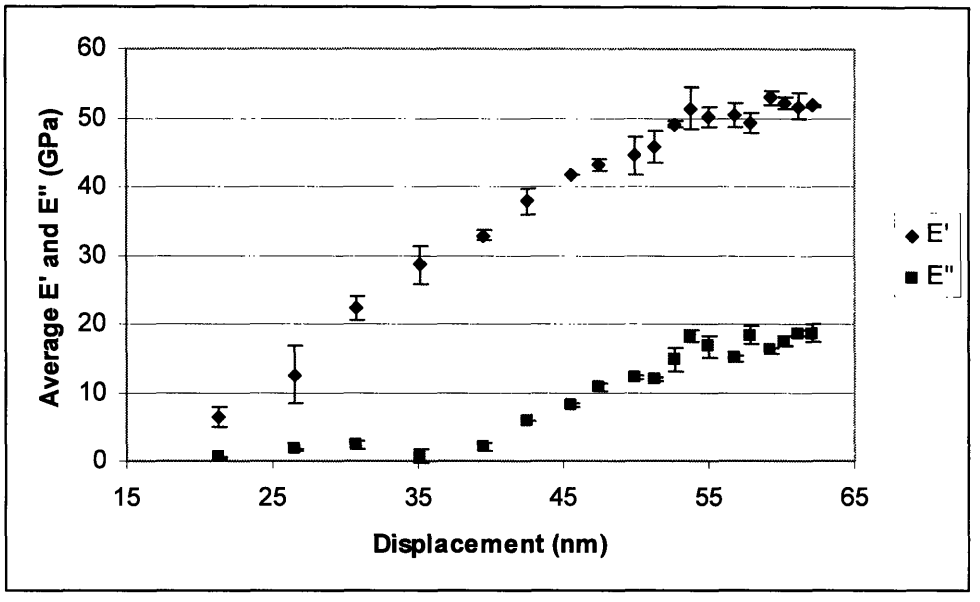

Figure B-10 Plot of average values of E' and E" vs. displacement for Sample 2.

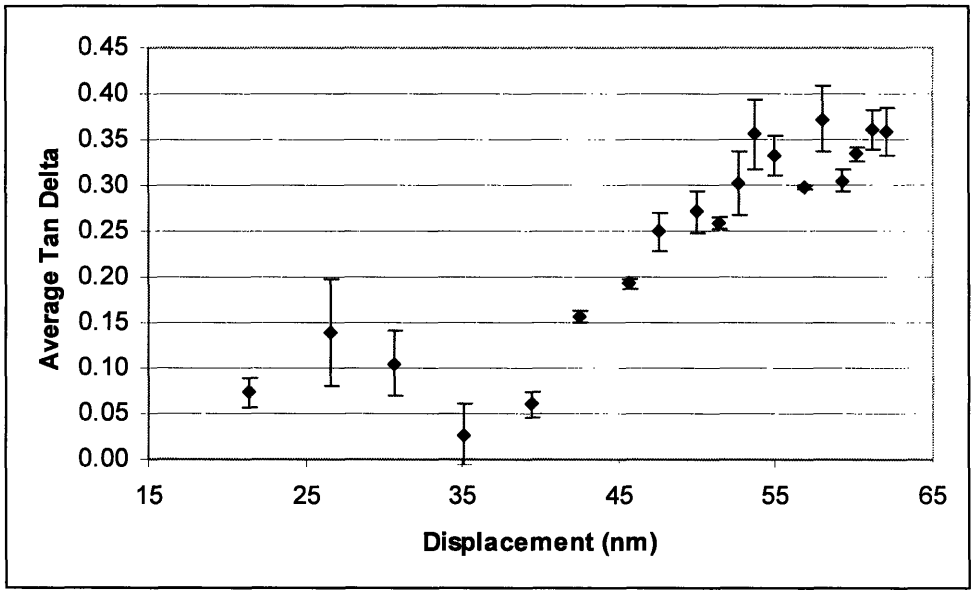

Figure B-11 Plot of average values of tan delta vs. displacement for Sample 2.

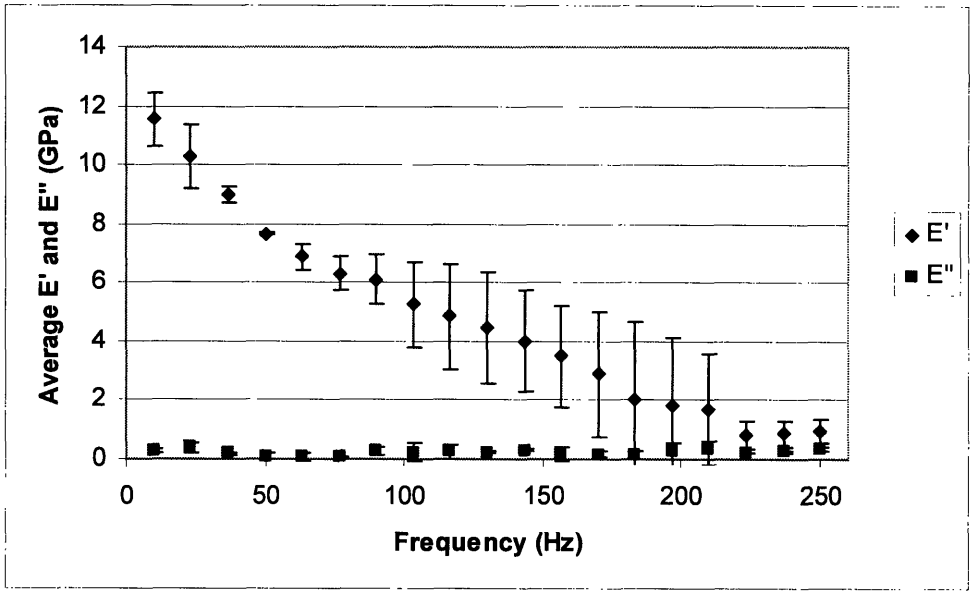

Figure B-12 Plot of average values of E' and E" for Sample 3.

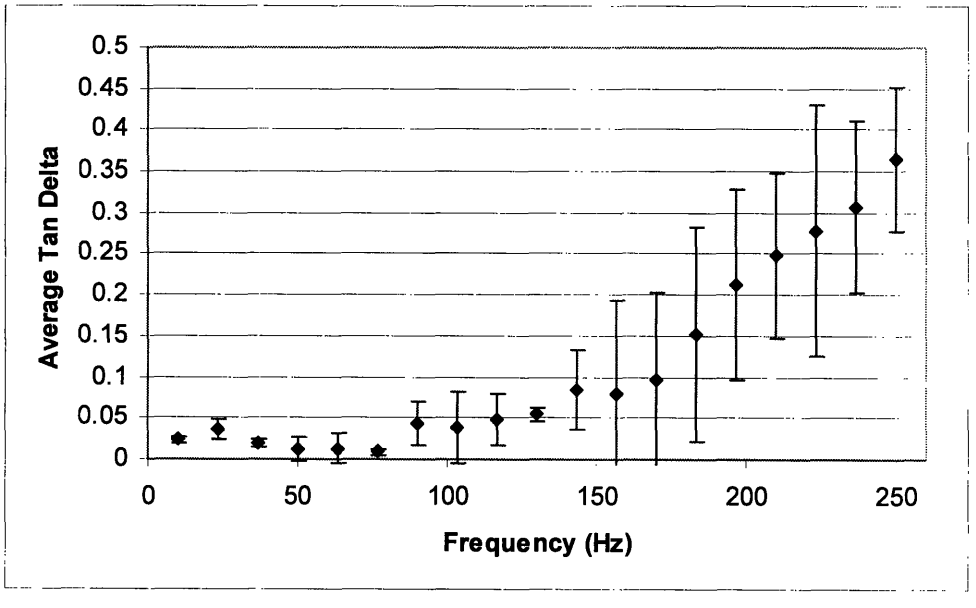

Figure B-13 Plot of average values of tan delta for Sample 3.

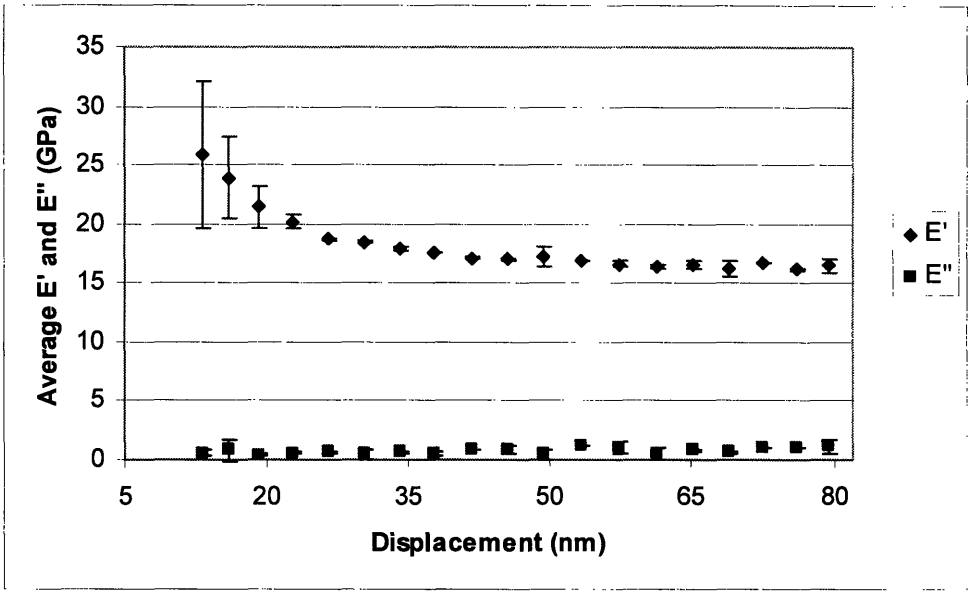

Figure B-14 Plot of average values of E' and E" for Sample 3.

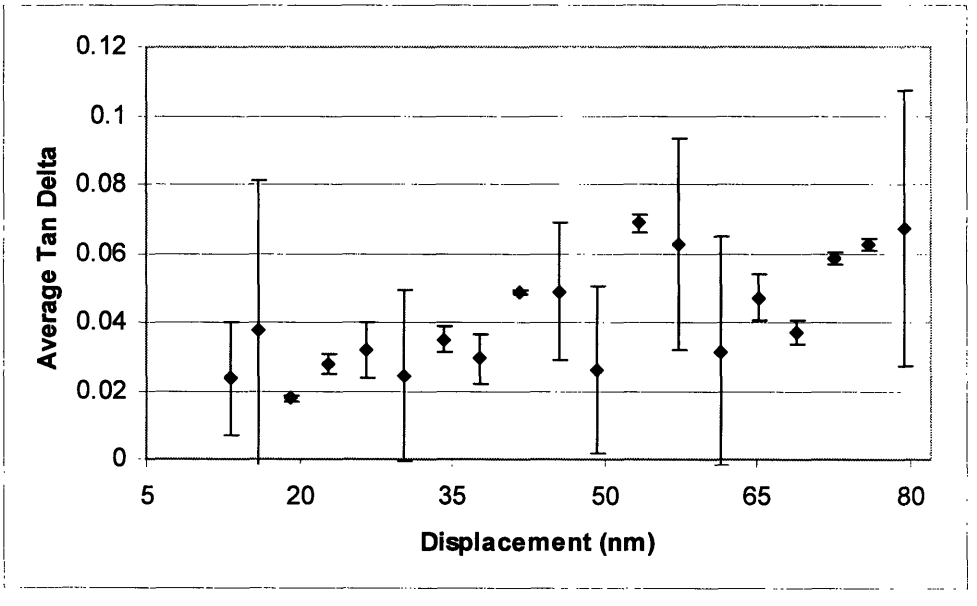

Figure B-15 Plot of average values of tan delta for Sample 3.

Appendix C Friction Coefficients for Additional Systems

The table below presents friction coefficients for additional PEM systems, on glass, silicon, and UHMWPE substrates. In all these tests, the uncoated and film-coated substrates were mounted on the lower slider (see Figure 2-3), and articulated against 1 or 2 mm diameter steel pins. Tests were carried out at ambient conditions; humidity levels were in the 20-40 % range.

Table C-1 Friction coefficients for additional PEM assemblies

No.	Substrate	Thickness (nm)	Normal Stress (MPa)	Average μ
1	UHMWPE	-	4	0.09
2	UHMWPE+(PAH 3.5/PAA 3.5)$_{15}$	62	4	0.13
3	UHMWPE+(PAH 3.5/PAA 3.5)$_{110}$	440	4	0.16
4	UHMWPE+(PAH 7.5/PAA 3.5)$_{8.5}$, PAH on top	82	4	0.14
5	UHMWPE+(PAH 7.5/PAA 3.5)$_9$, PAA on top	102	4	0.18
6	UHMWPE+(PAH 6.5/PAA 6.5)	96	4	0.15
7	UHMWPE+(PAH 3.5/PAA 3.5)$_{15}$+Ag	~65	4	0.18
8	Glass	-	0.25	0.44±0.24
9	Glass+(PAH 3.0/PSS 3.0)$_{20}$[$]	~10	0.25	0.45±0.06
10	Glass+(PAH 3.0/PSS 3.0)$_{120}$	33	0.25	0.56±0.22
11	Si <111> + (PAH 3.5/Nafion-117 3.5)$_{80}$	18	2.6	0.21
12	Glass + [(PAH 6.5/PAA 6.5)$_1$(PAH 6.5/MWNT 6.5)$_5$]$_2$[#]	44	0.25	0.25±0.01

13	Glass + $(PAH\ 5.0/PAA\text{-}MWNT\ 5.0)_{14+1\ PAH/PAA\ primer\ layer}^{*}$	115	0.25	0.30±0.22
14	Glass + $(PAH\ 5.0/PAA\text{-}MWNT\ 5.0)_{34+1\ PAH/PAA\ primer\ layer}^{*}$	380	0.25	0.21

[$]PSS is poly(sodium 4-styrene sulfonate), a strong polyelectrolyte.

[#]These composites were prepared using acid-treated MWNTs dispersed in water, similar to the constructs prepared in Chapter 4.

[*]For these assemblies, MWNTs were dispersed in PAA, through sonication, without any additional treatment. Dispersions were less stable than those prepared using acid-treated tubes. The loading in the suspension was 10% of the weight of PAA.

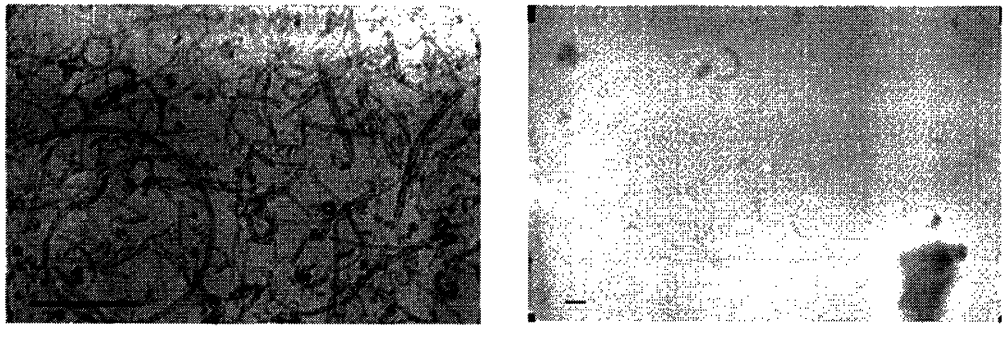

Figure C-1 TEM micrographs of the PEM constructs tested in lines 12(left) and 14 (right) of Table C-1. Scalebars depict 500 nm. In both cases, MWNTs are 1-5 μm in length and 20-50 nm in diameter.

Appendix D Effect of Supercritical CO_2 and Organic Additive Treatment on the Mechanical and Tribological Properties of Ultra-high Molecular Weight Polyethylene

D.1 Introduction

Ultra-high molecular weight polyethylene (UHMWPE) has been the preferred plastic bearing surface in total joint replacements for four decades [1]. In addition to its toughness, high elastic modulus, and impact strength, UHMWPE exhibits a low coefficient of friction, and is biocompatible in bulk form. The property of UHMWPE that supports its selection as a bearing surface in orthopedic implants is the high degree of entanglement between chains, owing to its molecular weight (in excess of 3 million); chain entanglements render the polymer extremely wear resistant.

In spite of the low wear rates of UHMWPE compared with other polymers, the life of a normal implant is usually limited by polymer wear particles produced at the metal/UHMWPE articulating interface. The wear debris is believed to induce bone resorption through a biological reaction, causing implant loosening, and necessitating a revision surgery [2]. Several attempts have been made to modify the polymer to reduce the wear rates, but without much success (for a comprehensive review, see ref. 3). In the recent past, radiation-induced crosslinking of UHMWPE has been shown to drastically reduce the wear rates of the polymer [4]; the treatment has been approved by the Food and Drug Administration (FDA) for use in total hip replacement prostheses. A reduction in wear, however, is accompanied by a decrease in ultimate mechanical properties (stress and strain at fracture) of UHMWPE [5]. These properties are important for the overall

mechanical stability of the hip implant, but are believed to be especially crucial for the functioning of knee joints, where the contact stresses are much higher.

It has been shown that the UHMWPE resin particles are poorly consolidated during the extrusion or compression molding process used to form the bulk material [6]; this is attributed to the high molecular weight which restricts molecular mobility and flow even in the melt. Olley and co-workers [6] proposed that the lower molecular weight fraction of the polymer (shorter molecules) is driven out of the particles into the interstitial zones during the sintering stage; the larger molecules remain near their originating particles. This material at the interfaces between particles plays a role in binding together the powder. It is, however, less strong than the material comprising the resin, and thus the initiation of wear is likely to occur at these particle boundaries, and especially in those cases where the amount of binding material is low. The objective of this project was to improve the consolidation of the powder particles of UHMWPE using a plasticizing agent. The first strategy evaluated the merit of supercritical carbon dioxide ($ScCO_2$) for this purpose. $ScCO_2$ is widely used as a solvent in polymer processing [7] and polymerization chemistry [8]. It is inexpensive, non-flammable, and certified by the FDA as non-toxic. The moderate critical conditions (T_c=31.1 °C, P_c=72.8 atm) make it a convenient fluid for experimentation. In addition, the strength of a supercritical solvent is a function of its density which, in the case of CO_2, can be controlled by varying the temperature and pressure. The use of $ScCO_2$ also obviates the need for elaborate separation procedures since CO_2 is a gas at ambient conditions. Though the associated quadrupole moment makes it a weak solvent for most non-polar polymers [9], $ScCO_2$ has been successfully used to swell both low and high-density polyethylene. This ability to

swell polyethylene has been used to impregnate the polymer with a monomer like styrene [10,11]; subsequent polymerization leads to composites with improved mechanical properties. $ScCO_2$ has also been used to create composites of UHMWPE with silver nanoparticles through impregnation [12]; the composite material was reported to exhibit improved wear behavior.

For a second strategy, we employed an organic additive to treat UHMWPE. Ethyl n-butyrate (EB) was chosen because of the close proximity of its solubility parameter (17.4 $(MPa)^{1/2}$) to polyethylene (16.5 $(MPa)^{1/2}$). Its chemical structure is depicted in Figure D-1. In addition, EB has been classified as "generally safe" by the FDA [13], and is used as a food additive.

The following sections include preliminary results from the $ScCO_2$ and EB treatment strategies. The treated specimens were tested for their mechanical and tribological properties. Further work and characterization is needed, however, to elucidate the fundamental nature of the induced modifications.

D.2 Experimental Section

D.2.1 Materials

UHMWPE GUR 1050 (M_w=5.5-6 x 10^6, Ticona, Bayport, TX) rod stock was purchased from Poly Hi Solidur, Inc. (Fort Wayne, IN). A part of the rod stock was gamma-irradiated in nitrogen at doses of 2.5, 5, and 10 MRad (Isomedix, Northboro, MA). After irradiation, the material was heated at 170 °C for 4 hours, and then annealed at 125 °C for 48 hours. Finally it was cooled to ambient temperature.

Ethyl butyrate was obtained from Sigma-Aldrich (Milwaukee, WI). Carbon dioxide (grade 5.5) and nitrogen (grade 5) were purchased from BOC Gases (Murray Hill, NJ). Bovine calf serum (79 g/l protein), employed as a lubricant during wear testing, was obtained from JRH Biosciences (Lenexa, KS). The serum was diluted to 23 g/l using deionized water, following recommended procedures [1]. The solution also contained 20 mM of the sodium salt of ethylenediaminetetraacetic acid (EDTA), and 0.2 % by weight of sodium azide. Both these chemicals were purchased from Sigma-Aldrich (Milwaukee, WI).

D.2.2 $ScCO_2$/ EB Treatment of UHMWPE

A pressure vessel (300 ml, Parr Instrument Company, Moline, IL) was utilized to treat the polymer with $ScCO_2$ and EB. The reactor was made of type 316 stainless steel with a maximum working pressure of 207 bar at a temperature of 350 °C; the inconel rupture disk was rated for 133 bar. A schematic of the test setup is illustrated in Figure D-2.

After flushing with air and weighing, UHMWPE specimens were placed in the reactor. The system was sealed and flushed with CO_2 using the inlet-outlet valves (see Figure D-2). The vessel was subsequently filled with CO_2 (~ 60 bar cylinder pressure), and heated. The pressure was stabilized around 100 bar by periodically releasing excess gas through the outlet valve. The specimens were kept inside the reactor for a period of 48 hours at 150 °C. The CO_2 was then released gradually without significantly decreasing the temperature. Finally, the reactor was allowed to cool and the samples were weighed.

For treating with EB, a similar setup was employed. Approximately 10-20 ml of the liquid, corresponding to 40-60 % of the weight of the samples, was added to the reactor; contact between EB and the polymer specimens was prevented by securing the samples in a wire brace along the inside of a 100 ml glass beaker placed in the vessel; the EB was added to the pressure vessel, outside the beaker. Prior to heating, the reactor was flushed with CO_2 to remove traces of air. The specimens were heated at 170 °C for 48 hours. The pressure of the EB (b.p. 121.5 °C)-CO_2 atmosphere in the system increased to about 6 bar during this period. At the end of the treatment period, the excess EB was released through the outlet valve, before allowing the system to cool to ambient conditions. The specimens were placed in a vacuum oven for 24 hours at 70-80 °C to remove any residual EB, prior to weighing.

D.2.3 Mechanical and Tribological Characterization

D.2.3.1Uniaxial Tensile Tests

Uniaxial tensile tests were conducted on an Instron 4201 testing machine at a *constant crosshead speed* of 5 mm/min (constant dL/dt). To prepare samples for testing, 1.5 mm-thick disks were cut from the cross-section of the rod stock. A die was used to punch out dog-bone specimens for tensile tests (ASTM D638-99, Type V); a schematic of the specimen geometry is depicted in Figure D-3. These specimens were also used in tensile experiments at a *constant true strain rate* ((1/L)dL/dt); an Instron 5582 testing machine was utilized for these tests conducted at an initial strain rate of 3.5 mm/mm/min.

D.2.3.2Tension Fatigue Tests

The specimen geometry recommended by Pruitt and co-workers [14] was used (see Figure D-4). A hydraulic Instron 8871 machine was employed for these measurements,

carried out to the point of crack inception. The inception point ($\triangle K_{incep}$) is defined as the stress intensity range corresponding to a crack growth rate (da/dN) of 10^{-6} mm/cycle (ASTM-E647). A sinusoidal constant force amplitude condition with a load ratio (min/max load ratio, R) of 0.1 was used at a frequency of 5 Hz. To attain the desired da/dN value, the fatigue load was incremented every 20000 cycles in steps of $\triangle K$=0.02 (MPa-$m^{-1/2}$), where $\triangle K$ is defined by the following equation:

$$\Delta K = \left(\frac{P}{T}\sqrt{W}\right) \times f\left(\frac{a}{W}\right)$$

Here P is the applied load, T and W are geometric parameters (see Figure D-4), *a* accounts for the crack length (see Figure D-4), and *f* is a function of *a* and W, specified in ref. 15. After each 20000-cycle run at a certain $\triangle K$, the crack lengths were measured using an Olympus Vanox-T optical microscope to ascertain if the desired da/dN value of 10^{-6} mm/cycle had been achieved.

D.2.3.3Pin-on-disk Wear Tests

Wear tests were carried out on an AMTI Orthopod pin-on-disk wear testing machine (located at Brigham and Women's Hospital, Boston, MA). UHMWPE pins, 9.5 mm in diameter and 2.5 cm long, were machined from the rod stock. Unmodified and EB-treated pins were made to articulate against zirconia disks; they were sonicated in water, dried, and weighed prior to testing. Bovine calf serum lubricant solution, described previously, was used as the surrounding medium; EDTA serves as an anti-chelating agent, while sodium azide is used as an antibacterial agent [16]. The temperature was maintained at about 37 °C using a water bath. The test was carried out over 500,000 cycles at a frequency of 1 Hz. To simulate motion in a hip joint, a square articulation path

(5 mm x 5 mm) was employed at a normal load of 192 N; this corresponds to a normal stress of 3 MPa. Physiological load levels in the human hip joint are reported to be in the 3-6 MPa range [1]. After about every 150,000 cycles, the lubricant solution was replaced with a fresh batch. During this replacement period, the disks were rinsed in water, while the pins were rinsed with water, ethanol, and finally acetone. They were dried and then weighed to determine weight loss due to wear, before being remounted in the wear tester.

D.2.4 DSC, TGA, and FT-IR Characterization

To elucidate the structure of the polymer after processing, differential scanning calorimetry (DSC) measurements were made (Q1000, TA Instruments). Circular samples, approximately 6 mm in diameter, were stamped out of the grip region of untreated and treated dog-bone specimens. These circular specimens were cut into two halves along the cross-section, and then cut in half across the diameter to yield samples 3-5 mg in weight. The samples were heated in aluminum pans from 80 °C to 170 °C at 10 °C/min. Curves were integrated between 100 and 150 °C to obtain values of $\triangle H_{fusion}$. The degree of crystallinity was calculated using a heat of fusion of 293 J/g for the polyethylene crystal [17]. To quantify the amount of EB remaining in the sample after the vacuum oven treatment, thermo-gravimetric analysis (TGA) was performed on a TG/DTA 320 instrument (Perkins Elmer). The sample geometry was identical to that used for DSC measurements. Overall weight loss was monitored over a temperature range of 20-220 °C; a heating rate of 10 °C/min was used. In addition, Fourier transform infrared spectroscopy (FT-IR) spectra were acquired for untreated and EB-treated samples using a Nicolet Model Magna 860 spectrophotometer with a Spectra Tech Nic Plan Microscope

(Spectra Tech ATR objective with zinc selenide crystal). The ATR objective probes the sample to a maximum depth of 1 μm.

D.3 Results and Discussion

D.3.1 Treatment of UHMWPE with $ScCO_2$

Figure D-5 depicts the best-case tensile stress-strain curves (constant crosshead speed) for specimens subjected to $ScCO_2$ treatment. At temperatures of 150 °C, UHMWPE is in the melt state; the high molecular weight of the polymer, however, restricts flow, retaining the geometric dimensions of the sample. Melt-state processing was used to allow for greater chain mobility, and hence facilitate interaction with $ScCO_2$. The tensile curves for the treated specimens resembled those for high density polyethylene (HDPE). The corresponding DSC results (Table D-1) for the peak temperature and % crystallinity of the treated samples revealed an increased proportion of crystalline domains compared with the unprocessed specimens. The degree of crystallinity for HDPE is reported to be in the 80-95 % range.

Subsequent treatment runs, however, were unable to reproduce the stress-strain behavior depicted in Figure D-5. The stress-strain curves for the treated specimens generally closely resembled those of the unmodified UHMWPE samples (see Figure D-5). Hence, no further fatigue or tribological characterization could be performed. Since all the subsequent runs were performed at the same conditions of time, temperature, and pressure, the lack of reproducibility was attributed to the release rates for CO_2, after the 48 hour treatment period. In the effort to control these rates with greater precision, a back pressure regulator (BPR), and various needle and metering valves were tested at the

outlet. Figure D-6 depicts typical release curves for these valve types. In the case of the needle valve, the release rate had to be manually increased each time it dropped to zero. It is evident that the valves, used in this study, did not offer good control over the release of the gas. Representative stress-strain curves for the treated specimens, when a BPR (0-400 bar operating range) and needle valve were employed for gas release, are presented in Figure D-7. The curves closely resembled those for untreated UHMWPE, except for a slight degree of softening post the yield point. No further mechanical characterization techniques were employed for these samples.

McCarthy and co-workers [18] have reported the welding of linear low density polyethylene films using $ScCO_2$ as a plasticization agent. In addition to a $ScCO_2$ pressure of 100 bar, a hydraulic press was utilized to apply further external pressure. Also, most studies on the phase behavior of polyethylene-CO_2 systems [9], or those employing binary mixtures of CO_2 with other organic compounds [19,20], utilize pressures well in excess of 100 bar. In the current study, we were able to demonstrate, in a single experiment, the potential to induce some structural changes in the polymer, and possibly affect its wear rate, using $ScCO_2$. A pressure vessel, capable of operating safely at higher pressures, might be required for reliable and reproducible results like the one illustrated in Figure D-5. There is also a need to control the release rates more accurately; a syringe pump, or a back pressure regulator with a narrow operating range, are possible alternatives. Finally, even small changes in stress-strain behavior could potentially be associated with large changes in the wear behavior. Wear tests on treated samples that might not show significant changes in a tensile test are recommended to ascertain that the wear behavior is unchanged.

D.3.2 Treatment of UHMWPE with EB

D.3.2.1 Uniaxial Tensile Tests

Uniaxial tensile stress-strain curves, at a constant crosshead speed, for unmodified and EB-treated dog-bone specimens are presented in Figure D-8. The corresponding values of elastic modulus, yield stress, and ultimate mechanical properties are tabulated in Table D-2. In all cases, the tensile curves for the treated samples extended to higher stresses and strains, beyond those for unmodified UHMWPE. The curves demonstrated a distinct softening past the yield point compared with the virgin material. The flat portion of the "best case" curve is attributed to the deformation of regions A-B and C-D (see Figure D-3); these regions are held between the grips during the test. When the gauge portion (B-C) has extended to a certain length, the levels of stress are sufficient to deform the grip portions. The flat portion, consequently, corresponds to the extension of the grip region, while the length of the gauge region remains unchanged. When the grip material has yielded, the entire sample further deforms, manifesting as a rise in the curve up to the point of failure. In a few cases, the deformation in the grip portions caused the sample to slip out of the holders.

The effect of EB-treatment on the tensile properties of radiation crosslinked UHMWPE is illustrated in Figures D-9 and D-10; in all cases the treated specimens were exposed to EB at 170 °C for 48 hours. For samples treated with a radiation dose of 2.5 MRad, the high extensions include the deformation of the grip regions, similar to the 0 MRad specimens. It is obvious that radiation-induced crosslinking limited the efficacy of the EB treatment with respect to increasing the ultimate properties; at doses in excess of 5

MRad, the properties remained almost unchanged after treatment. Table D-3 presents the ultimate properties for these specimens.

The dependence of ultimate properties on the time of treatment is presented in Figure D-11; in all cases, the temperature was maintained at 170 °C. For these 1.5 mm-thick dog-bone specimens, a treatment time of 12 hours may be sufficient to observe an increase in ultimate properties. For thicker samples, however, treatment times closer to 48 hours may be needed to allow for diffusion of the organic into the specimen.

To circumvent the undesirable deformation of the grip regions for the case of the EB-treated samples (0 and 2.5 MRad) in a constant crosshead speed experiment, a *constant true strain rate* test ((1/L)(dL/dt)) was employed. In these tests, the crosshead speed continually increases as the gauge portion extends (or L increases). This allows for sample deformation and fracture to be confined to the gauge length portion (B-C, see Figure D-3). The results of this test for virgin (0 MRad) and 5 MRad samples are depicted in Figures D-12 and D-13; *true* values of stress and strain were calculated based on a constant volume assumption, as described in ref. 21. In addition, a photograph of the untreated and EB-treated virgin material, after testing, is shown in Figure D-14. The 0 MRad-samples, when subject to EB treatment, exhibited a 77 and 20 % increase, respectively, in average ultimate true stress and strain over the corresponding untreated material. When the treated specimen was annealed in an atmosphere of nitrogen (170 °C, 3 hours), the effects of the treatment were lost; curves for the unmodified and EB-treated samples (0 MRad), after annealing, were virtually indistinguishable. The 5 MRad samples showed almost no change after treatment; this is unlike the case for the test at constant crosshead speed described previously, where these specimens exhibited a 29 and

8 % increase in true stress and strain over the unmodified counterparts (curves not shown here). From Figures D-9 and D-10, and from reported work, it is clear that the ultimate properties show a slight decrease with increasing doses of radiation for the untreated samples; a decrease in both stress and strain has a synergistic effect on the work of fracture. It is likely that for the treated 5 MRad samples, a constant true strain rate of 3.5 mm/mm/min could overwhelm the natural response of the material subjected to EB-treatment. Tests at lower constant strain rates are recommended for samples crosslinked with these higher doses of radiation.

D.3.2.2DSC, TGA, and FT-IR Characterization

To investigate the structure of the polymer after treating with EB, DSC was used; the % crystallinity and peak temperatures for the virgin, 2.5 MRad, and 5 MRad materials are presented in Table D-4. While the peak temperatures were only marginally affected by the treatment, the % crystallinity for the 0 MRad EB-treated material was approximately 12 % lower than unmodified UHMWPE. The 5 MRad samples also exhibited a 8 % decrease in crystallinity after treatment. The 2.5 MRad samples, however, showed almost no change in peak temperature or % crystallinity after the EB treatment. Sample DSC curves for all cases are depicted in Figure D-15.

TGA and FT-IR scans were used to elicit the amounts of residual EB in the samples. FT-IR spectra and corresponding normalized weights, both for 1.5 mm-thick dog-bone specimens, at various stages of the treatment process are presented in Figure D-16. After the vacuum oven treatment, the sample weights were almost identical to the initial values (before treatment); the corresponding FT-IR scan did not reveal any peaks associated with the ester. It must be noted, however, that scans were carried out using the

ATR objective, which penetrates the surface to a maximum depth of 1 μm. Hence, the technique is not suited to detect traces of EB in the bulk of the specimen. Although weight measurements did not reveal any residual EB amounts after the vacuum oven treatment, TGA scans (Figure D-17) showed a weight loss of approximately 2 % over the 20-220 °C range. It is likely that this weight loss corresponds to low levels of EB that are not detected by a macroscale balance, but a control scan for untreated UHMWPE was not performed. For the thicker samples used for fatigue, compact tension, and wear experiments, a 2-3 day vacuum oven treatment was used in the effort to remove all traces of EB; weight measurements, however, still revealed 3-7 % increases.

D.3.2.3Fatigue Tests

Fatigue tests were performed to evaluate the resistance to crack initiation of the EB-treated specimens. The inception points ($\triangle K_{incep}$) are graphically depicted in Figure D-18 for untreated and treated, 0 and 5 MRad specimens. While the 0 MRad samples exhibited a 9 % average increase in the stress intensity required for crack inception, after treatment, almost no effect of the EB treatment on the inception point was observed for the 5 MRad specimens. These results are in accordance with those from tensile tests (Figures D-9 and D-10); the efficacy of the treatment with respect to improving the mechanical properties of the polymer is lost at high radiation doses.

D.3.2.4Tribological Characterization

The volumetric wear over 500, 000 cycles for untreated and EB-treated virgin UHMWPE pins is depicted in Figure D-19. The average wear rates over the six stations used for each test were 7.5×10^{-9} cc/cycle for the treated pins and 5.3×10^{-9} cc/cycle for the unmodified UHMWPE material; the test with the treated samples, however, exhibited

large error bars and there was some overlap with the results from the control test. The EB-induced modification increases, at least marginally, the average wear rates of the bulk material under physiological conditions of load, number of cycles, and articulation pattern.

In summary, treatment of virgin UHMWPE specimens with EB resulted in an increase in ultimate mechanical properties of the polymer; the true tensile stress and strain at the point of fracture were higher by as much as 77 and 20 %. This was accompanied by a 9 % increase in fatigue crack inception points and some increase in wear rates. The efficacy of the treatment was drastically reduced for crosslinked specimens treated with doses of radiation in excess of 5 MRad. Specimens, crosslinked with radiation doses below 5 MRad, are expected to be able to avail the improved mechanical properties rendered by treatment with EB, without significantly affecting the wear rates. The ultimate objective of this work is to improve the tensile and fatigue properties of crosslinked UHMWPE without a significant adverse effect on the wear rate; currently UHMWPE bearing surfaces in hip replacements are treated with 6 MRad radiation doses.

DSC results for the 0 and 5 MRad samples exhibited a slight loss of crystallinity after the treatment. In addition, the effect of the treatment was lost after annealing the samples. Weight loss measurements and FT-IR spectra did not reveal traces of residual EB in the 1.5 mm-thick tensile specimens. One proposed hypothesis for the observed behavior of EB-treated polyethylene is a higher degree of entanglements of the material at the interstitial zones. This would explain a loss of crystallinity after EB-treatment, but not the increased wear rates. Another hypothesis is drawn from the work of Lemstra and

Smith [22,23]. They studied tensile properties for high molecular weight polyethylene fibers, produced by spinning from dilute solutions in decalin. Enhanced draw ratios were observed for these materials; a reduced degree of entanglements of the macromolecular network was cited as the principal cause for the high drawability of the processed specimens. The reduced entanglements might also explain the marginally increased wear rates in the present study; this reasoning, however, would require the crystallinity to exhibit an increase after EB-treatment, contrary to the observed behavior. Detailed characterization is thus still needed to elicit the precise nature of the EB-induced modification of UHMWPE.

D.4 Recommendations for Future EB-Related Work

A study of the effect of initial rate, in a *constant true strain rate* tensile test, on the stress-strain curves for untreated and EB-treated 5 MRad crosslinked UHMWPE specimens is recommended to clarify if such a test overwhelms the effects of the EB treatment at high doses of radiation. Further wear tests for the 0 MRad and the crosslinked samples will be useful in precisely quantifying the effect of the EB-induced modification on polymer wear. In addition, fatigue tests to the point of specimen failure are recommended; these tests have been reported to be of great significance to the performance of knee replacement prostheses [24] . FT-IR spectra, in transmission mode, would be useful in eliciting the levels of residual EB, if any, in the bulk of the sample. Also, TGA scans for untreated UHMWPE are needed to attribute the loss in weight for the treated sample (Figure D-17) to residual EB. X-ray diffraction and scanning electron microscopy are also useful tools to study the structure of the polymer, and possible changes due to the treatment with EB.

Once the nature of the EB-induced modification has been identified, an excursion in treatment temperature would enable the selection of optimal processing conditions. Finally, the choice of solvent has not been optimized. Elucidating the nature of the modification will assist the selection of the processing conditions, and possibly ideal solvent, for this process to achieve the final objective of improving the mechanical behavior of radiation crosslinked UHMWPE without compromising its wear rate.

D.5 References

(1) Wang, A.; Essner, A.; Polineni, V. K.; Sun, D. C.; Stark, C.; Dumbleton, J. H. In *New Directions in tribology*; Hutchings, I. M., Ed.; Mechanical Engineering Publications Limited: Bury St Edmunds, UK, 1997; pp 443-458.

(2) Ingham, E.; Fisher, J. *Proc. Instn. Mech. Engrs. Part H-Journal of Engineering in Medicine* **2000**, *214 (H1)*, 21-37.

(3) Kurtz, S. M.; Muratoglu, O. K.; Evans, M.; Edidin, A. A. *Biomaterials* **1999**, *20*, 1659-1688.

(4) McKellop, H.; Shen, F.; Lu, B.; Campbell, P.; Salovey, R. *J. Orthop. Res* **1999**, *17*, 157-167.

(5) Gomoll, A.; Bellare, A.; Wanich, T. In *Deformation, yield, and fracture of polymers: 11th International conference*, 2000; p 254.

(6) Olley, R. H.; Hosier, I. L.; Bassett, D. C.; Smith, N. G. *Biomaterials* **1999**, *20*, 2037-2046.

(7) Cooper, A. I. *J. Mater. Chem.* **2000**, *10*, 207-234.

(8) Kendall, J. L.; Canelas, D. A.; Young, J. L.; DeSimone, J. M. *Chem. Rev.* **1999**, *99*, 543-563.

(9) Kirby, C. F.; McHugh, M. A. *Chem. Rev.* **1999**, *99*, 565-602.

(10) Li, D.; Han, B. *Ind. Eng. Chem. Res.* **2000**, *39*, 4506-4509.

(11) Kung, E.; Lesser, A. J.; McCarthy, T. J. *Macromolecules* **1998**, *31*, 4160-4169.

(12) Webb, P. B.; Marr, P. C.; Parsons, A. J.; Gidda, H. S.; Howdle, S. M. *Pure Appl. Chem.* **2000**, *72*, 1347-1355.

(13) Ash, M.; Ash, I. *Handbook of food additives*; Synapse Information Resources: Endicott, NY, 2002.

(14) Baker, D. A.; Hastings, R. S.; Pruitt, L. *Polymer.* **2000**, *41*, 795-808.

(15) Anderson, T. L. *Fracture mechanics: fundamentals and applications*; CRC Press: Boca Raton, 1995.

(16) Liao, Y.; Benya, P. D.; McKellop, H. A. *J. Biomed. Mater. Res. (Appl. Biomater.)* **1999**, *48*, 465-473.

(17) Wunderlich, B.; Cormier, C. M. *J. Polym. Sci., Part A-2* **1967**, *5*, 987-988.

(18) Caskey, T.; Lesser, A. J.; McCarthy, T. J. *Polymer Eng. and Sci.* **2001**, *41*, 2259-2265.

(19) Xiong, Y.; Kiran, E. *J. Appl. Polym. Sci.* **1994**, *53*, 1179-1190.

(20) Kiran, E.; Zhuang, W.; Sen, Y. L. *J. Appl. Polym. Sci.* **1993**, *47*, 895-909.

(21) Crandall, S. H.; Dahl, N. C.; Lardner, T. J. *An introduction to the mechanics of solids*; The McGraw-Hill Companies, Inc.: New York, NY, 1999.

(22) Smith, P.; Lemstra, P. J. *Makromol. Chem.* **1979**, *180*, 2983-2986.

(23) Smith, P.; Lemstra, P. J. *Polymer* **1980**, *21*, 1341-1343.

(24) Baker, D. A.; Hastings, R. S.; Pruitt, L. *J. Biomed. Mater. Res.* **1999**, *46*, 573-581.

Table D-1 DSC analysis for $ScCO_2$ treated UHMWPE: best case results

	% Crystallinity	Peak Temp. [°C]
Unmodified	47.4 ± 0.2	139.4 ±0.8
CO2-treated	59.1 ± 2.6	143.8 ± 0.2

Table D-2 Mechanical Properties for unmodified and EB-treated UHMWPE from uniaxial tensile tests at constant crosshead speeds of 5 mm/min

	Unmodified	EB-treated
Modulus [MPa]	265.02 ±27.24	218.41 ± 22.58
Yield stress [MPa]	19.26 ± 0.32	19.17 ± 0.22
Engineering stress @ break [MPa]	44.43 ± 1.84	63.17 ± 5.50
Engineering strain @ break [mm/mm]	8.29 ± 0.38	27.96 ± 4.04

Table D-3 Ultimate properties for unmodified and EB-treated UHMWPE; uniaxial tests at constant crosshead speeds of 5 mm/min

		0 MRad	2.5 MRad	5 MRad	10 MRad
Engineering stress @ break [MPa]	Unmodified	44.43±1.84	44.70±0.15	43.46±1.43	40.18±1.04
	EB-treated	63.17±5.50	66.61±8.16	45.96±4.86	38.08±5.74
Engineering strain @ break [mm/mm]	Unmodified	8.29±0.38	7.25±0.00	6.30±0.17	4.72±0.30
	EB-treated	27.96±4.04	20.16±2.34	7.79±1.11	5.39±0.69

Table D-4 DSC results for unmodified and EB-treated UHMWPE subjected to various doses of radiation

Radiation Dose [MRad]	% Crystallinity Unmodified	% Crystallinity EB-Treated	Peak Temp. Unmodified [°C]	Peak Temp. EB-Treated [°C]
0	47.12 ± 3.32	41.33 ± 1.68	134.79 ± 0.26	133.53 ± 0.26
2.5	39.47 ± 1.06	40.25 ± 7.33	133.63 ± 0.14	134.87 ± 0.56
5	41.20 ± 0.33	38.04 ± 0.92	133.88 ± 0.13	132.20 ± 0.68

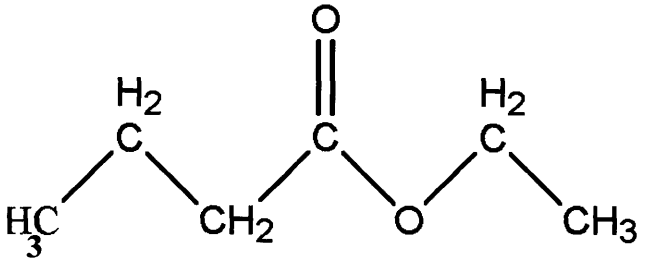

Figure D-1 Chemical structure of ethyl n-butyrate

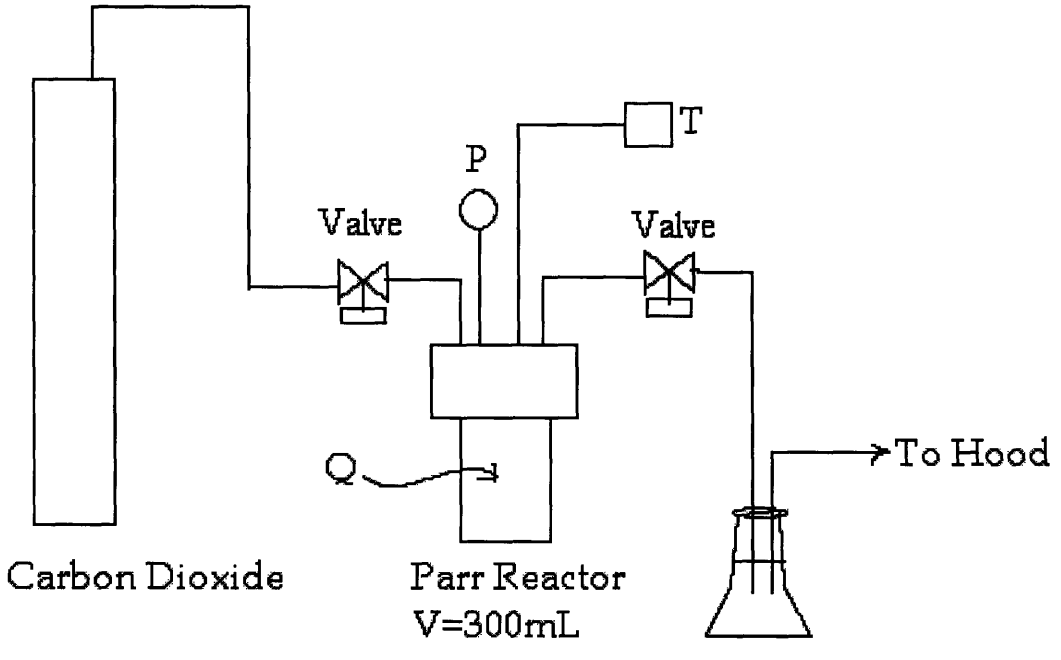

Figure D-2 Schematic of the test setup used for $ScCO_2$ and EB treatment of UHMWPE

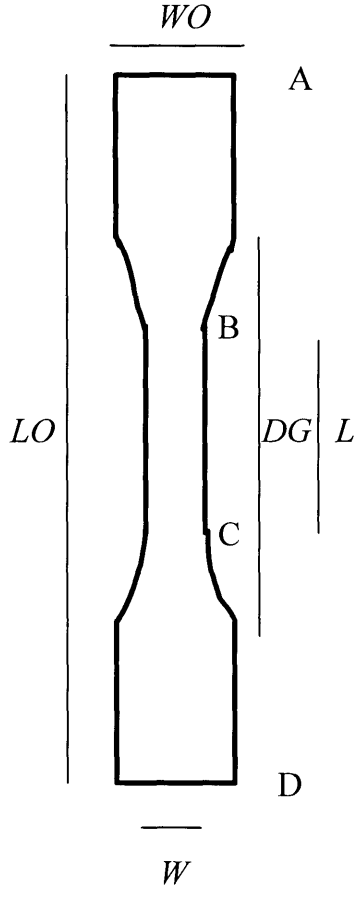

Dogbone: ASTM D638 Type V. W = 3.18 mm
L = 9.525 mm, DG = 25.4 mm, LO = 64 mm
WO = 10 mm, T (thickness) = 1.5 mm

Figure D-3 Specimen geometry for uniaxial tensile tests

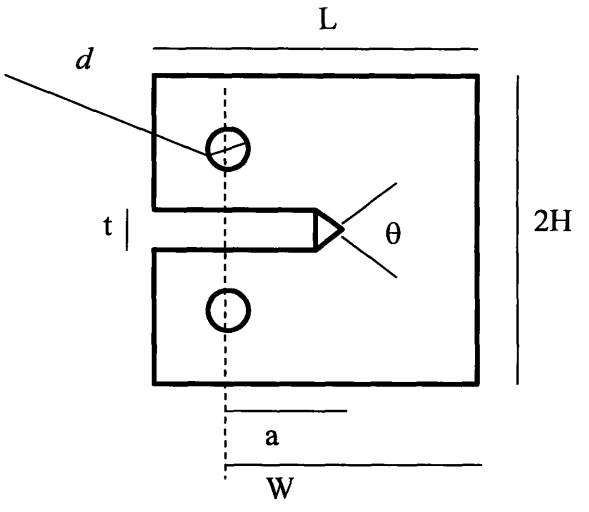

Fatigue Specimen: ASTM E647 Compact Specimen
L = 31.75 mm, d = 5.34 mm, t = 3.12 mm, 2H = 31.75mm
θ= 60°, a (initial) = 8.89 mm, W = 25.4 mm, T (thickness) = 8.13 mm

Figure D-4 Specimen geometry for fatigue tests

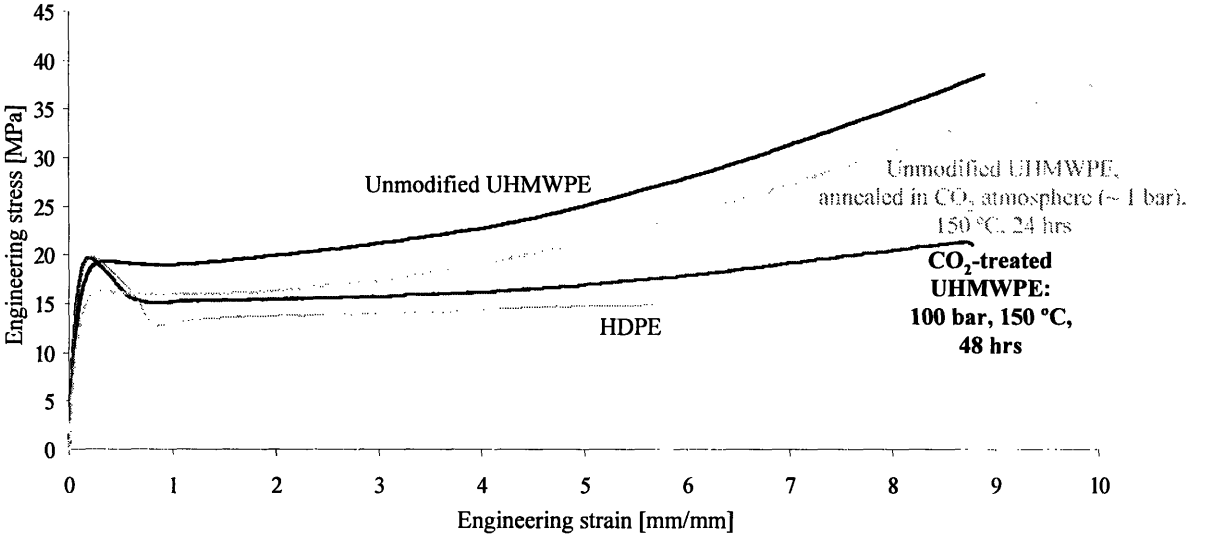

Figure D-5 Best-case tensile curves for ScCO2-treated UHMWPE. HDPE curve shown for comparison. All tests performed at a constant crosshead speed of 1 mm/min

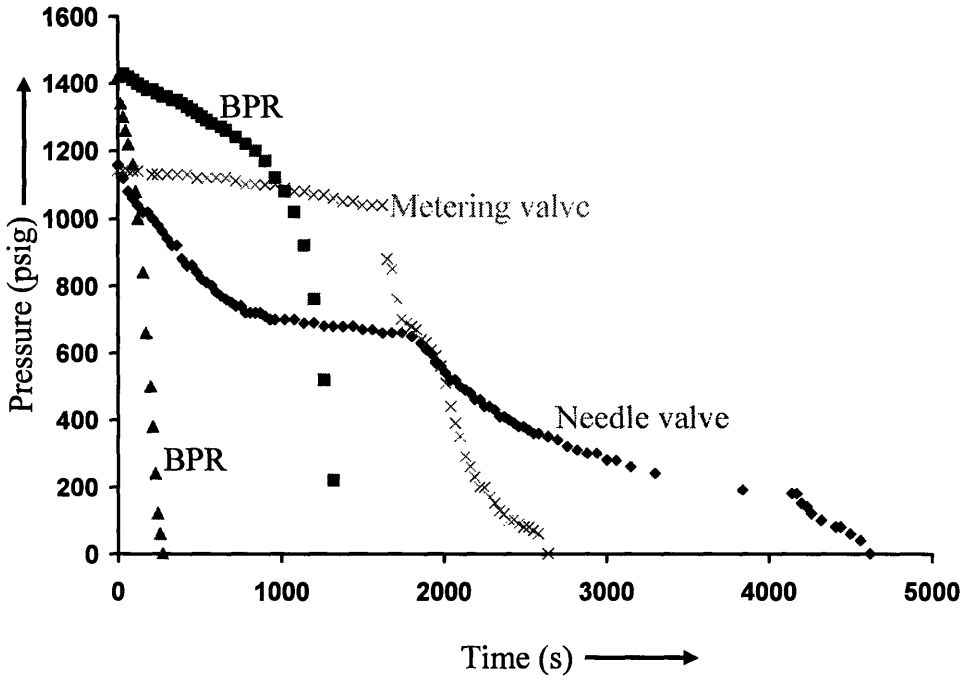

Figure D-6 Typical CO2 release curves for a back pressure regulator (BPR), needle valve (Cambridge valves) and metering valve (Autoclave).

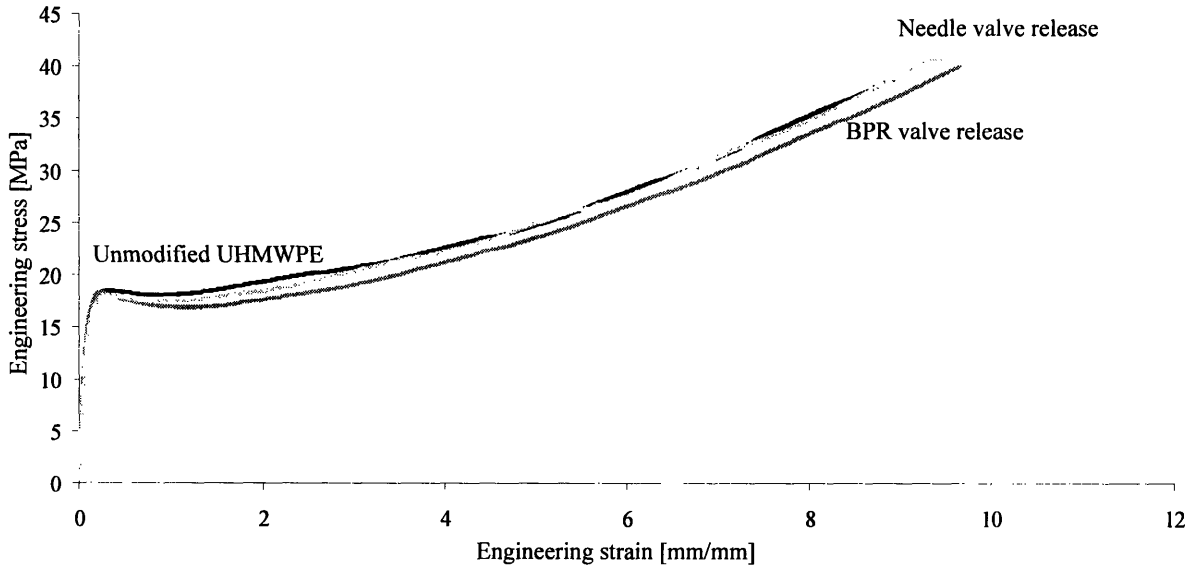

Figure D-7 Representative results when the BPR and needle valves were used for pressure release after $ScCO_2$ treatment; crosshead speed 1 mm/min.

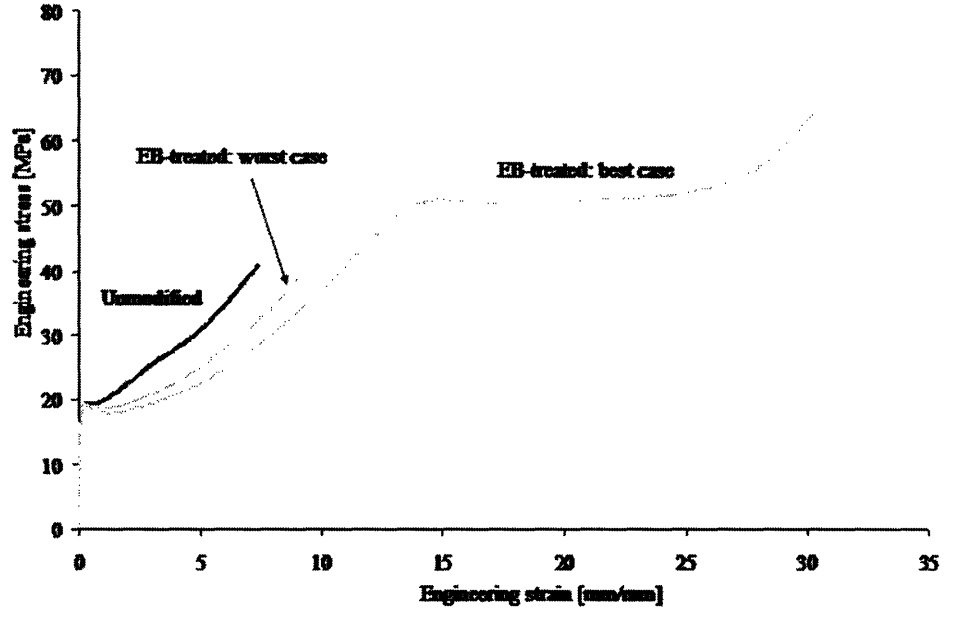

Figure D-8 Best and worst case tensile curve for EB-treated UHMWPE. Test performed at constant crosshead speed of 5 mm/min

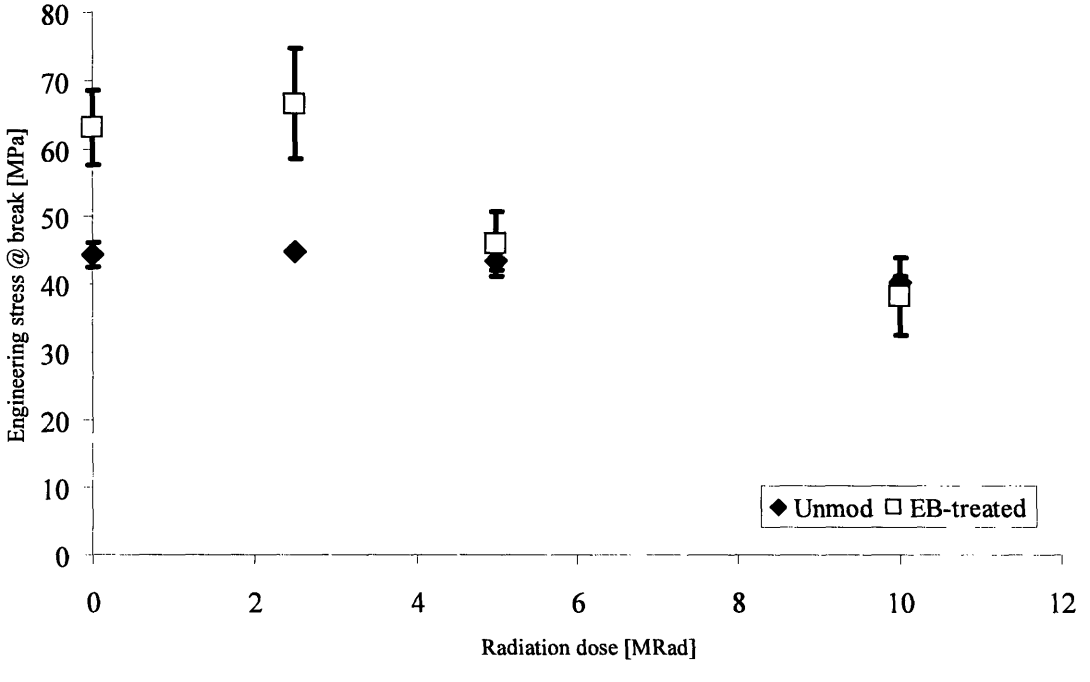

Figure D-9 Effect of radiation dose on the ultimate stress for unmodified and EB-treated samples. Uniaxial tensile tests performed at a constant crosshead speed of 5 mm/min.

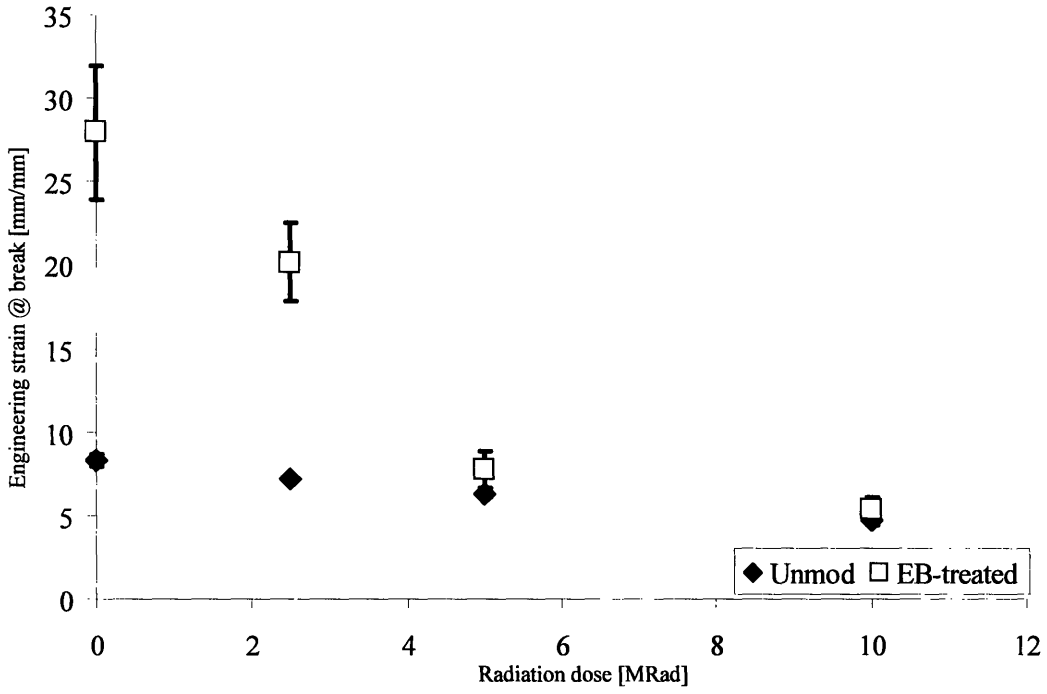

Figure D-10 Effect of radiation dose on the ultimate strain for unmodified and EB-treated samples. Uniaxial tensile tests performed at a constant crosshead speed of 5 mm/min.

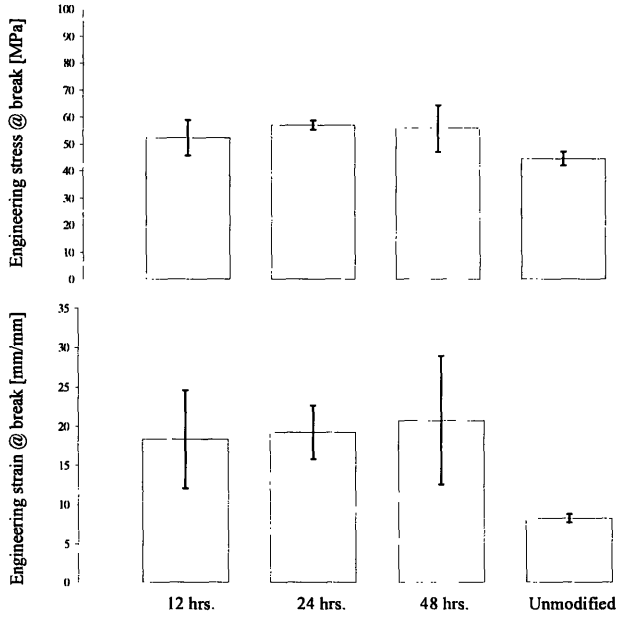

Figure D-11 Effect of EB-treatment time on the ultimate properties of UHMWPE; temperature 170 °C in all cases

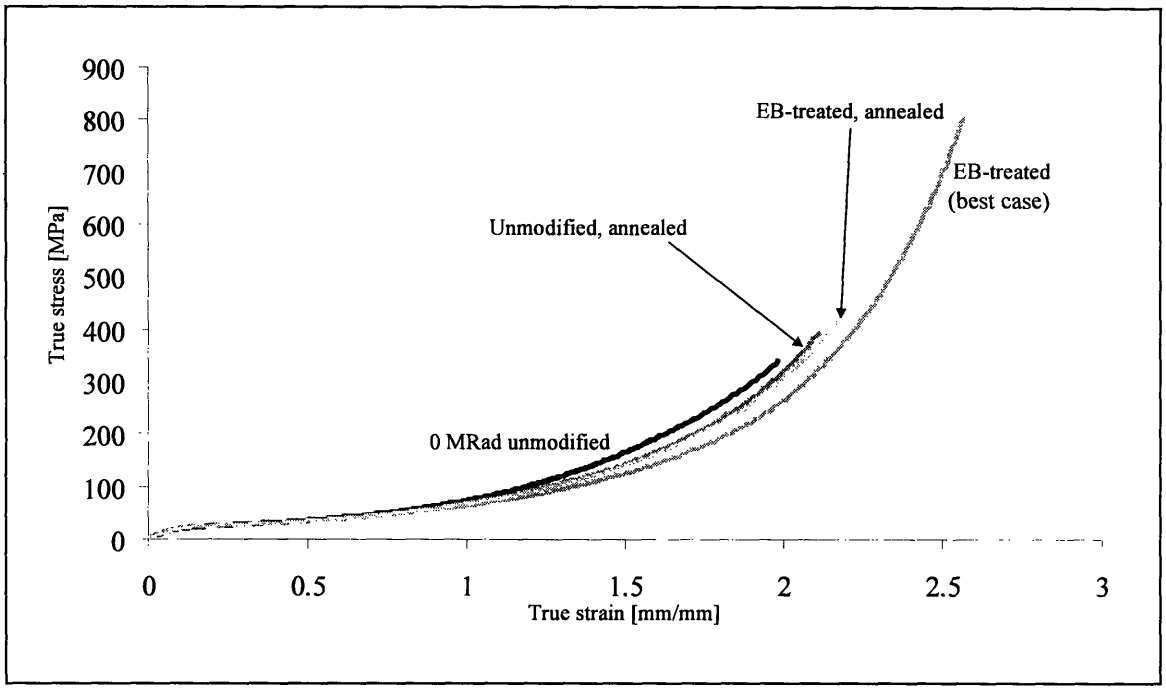

Figure D-12 True stress-true strain tensile curves for untreated and EB treated 0 MRad UHMWPE. Tests performed at an initial constant true strain rate of 3.5 mm/mm/min.

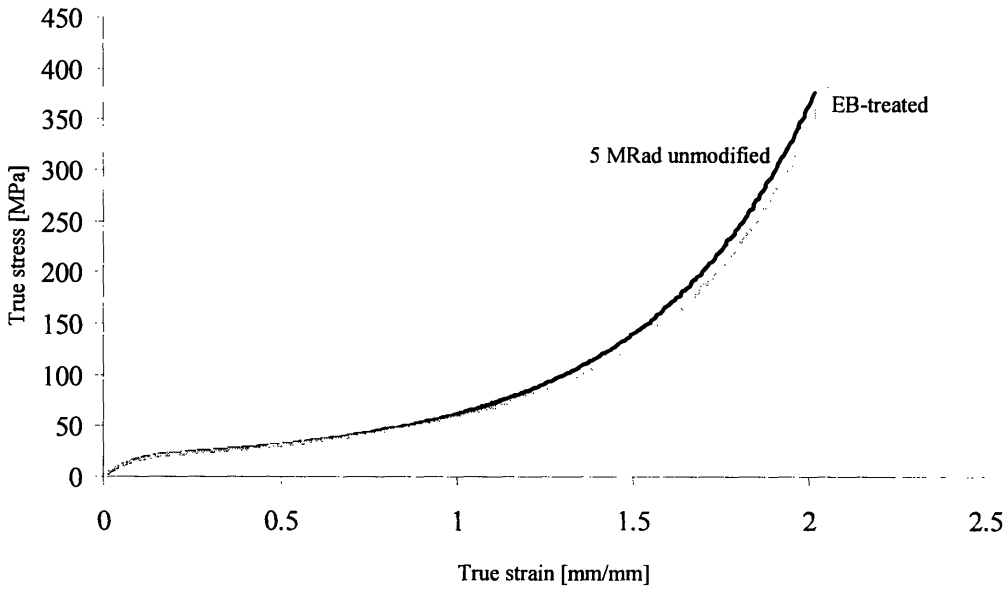

Figure D-13 True stress-true strain tensile curves for 5 MRad untreated and EB-treated samples; tests at a constant true strain rate (starting value 3.5 mm/mm/min)

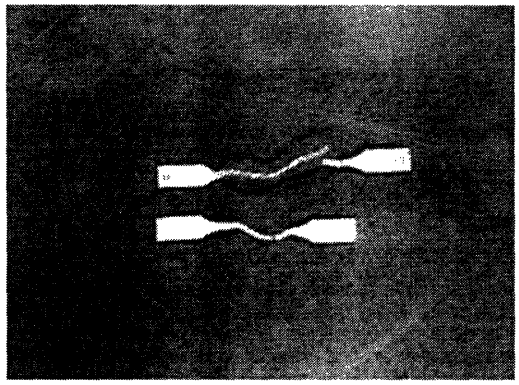

Figure D-14 Photograph of EB-treated (upper) and unmodifed (lower) UHMWPE (0 MRad) dog-bone specimens after constant true strain rate tensile tests.

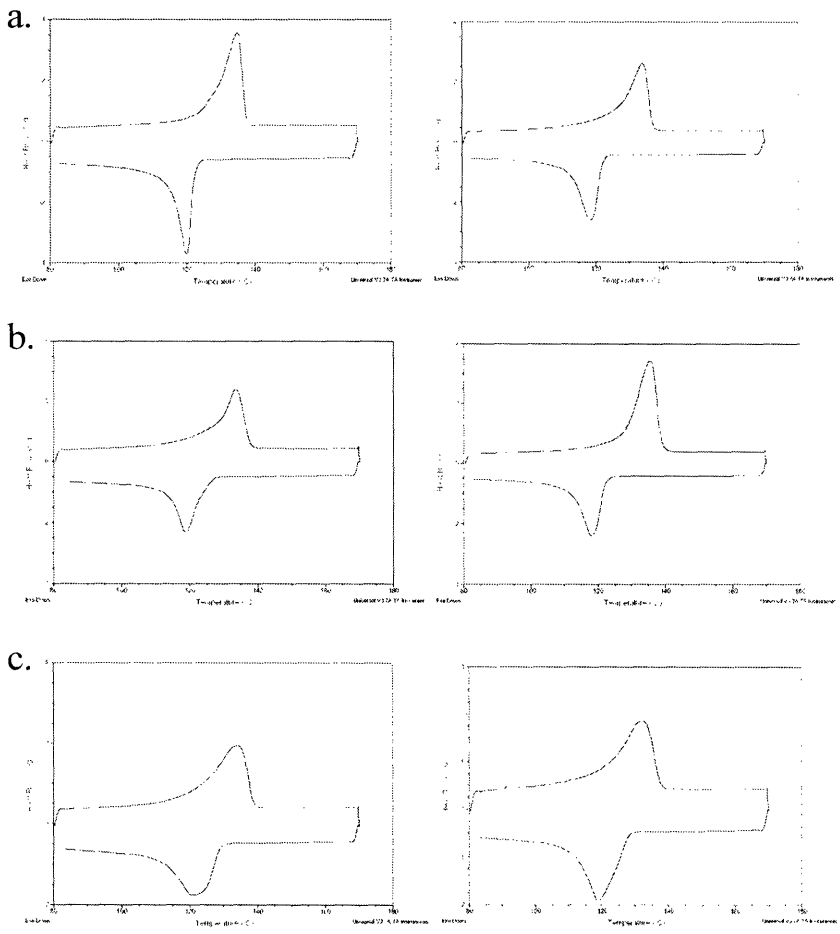

Figure D-15 Sample DSC curves for unmodified (left) and EB-treated (right) a. 0 MRad,b. 2.5 MRad, and c. 5 MRad samples

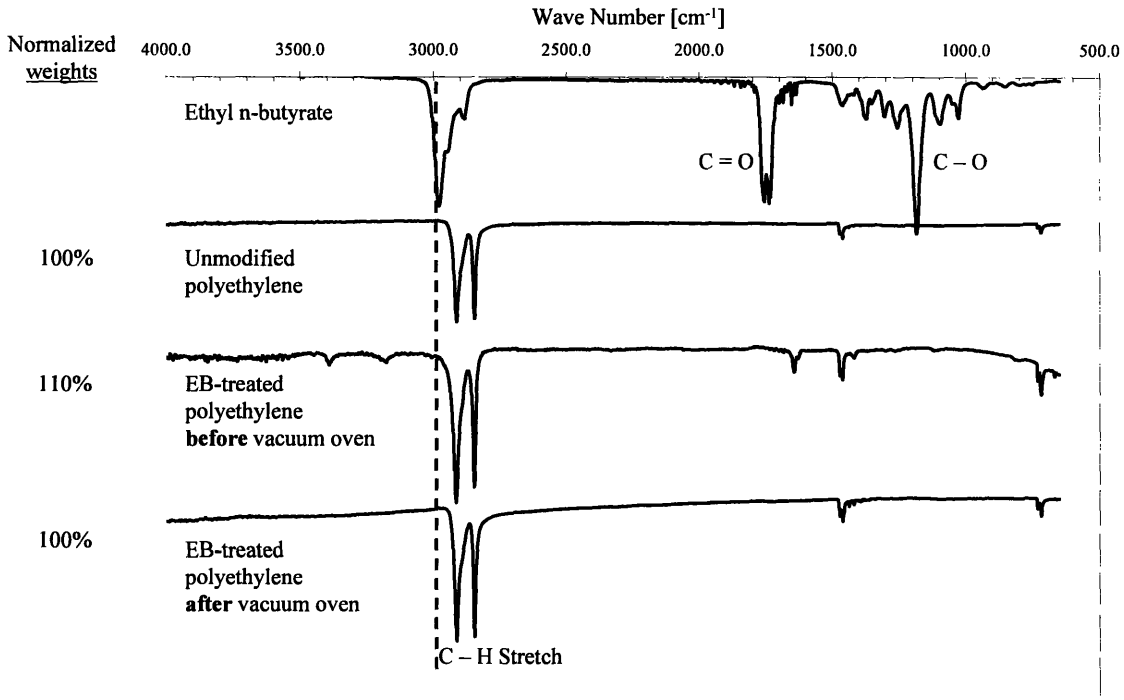

Figure D-16 FT-IR spectra and corresponding normalized weights for 1.5 mm-thick tensile test dog-bone specimens (0 MRad) at various stages of the EB-treatment process.

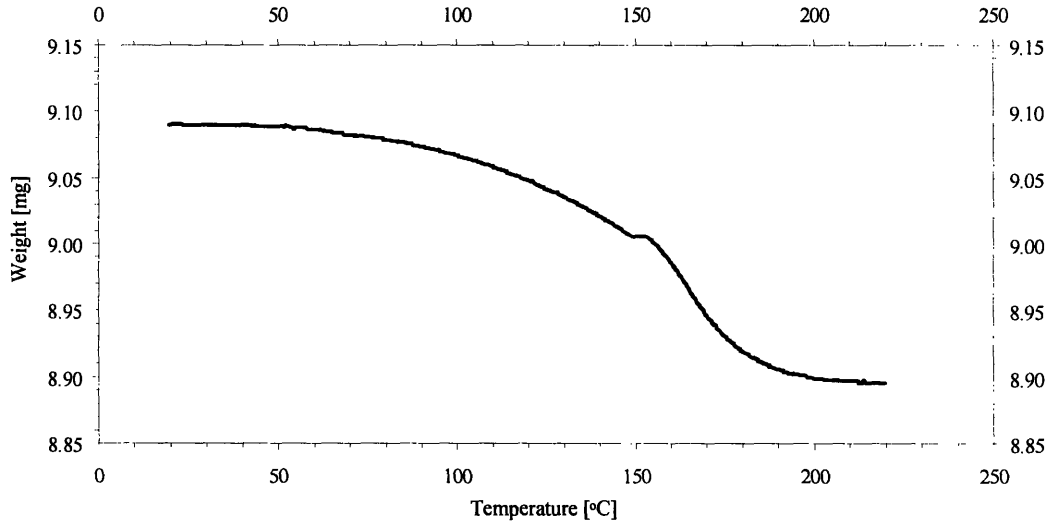

Figure D-17 TGA scan for EB-treated UHMWPE

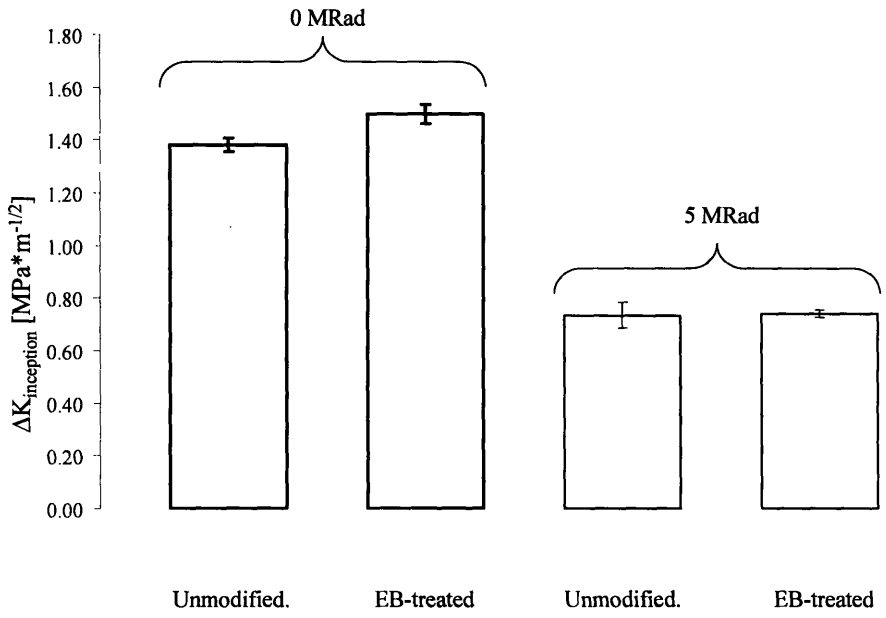

Figure D-18 Inception points for unmodified and EB-treated UHMWPE from fatigue tests

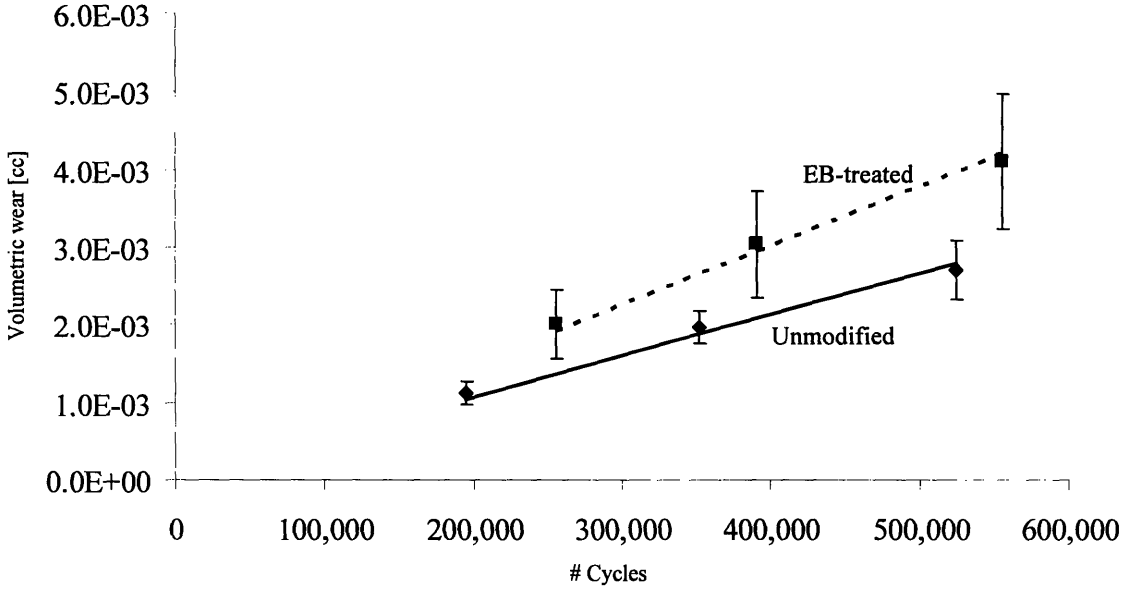

Figure D-19 Volumetric wear loss in a UHMWPE/zirconia pin-on-disk wear test

Appendix E PhDCEP Capstone Module: I-Shield Technologies[4]

This final section of the thesis describes a potential commercial venture that might be able to exploit some of the applications described previously. Specifically, we have focused on the use of the polyelectrolyte multilayer platform for biomedical applications. While our technology for increasing the longevity of orthopedic implants (see Chapter 3 for details) is an ideal foundation for a fledgling startup, any commercial venture that seeks to add value to an existing product needs to be more than just a one-product company. In the pages that follow, we describe I-Shield Technologies, a company that uses the versatile polyelectrolyte multilayer platform to provide coatings to solve medical problems of widespread clinical relevance, ranging from wear reducing coatings for hip and knee implants to antibacterial films for breast augmentations and reconstructions. In developing this business plan, we have also utilized polyelectrolyte multilayer applications beyond the work presented in this thesis; the antibacterial and drug delivery capabilities of these films were developed in the laboratory of Prof. Michael Rubner in the Department of Materials Science and Engineering.

The following is an adaptation of the *semifinalist* business plan submitted to the 50K Entrepreneurship Competition at MIT. Several of the plan's accolades have been enumerated in the section titled *External Reviews for Technology and Business Concept.*

[4] This chapter was co-authored by Michael Berg (Chemical Engineering) and David Lipman (MIT Sloan)

I-Shield Technologies

Confidential Business Plan

Please Do Not Distribute

This document does not represent
an offer to sell securities

I-Shield Technologies

www.ishieldtech.com

contact email: info@ishieldtech.com

I-Shield Technologies

Table of Contents

Executive Summary

I-Shield Technologies solves important biomedical problems by applying proprietary technologies developed in the laboratories of MIT. Our team is comprised of individuals who have developed the fundamental technologies involved, a medical specialist, and a businessperson with significant startup experience.

I-Shield will use a licensing business model to drive over $35MM in pretax cashflow by our third year. We will do so by exploiting our proprietary technology platform to address fundamental medical issues in artificial knees and hips, breast implants, post-operative adhesions, coronary stents, and other areas in a sequential manner. I-Shield will develop each solution and then license it to a leading existing device manufacturer, keeping overhead low and resources flexible.

I-Shield is a resilient company with many potential paths to success.

Technology: I-Shield uses ultra-thin coatings with proven ability to reduce wear and/or prevent biological encroachment by cell and bacteria. Our coatings are easy to apply, biocompatible (FDA approved), and do not change the material properties of the host device.

Market: I-Shield will optimize and then license its technology to one of five major hip and knee implant manufacturers. It will develop and license its technology to one of the two leading manufacturers of breast implants. Coronary stents, a potential home run, post-operative adhesions, and other markets will be exploited following a successful outcome in these two markets, or may be substituted in their stead if significant roadblocks are encountered in either market.

Team: I-Shield will comprise of 8 individuals after its first 3 months and currently has 4 founding members.

Scientists: Prem Pavoor and Michael Berg
Medical Doctor: Sridhar Durbhakula
Business/Finance: David Lipman

Financials: I-Shield's predicts over $35MM in pre-tax cashflow in its first 3 years. Peak predicted funding need is just over $2MM at the end of the first year.

Offering: I-Shield is looking for $500,000 to secure patent rights, further optimize our first product, and obtain our first licensing partner. We will gain the funds required to complete our first product and subsequent products from our first licensing partner in exchange for product rights and a small equity stake. Please Note: This document is not an offering to sell securities.

Introduction and Business Concept

I-Shield Technologies, www.ishieldtech.com, develops nanoscale coatings and films for important biomedical problems of widespread clinical relevance. Based on a common platform of patent-pending technologies developed at the Massachusetts Institute of Technology (Cambridge, MA), our product portfolio includes:

- Wear resistant coatings to improve the longevity of hip and knee total joint replacement implants
- Antibacterial and/or cell-inert coatings to enhance the performance and success rates of breast reconstruction and augmentation implants
- Cell-inert films to prevent post-operative adhesions
- Sustained drug eluting coatings for coronary stents

For the sake of brevity, this business plan will largely focus on I-Shield's products for the orthopedic and breast implant markets; these will lead I-Shield's foray into the medical device industry. The company is, however, actively pursuing the post-operative adhesion and drug delivery applications, and the following section provides a brief overview of these market opportunities for the reader's convenience.

Stage 1, Wear Reduction in Orthopedic Joint Replacements

Over 600,000 hip and knee total joint replacement procedures are performed annually in the United States alone; this represents a market of $3.5B with an annual growth rate of 9% (Standard and Poor's Reports, 2004). The most common configuration for the implants consists of a metal component articulating against a plastic (polyethylene) counterpart. Current artificial

joints have an average life of 10-15 years before replacement (revision) becomes necessary; for younger and more active patients, the life of the implant is often lower. The longevity of the implant is primarily limited by the formation of plastic wear debris at the articulating surfaces. The wear particles induce dissolution of the bone that holds the implant in place through an adverse cellular reaction to the wear debris (Ingham and Fisher, *Proceedings of the Institute of Mechanical Engineers, Part H: Journal of Engineering in Medicine*, 2000). Bone dissolution subsequently leads to implant loosening, necessitating a revision surgery. Revision surgeries are associated with significant health care expenditures (approximately $50,000 per surgery), prolonged hospitalization and patient dissatisfaction. Over the years, existing players have been able to capture significant market share even with only marginal improvements in wear reduction for these implants. With an aging baby boomer population, and as patients continue to lead more active lifestyles, there is a distinct need for a material that will minimize wear particle formation in order to avoid painful and expensive replacement procedures. To a 50-year old patient who wants to lead a normal lifestyle after a joint replacement, without the concern of revision surgeries every 10 years, a product that minimizes wear would be a godsend.

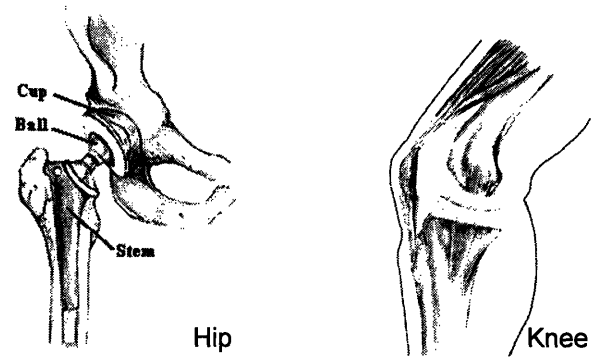

Figure 1. Schematic of hip and knee joint replacement implants (reproduced from Huddleston, *Arthritis of the Hip (Knee) Joint*, 2003)

I-Shield uses a patent-pending technology to transform the surface of the currently used implant materials in order to significantly reduce the formation of wear particles. I-Shield employs novel, biocompatible polymer coatings to achieve an improvement in implant longevity. The typical thickness of the coating is 100 nm (i.e. approximately one-hundredth the thickness of a strand of human hair). While the extremely thin coatings produce no physical/visible change to the existing implant materials, tests commissioned and run on orthopedic wear testers at the Massachusetts General Hospital have demonstrated up to a 40% reduction in wear particle production, for coatings that were not optimized. This is roughly equivalent to an additional 5 to 10 years added to product life (see Technology Section for details). The add-on coating technology provides improved performance utilizing existing implant materials. In addition to metal-on-plastic implants, the technology has been proven effective for wear reduction in other bearing surfaces such as the metal-on-metal articulation. Though the wear rates for the metal-on-metal implants are considerably lower than the conventional metal-on-plastic system, there are concerns about carcinogenicity from the metallic wear debris. In addition, high metal ion levels have been observed in the surrounding joint fluid when these materials are used. These factors have dampened the enthusiasm for the metal-on-metal implants in the United States.

Stage 2, Enhancement in Success Rates of Breast Augmentation and Reconstruction Implants

Approximately 270,000 breast augmentation and reconstruction surgeries were performed in the U.S. in 2000, according to the American Society of Plastic Surgeons. This represents a large and growing annual market of $250MM. In the same year, however, 54,000 implants were removed. Capsular contraction, along with chronic infection, was cited as the

major cause for these removals in 48% of cases. If the problems in these 48% of cases were prevented, over $100MM would be saved at a cost of $5,000 per revision surgery.

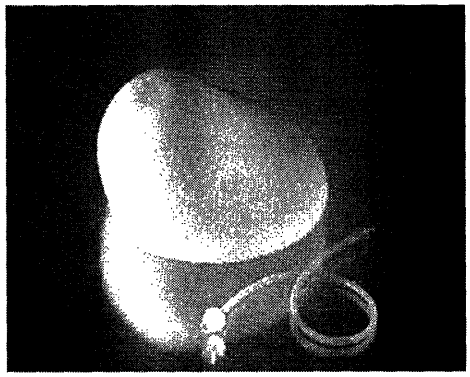

Figure 2. A typical saline-filled breast implant (courtesy Inamed Aesthetics)

During surgery, a pocket is made for the implant. Under normal conditions, the pocket remains open, thus allowing the implant to look and feel natural. However, in some patients, it tightens, squeezing the implant. This makes the implant feel hard, and distorts the appearance of the breast; the squeezing of the implant also causes the patient considerable pain and discomfort. While the exact cause of capsular contracture is unclear, it has been widely speculated in research literature that bacterial contamination of the implant shell causes an inflammatory reaction, which eventually leads to contraction (Pajkos, et. al., *Plastic and Reconstructive Surgery*, 2003).

I-Shield offers a cell-inert nanoscale coating that eliminates bacterial growth and non-specific tissue interaction to the extent of 99.9% (see Technology Section for experimental validation). Such a coating is expected to eliminate the incidence of capsular contracture in breast implants. The patent-pending technology, developed at MIT, would be the first of its kind for the breast implant market. The physical characteristics of the implant will be unaffected by the ultra-thin biocompatible coatings.

Stage 3+, Future Growth Opportunities for I-Shield

The following provides a brief overview of future growth areas for I-Shield. For the sake of conciseness, we will focus exclusively on the hip and knee, and breast implant markets in this business plan.

A. Prevention of Post Operative Adhesions

Post-operative adhesions occur with almost any surgery. Adhesions are fibrous formations that attach tissues or organs that should not normally be joined together. They are the unintended result of surgery, and their complications include bowel obstruction, infertility, restricted limb movement, pain, and often death. In 2001, an estimated 69 million procedures in the U.S. were applicable for use of an anti-adhesive sealant (National Center for Health Statistics); the number has increased from 36 million in 1996. This represents a market of approximately $8B in the U.S. alone. Abdominal, gynecological, and cardiovascular surgeries procedures frequently result in adhesion formation. About 93% of abdominal, 75% of gynecologic, and nearly 100% of open-heart surgeries result in adhesions.

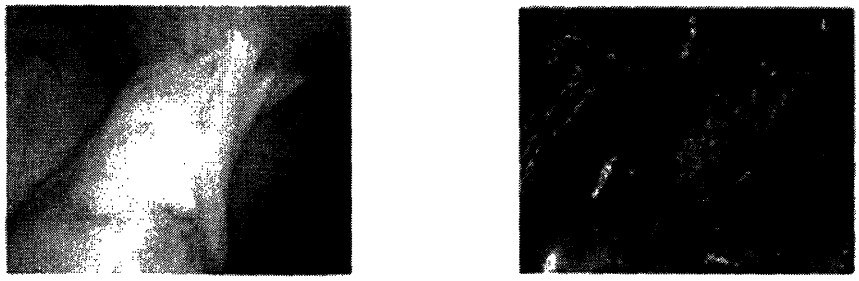

Figure 3. Illustrations of post operative adhesions – ovary to wall adhesion (left) and bowel adhesion (right). Reproduced from Surgical Biomaterials, Stephens, Inc., 2000.

Our technology could prevent post operative adhesion between tissues. We have developed nanoscale biocompatible polymer films that completely eliminate inter-tissue interaction.

Extensive tests in the laboratory have clearly demonstrated the technological superiority of our product over existing materials used to prevent adhesions currently on the market.

B. Sustained Drug Delivery Coatings for Coronary Stents

Standard and Poor's reports approximated the U.S. market for coronary stents to be $2B in 2003. Coronary stents are meshlike metal tubes that are inserted into diseased coronary arteries during angioplasty; the stent acts as a scaffold to keep the artery open. The insertion of the stent allows for unobstructed blood flow to the heart and often eliminates the need for an invasive bypass graft surgery. Sometimes, however, the vessel closes again at the site of the stent. A study published in the *New England Journal of Medicine* (2002) demonstrated that a major cardiac adverse event (leading to death, a heart attack, or the need for repeated revascularization of the targeted area) occurred in 31% of patients within six months after stenting.

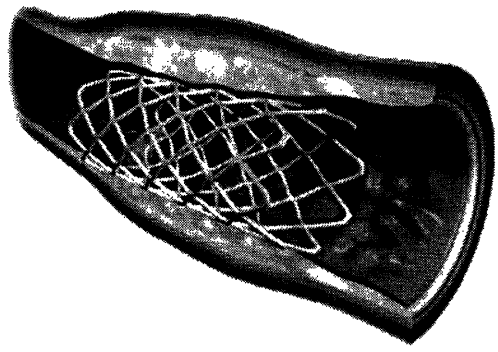

Figure 4. Schematic of a coronary stent (courtesy Endovasc, Inc.)

Medical device companies (Johnson & Johnson, Boston Scientific) have shown that drug-coated coronary stents can significantly reduce closing of the vessel after stenting. The drugs used to coat the stents are normally anticancer compounds that were developed to inhibit cell proliferation, and are typically applied to the stent via a polymer coating that allows for sustained release of the drug.

I-Shield's fourth product is a conformal coating for a coronary stent that is itself cell-inert. This product could prove to be a home run. With this coating, we eliminate the need to introduce a drug onto the stent. By preventing cell adhesion and hence proliferation, I-Shield's nanocoating will reduce the incidence of restenosis (vessel closing around the stent) to a minimum. *Alternatively, I-Shield also offers a coating that can be easily loaded with a drug. I-Shield's unique nanoporous coating facilitates the introduction of a drug molecule and allows for its sustained release over extended periods of time.* Extensive experimental validation at MIT has proven that I-Shield's biocompatible coatings can withstand physiological environments.

The following table provides a synopsis of the proprietary knowledge on I-Shield's founding team, some of which has been translated into patent applications that I-Shield eventually intends to exclusively license from MIT.

Stage	Application	Product Description	Patent Status
	Hip and knee implants	Wear resistant nanoscale coatings	Patent pending
Stage 2	Breast implants	Anti-bacterial and cell-inert nanoscale coatings to prevent capsular contracture	Patent pending
Stage 3+	Post-operative adhesions	Cell-inert films to prevent tissue interaction	Patent pending
Stage 3+	Coronary stents	Cell inert coatings Nanoporous coatings for sustained drug delivery	Patent pending Patent application filed

Overall Timeline

I-Shield's road from product development to commercialization for each of its stages can be summarized by the following table. For each of its stages, I-Shield will spend approximately one year to customize its product for the particular end application and issue an exclusive license for its use to a device manufacturer. The licensing will be typically accompanied by the FDA approval process, followed by the commercial launch.

Year 0 Months 1-2	**Year 0 Month 3**	**Year 0 Months 4-9**	**Year 0 Months 10-12**	**Year 1 Months 12-21**	**Year 1 Months 21-24**	**Year 2 Months 25-33**	**Year 2 Months 34-36**	**Year 3 Months 37-48**	**Year 4 Months 49-60**
Stage 1, Hip and Knee Implants									
	Equip Lab	Hire Lab Techs							
Carry out initial optimization in leased laboratory.		Finish Optimization in I-Shield Laborartory		Surgeon champion recruitment and product launch in small patient groups				Full market launch	
Refine deal with first customer	Receive initial funding from first customer		Premarket notification 510(k) filed by partner and approved by FDA (3 months)	First normal partner payments begin		Second year partner payments		Third and final year partner payment	
Stage 2, Breast Implants									
			Preliminary Optimization Work for Breast Implants	Product development at I-Shield		Surgeon champion recruitment and product launch in small patient groups			Full market launch
		Preliminary Industry Discussions		Negotiations with second partner	Premarket notification 510(k) filed by partner and approved by FDA (3 months)	First partner payments begin		Second year partner payment	Third and final year partner payment
Stage 3+, Future Opportunities									
			Preliminary Industry Discussion and Product Development			Stage 3 development begins		Surgeon trials for Stage 3	

Technology

A. Nanoscale Coating Technology

Our coatings for both orthopedic and breast implants are based on a single, but versatile, film assembly technology. The coatings are formed by the sequential adsorption of oppositely charged polymers from aqueous solutions, and rely on ionic and chemical linkages between the polymers for their structural integrity. A schematic of the film assembly process is depicted in the Figure 1 below. By varying the processing conditions during film assembly, the properties of the resulting coatings can be tailored to satisfy the needs of the end application. For hip and knee artificial joints, we use the technology to produce coatings that reduce the wear of the underlying implant materials. The same process used to manufacture films for breast implants results in coatings that demonstrate enhanced bacterial resistance and reduce the occurrence of capsular contracture. It must be emphasized that the coatings (each with their unique properties) and their end applications, and not the coating technology itself, are the subject of I-Shield's patent portfolio. The general method of coating provides several advantages:

- Adaptation to industrial is easy because various dip or spray-based methods can be used to coat materials and the films can be sterilized easily.
- The coatings are strongly adherent to a wide range of materials
- The coatings are conformal, providing contour coverage, and are uniform over large areas.
- All the processing is water-based and thus environmentally benign.
- The entities used to assemble the coatings have all been included in devices that have been FDA approved as biocompatible, and they are not chemically affected during film assembly, so should remain chemically equivalent to the approved compounds.

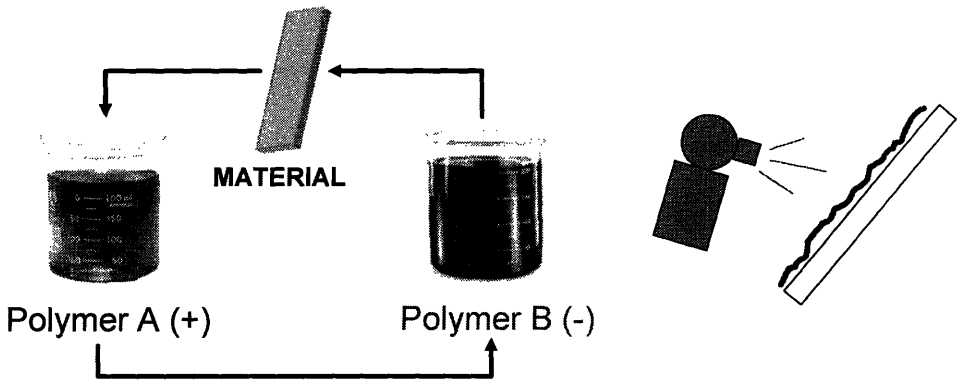

Figure 1. Schematic of the film assembly process using solutions of oppositely charged polymers. The films can also be sprayed onto the material, as illustrated.

B. Current Status of Product Development

An important part of I-Shield's contribution in the value chain (see Figure 2) will be to adapt the fundamental characterization of the coatings and our proprietary knowledge base to develop a customized product for the particular end application. This customization is expected to take up to one year for each application.

MIT: Fundamental original Ph.D. research	→ **I-Shield: Optimize coatings for medical implants, develop new coating applications**	→ Medical device manufacturer (e.g. JNJ, Inamed)	→ Regional distributors	→ Medical device representatives	→ Hospitals and surgeons

Figure 2. I-Shield's position in the value chain

Stage 1. *Wear reducing coatings for orthopedic implants*

Extensive fundamental friction-and-wear characterization of the coatings has been performed by a member of the founding team as part of his doctoral thesis. In addition, initial commissioned testing on orthopedic wear testers at the Massachusetts General Hospital has indicated considerably reduced wear (up to 40%) for the coated implant materials (see Figure 3);

this might itself translate into 5-10 years of additional life for an implant. Further optimization and testing of the coating are the next steps for I-Shield prior to entering into an agreement with a potential partner. The development phase will include:

a. Optimization of the polymer pair used for the coatings to further reduce wear

b. Hip and knee simulator tests (outsourced to an external testing facility)

c. Biological inflammatory response studies

d. Adaptation of technology to industrial scale

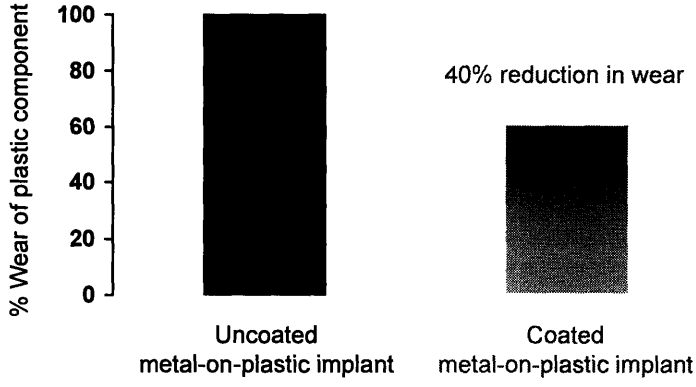

Figure 3. Unoptimized coatings demonstrated a 40% reduction in wear compared with their uncoated counterparts in wear tests over 6 months of equivalent human hip use

Stage 2. *Cell and bacterial inert coatings for breast implants*

Members of our advisory board and founding team have been involved in numerous mammalian cell and bacteria experiments to study the effectiveness of the coatings in biological applications. Results have conclusively demonstrated the cell-inert and anti-bacterial nature of our films; *the films resist cell adhesion to the extent of 99.9+%, without compromising the viability of the mammalian cells* (Yang et. al., *Biomacromolecules*, 2003). The resistance to cell adhesion is attributed to the ability of our films to swell upon hydration, which prevents cells from physically attaching to the surface. The antimicrobial properties of the films are the result

of the introduction of minute amounts of specific antibacterial agents (e.g. silver ions) into the coating. *The films are not passivated by protein adsorption, unlike some existing technologies.* I-Shield plans to enter into collaborative experiments with potential partners as the next phase of this process; this will allow for product customization and incorporation of the add-on technology into the existing manufacturing process. Inamed Aesthetics has expressed significant interest to enter this phase (see Subject Matter Expert Interviews Section). During this optimization phase, I-Shield will address the following issues:

a. Structural integrity of the coating under shear stresses

b. Corroborate adhesion of the coating to the breast implant

c. Further *in-vitro* testing to quantify bacterial adhesion

d. Animal studies (if necessary)

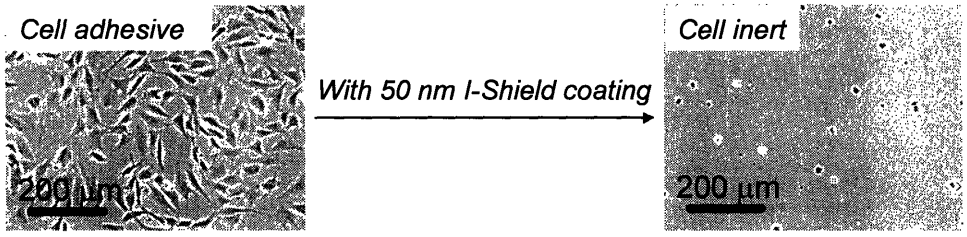

Figure 4. As an example of cell-inertness, I-Shield's coatings demonstrate resistance to fibroblast adhesion

C. Intellectual Property

Members of our founding team and advisory board have had several years of experience working with this coating technology and have developed considerable proprietary knowledge in that domain. The film assembly technique that I-Shield utilizes is a general one that is well reported in scientific literature. I-Shield's patents and proprietary knowledge are based on the materials, processing conditions, and use of the resulting films for specific applications. One or

more members of the team are co-inventors on all the patents used by I-Shield. In addition, Advisory Board member Spiegelberg brings considerable experience to the team on intellectual property licensing deals. I-Shield will license the following patents from MIT.

No.	Serial Number	Status	Title	Filing Date
1	10/278,774	Patent-pending	*Polyelectrolyte multilayers that influence cell growth, methods of applying them, and articles coated with them*	23-Oct-02
2	60/435,003	Patent-pending	*Method for making medical devices having antimicrobial coatings thereon*	19-Dec-02
3	10/453,453	Patent-pending	*Tribological applications of polyelectrolyte multilayers*	3-Jun-03
4	Case no. 10731	"h" application filed	*Loading and releasing molecules from porous polyelectrolyte multilayers*	31-Mar-04

D. Future Growth Strategies

I-Shield will continue to invent new coating products by leveraging its existing IP platform. As discussed in a previous section, I-Shield is currently researching products to be used in the following areas:

Prevention of post-operative adhesions. Post-operative adhesions are a major medical concern and result from non-specific tissue growth in undesirable areas after surgery. I-Shield is developing film and gel barriers that can be applied by the surgeon to prevent these undesirable tissue growths following surgery.

Stent and catheter coatings. Cell growth on stents and catheters can cause blockages that prevent the implant from fulfilling its purpose. I-Shield's cell inert coatings can solve this problem by improving the surface of the implant with regards to long-term cell resistance.

Drug-release coatings. Implants eluting drugs or growth factors from the surface can provide localized delivery that could dramatically help the patient's recovery. I-Shield is developing coatings that are not only engineered to reduce non-specific cell attachment and kill bacteria, but also release drugs or growth factors in a controlled manner.

In vitro diagnostic tests. Besides providing products for use in the body, I-Shield will develop coatings for cell arrays, drug-screening assays, and cell-based biosensors. We can creatively modify our cell-inert coatings by engineering patterns of molecules to interact with cells in a specific manner.

Anti-bacterial coatings. The anti-microbial properties of I-Shield's coatings can be used in many other applications besides preventing infection of breast implants. *Unlike some existing technologies, our coatings are not passivated by proteins.* There are opportunities on other medical implants as well as other applications such as textiles and scientific equipment.

Competitive Advantage

I-Shield's products for orthopedic joint replacements and breast implants are based on technologies that offer the following advantages:

- ***FDA approved materials***: All of I-Shield's ultra-thin coatings utilize polymers that are approved for use in existing medical devices. Since the resulting coating does not alter the chemical nature of its constituents, our products will NOT have to go through a capital and time intensive human clinical trial stage before introduction.

- ***Superior technologies***: I-Shield's competitive advantage lies in its products being technologically superior to those offered by its competition.

Type of Implant	**Potential Competing Technology**	**Disadvantages**
Hip	Radiation treatment	Weakens implant mechanically Cannot be applied to knee (only hip)
Breast	Phosphorylcholine polymer coatings	Not as easily applied to surfaces Materials require tedious synthesis with much higher number of processing steps increasing complication Only 70% reduction in bacterial attachment vs. 99.9% for I-Shield

- Our products provide an ***add-on technology*** that does not replace the currently used implant material combination. It only improves the materials through addition of a 100 nm coating. Complete re-training of the sales force and surgeons is not required.

- ***Low capital and labor expenditure:*** The transformation of the implant materials can be achieved via an automated process that is easily scalable and requires minimal capital expenditure. The process is environmentally-benign and water-based.

- ***Patent-protected technologies***: Our products are based on 4 patents filed by MIT through Foley Hoag, LLP (see Subject Matter Expert Interviews Section). Each of our offerings is based on 3-5 years of original doctoral research, and the intricacies of the technologies would be very difficult to replicate.

Stage 1, Hip and Knee Implants

There are currently 5 major manufacturers of hip and knee replacements. Four out of the five use a radiation-treated version of the plastic component for the hip implant (the metal surface is identical for all manufacturers). It has been demonstrated in clinical trials that this version of the plastic is associated with a lower wear rate compared with its untreated counterpart.

Radiation treatment, however, adversely affects the mechanical strength of the plastic component, affecting the longevity of the implant, particularly for the case of the knee which experiences larger forces than the hip. The treatment has, subsequently, not been approved by the FDA for use in knee implants.

Our technology addresses the problems with radiation treatment by providing an add-on coating to the existing implant materials, i.e. the properties of the underlying plastic are unaffected (unlike radiation treatment). The coatings are only 100 nanometers thick, but still drastically reduce wear rates without any reduction in structural or mechanical integrity. Hence

they can be applied both for the hip and the knee.

Stage 2, Breast Implants

There are currently 2 manufacturers of breast implants in the US market. In this $250MM US market, none of them has a product, on market or planned, that claims to reduce the incidence of capsular contracture. I-Shield's product is thus unrivaled; extensive studies have shown that our product is cell and bacteria inert hand would resist interaction with the surrounding capsular tissue to the extent of 99.9 % (see Technology Section).

B. Competitor Profiles

Orthopedics

Currently Zimmer, Stryker, JNJ/Depuy, and Smith and Nephew offer hip implants that claim reduction in wear.

Company	Product Name	Technology
Zimmer	Longevity	Radiation Treatment
Stryker	Crossfire	Radiation Treatment
JNJ/Depuy	Marathon	Radiation Treatment
Smith and Nephew	Reflection	Radiation Treatment

Radiation treatment reduces wear, but it also greatly reduces the mechanical strength of the implant. For this reason, the treatment can only be performed on hip implants and not on knee implants. No company manufacturers a knee implant with reduced wear properties. Our coatings do not alter the bulk properties of the implant making it an attractive product for both hip and knee implants.

Bio-Inert Coatings for Breast Implants

No breast implant manufacturer currently markets a product claiming to reduce the occurrences of infection or capsular contraction. Biocompatibles and SurModics, however, produce coatings designed to reduce cell adhesion and bacterial infection. Currently, their coatings are not designed for breast implants, but they could be potential competitors.

Biocompatibles specializes in making biomedical polymers for drug delivery and medical devices. Their products include drug-eluting coatings for stents and various technologies for the treatment of tumors. Their stent coatings claim reduction in cell adhesion and protein adsorption as well as discouragement of bacterial growth. The coatings use PC Technology™, which utilizes polymers containing phosphorylcholine. In scientific literature, phosphorylcholine has been reported to reduce adhesion of cells, proteins, and bacteria. Particularly in the case of bacterial adhesion, however, this chemical only reduces adhesion by approximately 70% leaving a large amount of bacteria to grow on the surface (Ostoni, et. al. *Langmuir*, 2001). I-Shield's coating for breast implants is superior since it reduces bacterial adhesion by 99.9% and virtually eliminates the interactions of mammalian cells with the surface.

SurModics provides surface modifications for biomedical applications. Their core technologies include a patented drug delivery polymer platform and surface modification technology called PhotoLink®. The PhotoLink® modification claims reduction in platelet attachment and a decrease in friction. They make no claims about antimicrobial properties, or interactions with other cell types besides platelets. I-Shield's coating addresses both of these areas.

Manufacturing and Operations

A. Initial Activities

I-Shield will conduct its initial optimization work on rented equipment for its first three months, addressing any proof of concept questions brought by potential partners during negotiations. Lab costs will be based on hours used and should not exceed $100,000. Additionally, the initially $500,000 will cover over $200,000 in outsourced testing, basic coating and characterizing equipment, some of which is included in section "C" below, rent of temporary lab space, any additional materials and research, as well as initial payrolls and fees.

B. Facilities

Upon funding from partner, I-Shield will lease approximately 4000 ft^2 of laboratory and office space in the Greater Boston area to develop its biomedical coatings. The laboratories will include equipment for cell culture, thin film processing, and characterization. The necessary equipment will cost approximately $150,500 and rent will be approximately $120,000 per year. For orthopedic implant testing, we will outsource hip and knee simulation for $500,000 for Stage 1. Approximately half of this testing will take place before our first partner is signed. For Stage 2 we will spend an additional $250,000 for testing. I-Shield does not need a manufacturing area since we plan to license or partner with existing implant manufacturers who will integrate our technologies into their manufacturing operations.

C. Equipment

Our laboratory equipment will consist of facilities for producing coatings, performing tissue culture, and characterizing the properties. The total cost for equipment needed for start-up is approximately $150,500. The following table provides a breakdown of these costs:

Equipment	Qty.	Price($)	Total Cost($)	Manufacturer	Supplier
Coating Equipment	2	12,500	25,000	Microm	Microm
Vacuum Oven	1	1,400	1,400	VWR	VWR
Vacuum Pump	1	1,500	1,500	VWR	VWR
Incubator	2	9,200	18,400	Barnstead	VWR
Water Bath	1	700	700	VWR	VWR
Orbital Shaker	1	800	800	VWR	VWR
Freezer	1	2,500	2,500	VWR	VWR
Low Temp Freezer	1	7,100	7,100	VWR	VWR
Refrigerator	2	2,100	4,200	VWR	VWR
Cryogenic Storage Unit	1	9,700	9,700	VWR	VWR
Vortex	1	200	200	VWR	VWR
Ultrasonic Cleaner	1	400	400	VWR	VWR
Centrifuge	1	3,500	3,500	Eppendorf	VWR
Microscope + Computer	1	45,000	45,000	Zeiss	Zeiss
Balance	1	1,900	1,900	Mettler-Toledo	VWR
Stirrer/Hot Plate	2	200	400	VWR	VWR
pH Meter	2	600	1,200	Beckman	VWR
Plasma Cleaner	1	2,500	2,500	Harrick	Harrick
Milli-Q Water System	1	7,500	7,500	Millipore	Millipore
Chem. Storage Cabinet	2	1,500	3,000	VWR	VWR
Tissue Culture Hood	1	4,800	4,800	Labconco	VWR
Chemical Fume Hood	1	4,800	4,800	Labconco	VWR
Miscellaneous Supplies	1	2,500	2,500	VWR	VWR
TOTAL COST			$150,500		

C. Chemicals and Consumables

In addition to start-up equipment, I-Shield will use approximately $7,500 per year in chemicals and other laboratory consumables. The following table provides information on these costs:

Item	Yearly Cost	Supplier
Polymers	2,000	Sigma, Polysciences
Solvents	500	Sigma, VWR
Cell Culture Supplies	2,000	Invitrogen, Sigma, VWR
Proteins and Peptides	1,000	American Peptide, Invitrogen, Sigma
Water Filters	1,000	Millipore
Miscellaneous Lab Supplies	1,000	VWR
TOTAL YEARLY COST	$7,500	

FDA Regulation and Product Launch

FDA Device Classification

Medical devices are classified by the U.S. Food and Drug Administration (FDA), which evaluates them for safety and effectiveness before granting marketing approval. Devices may fall into one of the following three classifications for new submissions, depending on their potential risk.

Class	Examples	Control Type	Potential Patient Risk	Pre-Approval Stipulations
I	Stethoscopes, surgical scalpels	General controls	Low	Sufficient evidence to prove safety/effectiveness
II	X-ray machines, endoscopes, I-Shield coated hip, knee, and breast implants	Special controls	Moderate	Insufficient evidence to support safety/effectiveness. Substantial equivalence to a predicate device
III	Cardiac pacemakers, angioplasty catheters	Pre-market approval	High	Insufficient evidence to support safety/effectiveness. No substantial equivalence to a predicate device

After consulting with several implant manufacturers (Zimmer, Biomet Orthopedics, see Expert Interviews Section), we expect that our coated end-products (hip and knee implants, and breast implants) will classify as Class II medical devices. The materials used to assemble our coatings are all biocompatible and included in existing FDA-approved devices. Additionally, the coatings will be applied to previously FDA approved devices (orthopedic and breast implants). Therefore, substantial equivalence can be established to pre-existing devices, allowing for a Class II status.

Timeline to FDA Approval and Market Launch

For all Class II devices, medical device manufacturers can obtain FDA clearance via the agency's premarket notification process, known as the 510(k) filing. The manufacturer must submit a 510(k) to the FDA at least 90 days before introducing any new device on the market for the first time. A 510(k) is also required when proposing a major change in intended use for a device that is already in commercial distribution. A 510(k) includes descriptive and performance data to demonstrate that the device to be marketed is safe and effective, or substantially equivalent to a legally marketed device (predicate device).

I-Shield will take one year to optimize, test, and customize its product for each end application. During this one year interim, the company will also engage in negotiation with prospective partners. The rigorous laboratory data will allow us to market the product more effectively to potential clients. We expect that the 510(k) notification will be filed with and approved by the FDA before the end of the year. Once FDA approval has been received, the product is ready to be launched commercially. Most implant manufacturers recruit surgeon champions to implant the product in a select group of patients. It is generally believed that the market, as a whole, embraces the new product approximately two years after the first implants have been used by the surgeon champions (and clinical performance data is available), and the device has been introduced at major medical conferences. The timeline for this process is illustrated below.

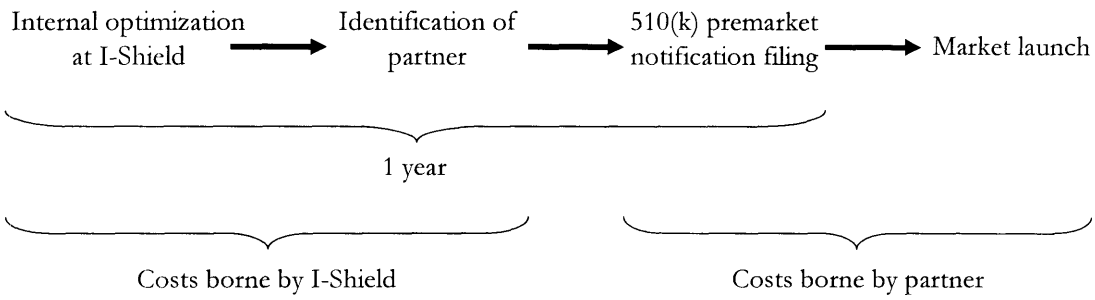

Road to FDA Approval and Product Launch for I-Shield's Class II Devices

Marketing and Potential Customers

Stage 1, Hip and Knee Implants:

After one year of product development, optimization, and testing in Year 0, I-Shield will sell an exclusive license for its implant coatings to one of the five major producers in the hip and knee implant market (see Timeline Section). I-Shield will closely collaborate with the partner as it completes the necessary FDA trials and production optimization needed to allow volume market production. The chart below depicts the industry scenario in the annual $3.5B hip and knee implant market.

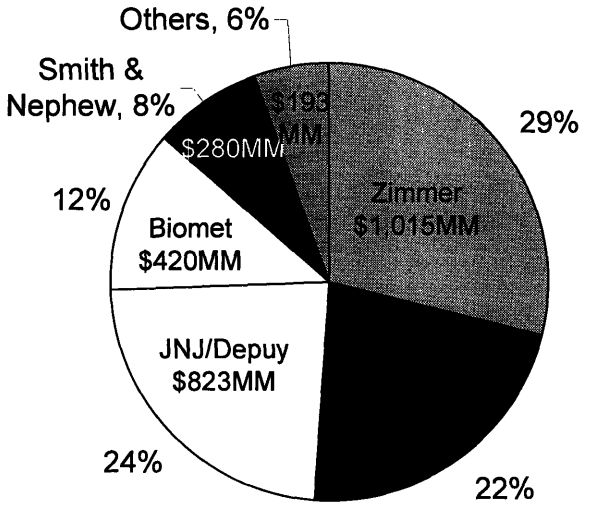

(Courtesy Standard and Poors Reports, 2004)
Hip and Knee Implant Producers in the U.S.

Currently, four of the manufacturers (JNJ, Zimmer, Stryker, and Smith & Nephew) use radiation treatment to lower the wear of the plastic implant component. While we are currently initiating discussions with Biomet Orthopedics, I-Shield's technology will also offer a compelling value proposition to any producer who has already invested in radiation technology because our technology is superior and applicable to the knee (radiation treatment is not approved for use in

the knee). With a product that offers superior performance, our partner will be able to gain market share and raise prices. The format of the sale as an exclusive license will create a bidding environment that will allow I-Shield to extract a relatively large share of the value created by its technology. As shown in the table on the next page, most of the potential buyers of I-Shield's hip and knee technology are large and could easily afford an exclusive license for our technology.

I-Shield's strong associations with the orthopedic surgery department at Brigham and Women's Hospital and an orthopedic surgeon on its founding team will make it easier to reach out to these manufacturers. Already, we are in the process of beginning discussions with Biomet Orthopedics.

Key Statisitics

Name of Company	Total Sales	Estimated US Hip and Knee Sales	Market Cap	Net Income	PE	Cash On Hand	Competitive Antiwear Technologies for Hip	Competitive Antiwear Technologies for Knee
Zimmer	$1.9B	$1,015MM	$19.4B	$291MM	67	$77.5MM	Radiation	None
Stryker	$3.64B	$770MM	$19.9B	$453.5MM	44	$65.9MM	Radiation	None
JNJ Depuy	$3.0B (Depuy)	$823MM	$160.65B	$7.62B	21	$9,520MM	Radiation	None
Biomet	$1.55B	$420MM	10.27B	$323.5MM	32	$463.6MM	None	None
Smith & Nephew	$2.1B	$280MM	$9.77B	$263.8MM	37	$47.71MM	Radiation	None

Recent Deals

Name of Company	Date	Details
Zimmer	June 2003	Purchased Centerpulse, a leader in European Orthopedics, for $3.2B in cash and stock.
	November 2003	Purchased Implex, developer of trabecular metal technology, for $89MM in cash.
Stryker	July 2002	Purchased Surgical Dynamics spinal business for $135MM in cash.
	August 2000	Purchased Image Guided Technologies (optical localizers) in all stock deal.
JNJ/Depuy	May 2003	Purchased Link Spine, maker of artificial disc, for $325MM up front, plus milestone payments.
	January 2003	Purchased most of Orquest, a bone graft company, for undisclosed amount.
Biomet	March 2004	Announced purchase of Interpore, spinal products, for $280MM in cash.
	September 2000	Purchased Biolectron, spinal fusion products, for $90MM in cash.
Smith & Nephew	March 2004	Purchased Midland Medical Technologies, metal on metal hip implants, for $160MM cash.
	November 2002	Purchased Dermagraph for $12MM in cash.

Source: public filings & company websites. US Hip and Knee sales estimated by Standard and Poors.

Stage 2, Breast Implants:

Using the revenues generated by the licensing agreement for its joint replacement technology, I-Shield will develop and optimize its coating for breast implants in Year One (see

Timeline). I–Shield will then sell an exclusive license to one of the two existing producers of breast implants in the $250MM+ per year US market, Inamed/McGrath or Mentor. I-Shield might also serve as a partner in commercialization and getting FDA approval. Currently, neither of these producers offers a product that is differentiated or can claim to address the important problem of capsular contraction. Also, each has approximately 50% share of the US market, and each has cash on hand in excess of $80MM and a market cap over $1B. Please see the table on the next page for more details.

With I-Shield's patent-pending technology that eliminates bacterial infection and hence the potential risk of contraction for the implant, our partner will enjoy an increase in both market share and average selling prices, making the partnership an important source of value for both offensive and defensive strategic reasons. *In phone conversations, Inamed has expressed significant interest in our technology. We are currently discussing the possibility of collaborative tests to demonstrate the efficacy of our coating.*

Potential Breast Implant Partners

Key Statisitics								
Name of Company	Total Sales	Estimated US Breast Implant Sales	Estimated Worldwide Breast Implant Sales	Market Cap	Net Income	PE	Cash On Hand	Competitive Anti-Contraction Technologies
Inamed	$332.6MM	$125MM	$170MM	$1.93B	$53.0MM	36	$80MM	None
Mentor	$405.9MM	$125MM	$180MM	$1.42B	$53.4MM	27	$170MM	None

Recent Deals		
Name of Company	Date	Details
Inamed	October 2002	Deal with Genzyme to license dermal filler. Payments based on milestones and sales.
	July 2002	Deal with Ipsen to sell botulinum toxin type A in the United States.
Mentor	October 2003	Acquired Inform Solutions, a practice management software company.
	November 2002	Acquired Mills Biopharmaceuticals, a prostrate treatment product.

Source: public filings & company websites. Breast Implant sales estimated by Suntrust Robinson Humphrey

Stage 3 and Beyond (Future Growth Opportunities):

As we develop new applications for I-Shield Technologies after Stage 2, we will apply lessons learned in Stage 1 and Stage 2 to refine our business model. Rather than being a manufacturer of medical devices and being involved in the capital intensive and low margin distribution side of the business, I-Shield will leverage its unique position in the value chain (see Technology Section, Figure 2) and its core competencies in product innovation to continue on as a developer of technologies.

Key Risks

I-Shield Technologies is an early stage technology company and its business plan has many outstanding risks and uncertainties. The following summary of key risks may not be all-inclusive, but does represent I-Shield management's view of the general potential hurdles ahead.

Technology Risk: Based on the expertise of its founding members in the coating technology arena, I-Shield estimates that it will take nine months to optimize its first product for the hip and knee implant market. While delays caused by unforeseen technical hurdles are not likely given our technical expertise and proprietary knowledge base, they could have material effect on I-Shield's viability. The risks of delays in technology customization are hedged, however, by our ability to shift focus to other applications (i.e. breast implants, coronary stents, post-operative adhesion prevention, etc.) if needed.

FDA Risk: Based on discussions with implant manufacturers like Biomet, I-Shield expects the end use coated devices to be classified as "Class I" or "Class II" by the FDA. As outlined in the FDA Section, we believe that since its coating materials are already biocompatible, and since the material properties of the previously FDA approved devices are virtually unchanged, there would be only a 3-month 510(k) pre-market notification process to get approval, and a subsequent 2-year trial period before full-scale market penetration occurs. There remains a slight risk, however, that our products might be classified as "Class III"; though the overall timeline remains the same, formal FDA approval for the device is obtained only at the end of the 2 year trial period. This might dampen market acceptance of the device and hence the time to significant market could be impacted by 1 to 2 years as a result. In such a case, our partner might have to

step up its marketing efforts during the approval stage to generate awareness and interest in the product.

Competitive Risk: I-Shield's product for the hip and knee implant market has a substitute technology that also achieves wear rate reduction (see Competitive Advantage Section). In addition, in the breast implant arena, there are other coating technology companies, most notably Biocompatibles, which could potentially offer a competing product. I-Shield's founding team is comprised of two scientists who have worked extensively with the coating technology and its applications for imparting wear resistance and cell-inertness as part of their doctoral theses. We have surveyed the competitor landscape extensively and are confident that our coatings are technologically superior to the competition (see Competitive Advantage Section for details).

IP Risk: There are two general risks faced by I-Shield in regards to intellectual property. I-Shield must first acquire these rights from MIT and then protect these rights from potential competitors, and from potential customers. As outlined in our technology section, the involvement of our team in the creation of the technologies to be utilized, and backing of the lead professors (and Advisory Board Members) involved, should allow us to reach an agreement with MIT. In addition, the patents were filed by MIT through Foley Hoag, LLP; in collaboration with the founding team members, the lawyers at Foley Hoag have performed a comprehensive search of existing patents and research literature. In the absence of prior work in this area, the resulting patent applications, which we plan to license, are broad, covering diverse materials and applications; we are quite confident that they will be defensible from attack.

Team Risk: I-Shield has a well-rounded team, with scientific, business, and medical experience. We realize, however, that the team is stronger on the technical side than the business side, without much experience in medical device marketing and IP licensing. As depicted in our proposed organizational chart (see Organizational Structure and Personnel Profiles Section), we are actively looking to recruit individuals with the relevant marketing and sales-and-negotiations backgrounds. We are utilizing the MIT Venture Mentoring Service, the 50K Mentor Program, and our own personal contacts for this purpose.

Partner Risk: In I-Shield's current plan, a partner is signed for our Stage 1 product early in the development stage, and begins cash payments within Year 0. While we feel confident in our ability to secure this partnership, there is a risk that negotiations might be prolonged. This risk is hedged by our ability to prioritize Stage 2, breast implants, ahead of Stage 1 if market conditions dictate. We do not foresee that risk in the amount of partner payments could have material impact on the viability of I-Shield as our cash requirements are small in relation to expected partner payments.

Financing Risk: I-Shield requires funds after our initial $500k to move forward. If I-Shield is unable to secure initial funding, alternate means of funding (like SBIR grants) will be pursued, and potentially another $500K will have to be raised. This risk is hedged, at least somewhat, by the fact that we will not raise the initial $500K unless we are reasonably close to having a deal formed with a hip/knee implant manufacturer.

Financial Plan

The following financial plan only considers the first two stages of I-Shield's plan. The first stage is to license its technology to a manufacturer of artificial knees and hips. The second stage is to use the license proceeds from Stage 1 to fund development of the breast implant product, and to license it to a breast implant manufacturer. Please note that we have not modeled proceeds from international opportunities, the surgical adhesions business, or the cardiac stent business in this plan and that they represent areas of significant opportunity and upside.

We expect I-Shield to become cashflow positive during its first year through the license proceeds gained by selling the artificial knee and hip licenses. On a cumulative basis, I-Shield will create over $35MM of pretax cash-flow in the first 3 years from the knee/hip implant and breast implant markets.

Revenue

Stage 1, *Knee and Hip Implants*

Revenue: I-Shield's technology will be licensed to a knee and hip implant device manufacturer with a ~12% market share. To be conservative, we assume that our technology will be substituted in only 50% of the manufacturer's implants. This represents a current partner addressable market of:

$3.5B * 12% market share * 50% share of products = ~$210MM annual

We believe that the value added by I-Shield is conservatively approximated by:

Volume due to increase in market share (20% increase in volume to ~12% market share):

Partner Addressable Market	X	Increase In Volume	X	Contribution Margin	=	Profit Created
$210MM		20%		70%		$29.4MM annual

Price (20% increase, the same as irradiated implants):

Market Size (Reflects Increase in Volume)	X	Increase In Price	X	Contribution Margin	=	Profit Created
$252MM		20%		90%		$45.4MM annual

The total additional profit gained through I-Shield technology is therefore conservatively estimated at ~$74.8MM per year. Using a PE multiple of 15 (lower than that of any potential partner) and a corporate tax rate of 40%, this would imply an increase in partner market value of: $74.8MM X 15 X (1 – 40%) = ~$672.8MM.

As our deal payments would begin at the end of Year 0, 2 years before profitability begins, we would discount this value for 3 years (discounting fully the first year of profitability) at a steep discount rate of about 35%, lowering the net present value at the time of deal to $273.5. We would expect to sell the technology for ~20% of this value, or roughly $54.7MM. We assume proceeds of $18.2MM at time of deal, with annual progress payments of $18.2MM and $18.2MM making the balance. As part of our partnership agreement, we also expect to sell an equity stake in the third month of Year 0 for $2.5MM, sufficient to fund over 12 months of operations. There are no future royalties expected from stage 1.

Stage 1 Revenue Summary:

$MM	Year 0	Year 1	Year 2	Year 3	Year 4	Year 5	Total
Stage 1	$ -	$ 18.2	$ 18.2	$ 18.2	$ -	$ -	$ 54.7

We believe that many of our most likely potential customers have sufficient cash, Biomet has over $450MM in cash, JNJ has over $9B in cash, to make up-front cash payments, as we

have modeled them, to be the most attractive form of deal. Our business plan is flexible as to whether these payments are structured as mostly upfront/progress, or partial upfront/progress and partial royalty-based provided that our operating cash needs are met and the NPV is not decreased. A typical royalty deal would give us smaller upfront payments of perhaps $7MM as a licensing fee, and then ~4% per year on all I-Shield coated devices sold, or roughly $12MM per year, starting in Year 3.

Stage 2, *Breast Implants*:

Revenue: I-Shield will partner with a breast implant manufacturer with approximately 50% market share, or $125MM per year. All of the market is addressable using I-Shield Technology.

We believe that the value added by I-Shield is conservatively approximated by:

Volume due to increase in market share (10% increase in volume, taking partner from ~50% market share to ~55% market share):

Partner Addressable Market	X	Increase In Volume	X	Contribution Margin	=	Profit Created
$125MM		10%		70%		$8.75MM annual

Price (20% increase, justified by the differentiated, premium product):

Market Size (Reflects Increase in Volume)	X	Increase In Price	X	Contribution Margin	=	Profit Created
$210MM		20%		90%		$24.75MM annual

The total additional profit gained through I-Shield technology is therefore conservatively estimated at about $33.5MM per year. Using a PE multiple of 15 (lower than that of any potential partner) and a corporate tax rate of 40%, this would imply an increase in partner market value of:

$33.5MM X 15 X (1 – 40%) = ~$301.5MM.

As our deal would take place at the beginning of Year 2, 2 years before partner profitability, we would discount this value for 3 years (discounting fully the first year of profitability) at a steep discount rate of about 35%, lowering the net present value at the time of deal to $122.5MM. We would expect to sell the technology for ~20% of this value, or roughly $24.5MM. We assume proceeds of $8.2MM at time of deal, with annual progress payments of $8.2MM and $8.2MM making the balance. There are no future royalties expected from Stage 2.

Stage 2 Revenue Summary

$MM	Year 0	Year 1	Year 2	Year 3	Year 4	Year 5	Total
Stage 2	$ -	$ -	$ 8.2	$ 8.2	$ 8.2	$ -	$ 24.5

As with Stage 1, we believe that both of our potential customers have sufficient cash. Inamed has over $80MM in cash and Mentor has over $170MM in cash. This will likely make up-front cash payments, as we have modeled them, to be the most attractive form of deal. Our business plan is flexible as to whether these payments are structured as mostly upfront/progress, or partial upfront/progress and partial royalty-based provided that our operating cash needs are met and the NPV is not decreased. A typical royalty deal would give us smaller upfront payments of perhaps $3MM as a licensing fee, and then ~4% per year on all I-Shield coated devices sold, or roughly $6.6MM per year, starting in Year 4.

Stage 3 and Beyond, *Additional Products*:

I-Shield will continue to expand its research and industry partnerships into new applications beginning in Year 2. We do not expect any revenue from this activity prior to Year 3, and have not modeled any cash flow beyond Stage 3.

I-Shield Revenue Summary

Only Revenue through year 3 appears in financial plan as revenue after Stage 2 is not included in our financial plan.

	Year 0	Year 1	Year 2	Year 3	Year 4	Total
Stage 1	$ -	$ 18.2	$ 18.2	$ 18.2	$ -	$ 54.7
Stage 2	$ -	$ -	$ 8.2	$ 8.2	$ 8.2	$ 24.5
Stage 3-on	$ -	$ -	$ -	?	?	?
Total	$ -	$ 18.2	$ 26.4	$ 26.4	$ 8.2	$ 79.2

I-Shield Revenue Sensitivity

(Baseline 3 Year revenue total is $44.6MM)

Changes to first 3 years of revenue (Year 0 through Year 2)
Revenue, $MM

Invisible Shield Share of Value Created

PE Rate	10%	15%	20%	25%	30%	35%
8	-52.1	-42.6	-33.1	-23.7	-14.2	-4.7
10	-47.4	-35.5	-23.7	-11.8	0.0	11.8
12	-42.6	-28.4	-14.2	0.0	14.2	28.4
14	-37.9	-21.3	-4.7	11.8	28.4	45.0
15	-35.5	-17.8	0.0	17.8	35.5	53.3
16	-33.1	-14.2	4.7	23.7	42.6	61.6
18	-28.4	-7.1	14.2	35.5	56.8	78.1
20	-23.7	0.0	23.7	47.4	71.0	94.7
22	-18.9	7.1	33.1	59.2	85.2	111.3
24	-14.2	14.2	42.6	71.0	99.4	127.9

Discount Rate Used in Negotiation
(3 Year Discount on Earnings)

Change in Rev	20%	25%	30%	35%	40%	45%	50%
	30.1	18.4	8.5	0%	-7.3	-13.7	-19.2

Costs

As outlined previously, I-Shield will require 1 year to optimize its technology in hip and knee implant devices (i.e., Year 0) before initial payments. In addition, I-Shield will need 1 year, starting at the end of Year 0 (i.e., Year 1) to prove and optimize its technology for breast implants. I-Shield has costs that are general, as well as costs that relate specifically to Stage 1 and Stage 2. Costs associated specifically with Stage 3-on are not included in our cost estimates, nor is the associated revenue.

General Costs:

General Recurring Operating Expenses

Lab Space: 3,500 Sq. Ft. X $15/square foot = $52,500 per year

Adjoining Office Space: 500 Sq. Ft. X $15/square foot = $7,500 per year

3 Lab Techs @ $100,000 per year loaded Salary = $300,000 per year

2 Management Employees @ $120,000 per year loaded salary = $240,000 per year.

2 Lead Scientists @ $120,000 per year loaded salary = $240,000 per year.

1 Medical Doctor 1/2 time @ 100,000 per year loaded fee = $100,000 per year.

Legal Expenses and other professional fees = $25,000 per year.

Travel and Marketing = $50,000 per year.

Utilities, Phone & Misc. = $17,500 per year.

Material Costs = $7,500 per year

Total Recurring General Operating Expenses = $1.1MM per year.

General One Time Expenses (Year Zero):

Tenant Improvements @ $15 per square foot = $60,000

Laboratory Equipment (film coating setup, cell culture facilities, film characterization equipment) = $150,500 (see Manufacturing and Operations Section)

Stage One Specific Costs:

Patent License Set up Fee with MIT = $100,000 in Year 0.

Patent Royalty Fee @ 10% of revenue = $1.82MM per year in Year 1, Year 2, and Year 3. (Detailed negotiations with the TLO are ongoing)

Outsourced Testing = $500,000 in Year 0.

Legal/Deal Fees = $100,000 per year in Year 0 and Year 1.

FDA Trials/Testing under $1MM and paid by partner, as is typical.

Stage Two Specific Costs

Patent License Set up Fee with MIT = $100,000 in Year 1.

Patent Royalty Fee @ 10% of revenue = $817,000 per year in Year 2, Year 3, and Year 4.

Legal/Deal Fees = $75K per year in Year 1 and Year 2.

Additional Testing at I-Shield = $250,000 in Year 1.

FDA Trials/Testing under $1MM and paid by partner, as is typical.

Cost Summary (Cash Basis)				
$K	**Year 0**	**Year 1**	**Year 2**	**Total**
Operating Costs				
General Operating Costs				
Space	60	60	60	180
Scientific Salaries	500	640	640	1,780
Management	240	240	240	720
Legal Expense	25	25	25	75
Travel and Marketing	50	50	50	150
Utilities & Misc.	25	25	25	75
Total Gen. Operating Costs	900	1,040	1,040	2,980
Stage One Operating Costs				
Patent Royalty to MIT	-	1,823	1,823	3,646
Legal/Deal/Patent Fees	100	100	-	200
Outsourced Testing	500	-	-	500
Total Stage 1 Op. Costs	600	1,923	1,823	4,346
Stage Two Operating Costs				
Patent Royalty to MIT	-	-	817	817
Legal/Deal/Patent Fees	-	75	75	150
Additional Testing	-	250	-	250
Total Stage 2 Op. Costs	-	325	892	1,217
Total Operating Costs	**1,500**	**3,288**	**3,755**	**8,543**
Capital Expenses	**Year 0**	**Year 1**	**Year 2**	**Total**
General Capital Expenses				
Tenant Improvement	90	-	-	90
Lab Equipment	151	-	-	151
Total General CapEx	241	-	-	241
Stage 1 CapEx (Patent License)	100	-	-	100
Stage 2 CapEx (Patent License)	-	100	-	100
Total CapEx	**341**	**100**	**-**	**441**
Total PreTax Cash Expenses	**1,841**	**3,388**	**3,755**	**8,983**

I-Shield Cash Flow

$K	Year 0	Year 1	Year 2	Total
Revenue				
Stage 1 Rev.	-	18,230	18,230	36,459
Stage 2 Rev.	-	-	8,169	8,169
Total Revenue	-	18,230	26,398	44,628
Operating Costs				
General	900	1,040	1,040	2,980
Stage 1	600	1,923	1,823	4,346
Stage 2	-	325	892	1,217
Total OpEx	1,500	3,288	3,755	8,543
Capital Expenses				
General	241	0	0	241
Stage 1	100	0	0	100
Stage 2	0	100	-	100
Total CapEx	341	100	0	441
Total Pretax Cashflow	(1,841)	14,842	22,643	35,644
Taxes	-	5,273	8,999	14,271
After Tax Cashflow	**(1,841)**	**9,569**	**13,645**	**21,373**
Sale of Equity	**3,200**	**-**	**-**	**3,200**
EOP Cash	**1,360**	**10,929**	**24,573**	**24,573**
IRR	**536%**			
NPV @ 35% Discount	**$9,433**			

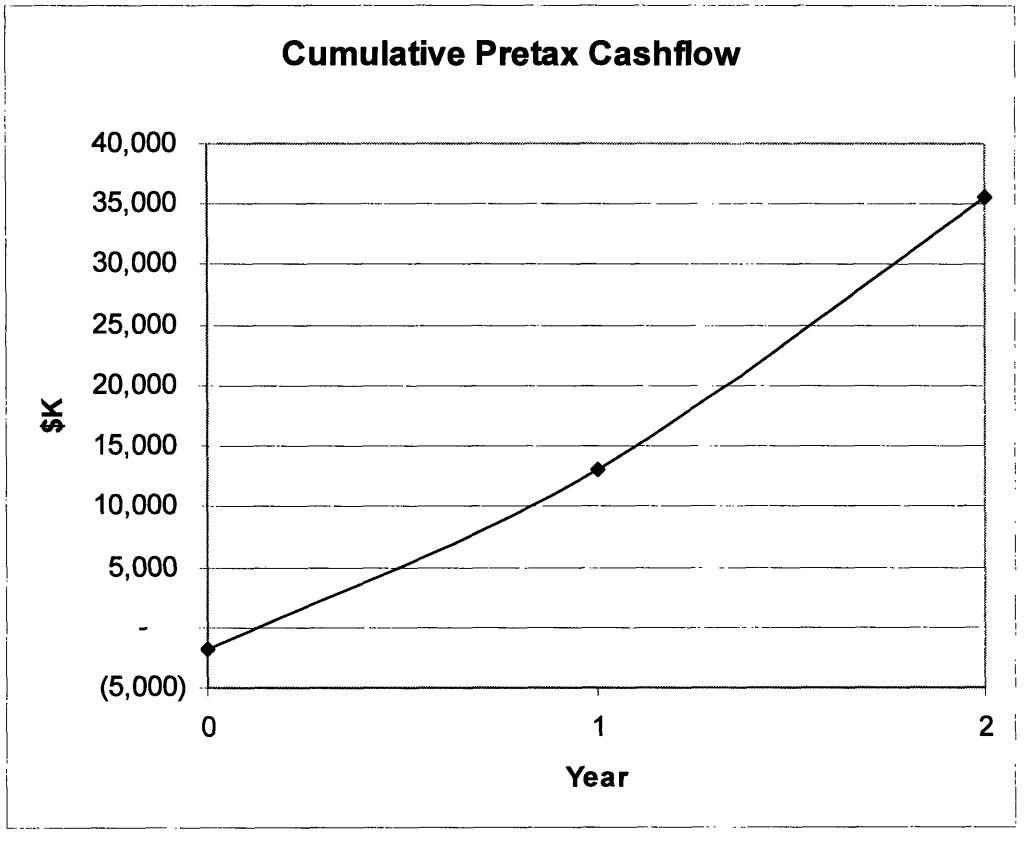
Cumulative Pretax Cashflow
40,000
35,000
30,000
25,000
20,000
15,000
10,000
5,000
-
(5,000)
$K
0
1
2
Year

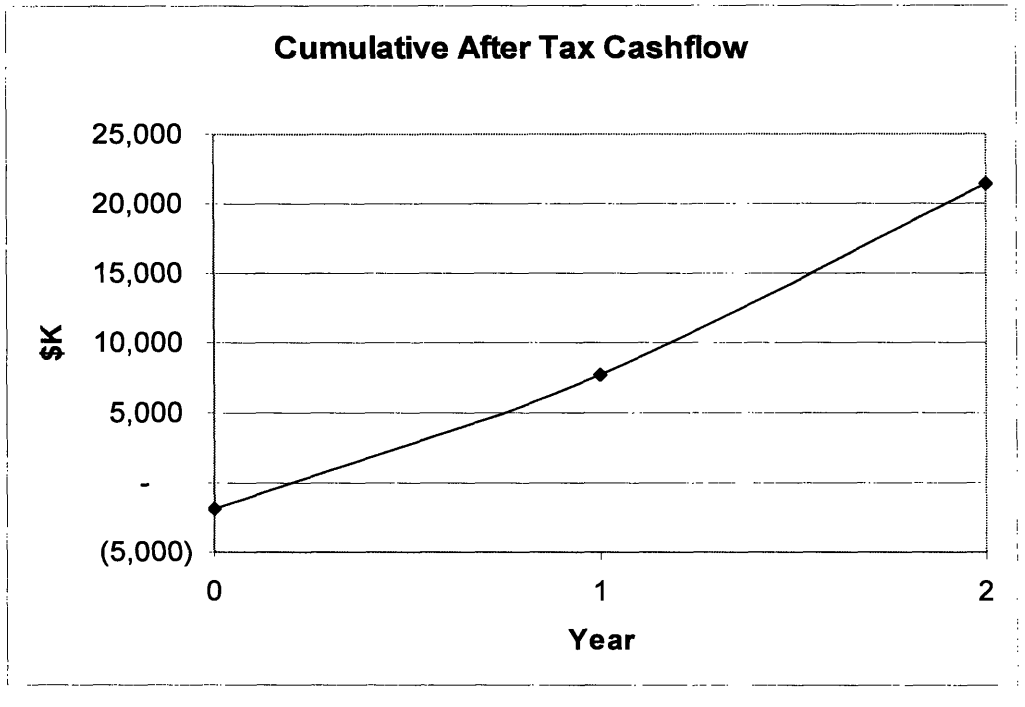
Cumulative After Tax Cashflow
25,000
20,000
15,000
10,000
5,000
-
(5,000)
$K
0
1
2
Year

Income Statement

(Simplified with no working capital and revenue recognition on cash rec

$K	Year 0	Year 1	Year 2	Total
Revenue				
Stage 1 Rev.	-	18,230	18,230	36,459
Stage 2 Rev.	-	-	8,169	8,169
Total Revenue	-	18,230	26,398	44,628
Operating Costs				
General	900	1,040	1,040	2,980
Stage 1	600	1,923	1,823	4,346
Stage 2	-	325	892	1,217
Total OpEx	1,500	3,288	3,755	8,543
EBITDA	**(1,500)**	**14,942**	**22,643**	**36,085**
EBITDA Margin	*N/A*	*82%*	*86%*	*81%*
Depreciation (3 Year)				
General	80	80	80	241
Stage 1	33	33	33	100
Stage 2	0	33	33	67
Total Depreciation	113.5	147	147	407
EBIT	(1,614)	14,795	22,497	35,678
EBIT Margin	*N/A*	81%	85%	80%
Interest (assumed zero)	0	0	0	0
Tax @ 40%	(645)	5,918	8,999	14,271
Net Earnings	**(968)**	**8,877**	**13,498**	**21,407**
Net Margin	*N/A*	*49%*	*51%*	*48%*

Offering

I-Shield is looking for $500,000 to secure patent rights, further optimize our first product, obtain key personnel, and obtain our first licensing partner. I-Shield is prepared to give a 10% equity stake for this initial funding. We will gain the $2.5MM required to complete our first product and subsequent products from our first licensing partner in exchange for product rights and a 5% to 10% equity stake.

External Reviews for Technology and Business Concept

I-Shield has received acclaim from numerous industrial and academic institutions, both for its state-of-the-art technologies and business plan. The following section briefly outlines I-Shield's accomplishments to date.

1. IdeaStream Business Plan Presentation at the Deshpande Center for Technological Innovation

In April 2004, I-Shield was selected to present its business plan at the annual conference organized by the Deshpande Center for Technological Innovation at MIT. I-Shield's technologies were profiled as some of the most exciting work coming out of MIT with a real prospect for commercialization. The entry-by-invitation only conference was attended by over 250 entrepreneurs, venture capitalists, and technologists from the Cambridge-Boston area. I-Shield's presentation received an enormous degree of positive and enthusiastic feedback, including a request from Alza, Johnson & Johnson's drug delivery division, for discussions regarding I-Shield's antibacterial coatings. We are in the process of following up on that request.

2. Collaborative Experiments with Inamed Aesthetics

Inamed Aesthetics, one of the two largest players in the breast implant market, has expressed significant interest in I-Shield's coatings for potentially reducing capsular contracture in breast implants. After initial discussions with them, I-Shield is considering initial collaborative experiments with Inamed. The experiments will facilitate development of a customized product, in addition to accelerating I-Shield's internal product optimization cycle.

3. MIT Polymer Research Awards for I-Shield's Technologies

I-Shield's coatings for wear reduction and resistance to cell and bacterial adhesion have both been subjects of Ph.D. theses of its founding members. The founding members were recently joint recipients of the 2004 OMNOVA Signature Award, MIT's premier award for excellence in polymer research; this is a clear indication of I-Shield's technological expertise.

4. Review of Business Plan by Advisory Board and External Experts

I-Shield's business plan has been carefully scrutinized and critiqued by an independent panel comprising entrepreneurs and MIT professors; the list includes Stephen Spielgelberg (President, Cambridge Polymer Group and I-Shield's Advisory Board Member), Terence Russell (2002 50K finalist and current entrepreneur), and Robert Cohen (Professor, MIT, co-founder, MatTek Corporation and I-Shield's Advisory Board Member).

Subject Matter Expert Information/Interviews

The following section is a compilation of I-Shield's discussions/interviews with various subject matter experts. We have only provided a synopsis of these interviews and have not revealed all names owing to a lack of formal signed contracts. Discussions with these individuals make this business plan more realistic and have helped prepare I-Shield's management team to face the challenges and opportunities of starting a new venture.

Foley Hoag, LLP: The patents that I-Shield plans on licensing from MIT have been filed by the law firm Foley Hoag, LLP. I-Shield's founding members worked closely with the lawyers while filing the patent application. A comprehensive search was performed to survey the competitive landscape with regards to I-Shield's coatings. While there are many potential competing coatings, it was clear that our coatings were technologically superior. Comprehensive patents were subsequently filed, reducing the risk of IP infringement.

Inamed Aesthetics: I-Shield has been involved in several discussions with Inamed Aesthetics, one of the two major players in the breast implant market; one of I-Shield's founding members has had numerous phone and e-mail exchanges with the business development manager and also the general manager for the breast implants division. The conversations have led to the possibility of initiating collaborative experiments with Inamed to test and then optimize I-Shield's anti-bacterial and cell-inert coatings for breast implants. Inamed has also expressed an interest to study I-Shield's coatings for coronary stents.

Biomet Orthopedics and Wright Medical Technologies: An initial phone conversation with Wright Medical Technologies has led to the company sending a Non-Disclosure Agreement to I-Shield to enable detailed discussions for the hip and knee implant coatings. Initial discussions led

by our medical doctor have elicited considerable interest from Biomet Orthopedics also. We are currently scheduling a lunch appointment with their Vice-President during his next visit to the city in early May.

U.S. Food and Drug Administration and Biomet: I-Shield's medical doctor has had extensive interviews with individuals at the FDA and at major implant manufacturers, including Bill Kolter (V.P. Sales, Biomet Orthopedics). All of them are confident that the I-Shield-coated end products will be classified as Class II during the FDA approval process. They also supplied I-Shield with a detailed timeline for a typical licensing deal; their information is reflected in the FDA, Marketing, and Financial Plan Section.

Stephen Spielgelberg: We have had extensive discussions with Stephen Speigelberg, I-Shield's Advisory Board Member and President, Cambridge Polymer Group. Stephen's experience as a co-founder of a polymer company and a licensing expert in the orthopedics space has enabled us to obtain accurate estimates of the costs involved in setting up a development center, the timeline for a typical licensing deal, and the price premiums that might be levied for our coated end products.

Organizational Structure and Personnel Profiles

Organization Chart

The following chart describes I-Shield's projected organizational structure:

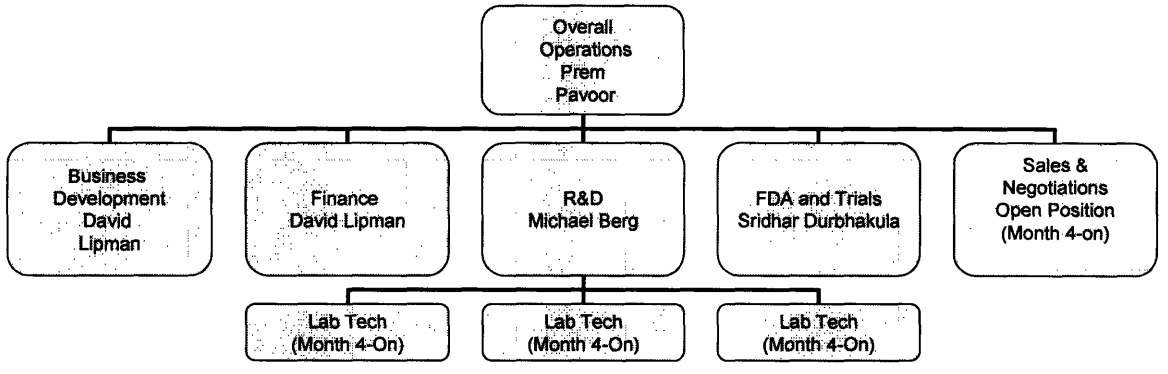

Personnel Profiles

A. Management Team

Prem Pavoor is a fourth year Ph.D. candidate in the Department of Chemical Engineering at MIT, and a first year MBA student at MIT Sloan. At MIT, Prem's research has focused on the development and successful application of nanoscale coatings for enhancing the performance of orthopedic joint replacement implants, work that has led to a patent application filed by MIT and several publications in peer reviewed journals. In addition, Prem has served as engineering consultant to a multinational chemical/petrochemical corporation in Japan and a drug delivery company (Cambridge). Prem holds a Bachelors degree in Chemical Engineering with honors from the University of Mumbai, and a M.S. in Chemical Engineering Practice from MIT. At I-Shield, Prem will supervise overall operations and technical logistics.

Michael Berg currently works on thin film coatings for biological applications as a fourth year Ph.D. student in the Chemical Engineering Department at MIT. His research has focused on making surfaces inert to proteins, bacteria, and mammalian cells through the application of nanoscale films. Michael's work has led to several publications and is being considered for patents by MIT. Before joining MIT, Michael was a process and research engineer for Kimberly Clark and W.L. Gore. Michael has also worked for a polymer start-up company, Airak, in its early stages. He holds a B.S. degree in Chemical Engineering with high honors from Virginia Tech. Michael will be in charge of product development for I-Shield.

Sridhar Durbhakula, M.D. is a Fellow in joint reconstruction at the Massachusetts General Hospital. He has also completed a residency in orthopedic surgery at Albany Medical Center, including a one-year research fellowship. Sridhar completed a seven-year accelerated program at Northwestern University, where he earned a B.S. degree in Biomedical Engineering as well as an MD degree. He has co-authored several publications related to total joint replacement surgery. Sridhar's current research projects involve bearing surface technology such as radiation-treated polyethylene. Sridhar has been invited to serve as a clinical faculty member at the Johns Hopkins Medical Institute. Sridhar will oversee clinical trials and regulatory issues for our products.

David Lipman is a MBA candidate for the class of 2005 at the MIT Sloan School of Management. David's four years of professional experience includes business development as well as strategic and financial planning for both startups and a strategy consulting firm. At Velocita, a telecommunications startup, David authored a business plan which enabled the company to win $497MM in funding in the Spring of 2001. David is a graduate of Dartmouth

College where he graduated with honors with a B.A. in History. David will be responsible for business development and financial planning.

B. Advisory Board

Anuj Bellare is the Director of the Orthopaedic Nanotechnology Group and Assistant Professor in the Department of Orthopaedic Surgery at the Harvard Medical School. Anuj is an expert in the field of orthopedic implants and holds an important patent that has facilitated improved medical imaging of bone cement used for joint replacements. Anuj graduated from the Indian Institute of Technology (Chennai, India) with a Bachelors degree in Chemical Engineering, and holds a Ph.D. in Polymer Science and Technology from MIT.

Robert Cohen is the St. Laurent Professor in the Department of Chemical Engineering at MIT. Robert's work over the past three decades has had great impact in the field of polymer chemistry and physics, and in 2000 he was awarded the Charles M.A. Stine Award by the American Institute of Chemical Engineers for pioneering research contributions to polymer science and engineering, leadership in groundbreaking educational initiatives, and development of new products and processes. Robert has consulted for several chemical and materials companies during his tenure at MIT and is currently the Co-Director of the Dupont-MIT Alliance. He is also the co-founder of MatTek Corporation, a successful, privately-held biomaterials/tissue engineering company. Robert holds a B.S. in Chemical Engineering from Cornell University and a Ph.D. in Chemical Engineering from the California Institute of Technology.

Michael Rubner is TDK Professor of Polymer Materials Science and Engineering at MIT. He is also the Director of MIT's Center for Materials Science and Engineering. Michael's research has focused on the design, fabrication, and properties of ultra-thin films of polymers for electrical, optical, and biomaterial applications. In addition to his work at MIT, Michael serves as a consultant to several materials companies in the U.S. He holds a B.S. in Chemistry from the University of Lowell and a Ph.D. in Polymer Science from MIT.

Stephen Spiegelberg is co-founder and President of the Cambridge Polymer Group, a contract research laboratory that serves several large biomedical product manufacturers. Stephen brings several years of experience with intellectual property licensing deals to I-Shield. He is often invited as an expert witness in biomedical product litigations. In addition, Stephen has designed test methodologies and processing steps for orthopedic implant materials used in hip and knee replacements, and is an expert in instrument design and fabrication. He has a B.Sc. in Chemical Engineering from the University of Wisconsin-Madison, and a Ph.D. in Chemical Engineering from MIT.

C. Open Positions:

Sales and Negotiations: I-Shield needs an individual who has been involved in technology licensing deals and who has contacts within the medical devices industry.

Lab Technicians: I-Shield will recruit 3 laboratory technicians and will hire them within 3 months of initial funding. I-Shield expects to staff these positions relatively quickly from contacts within MIT.

I-Shield Technologies

www.ishieldtech.com

contact email: info@ishieldtech.com